

A Green Pathway for the Production of Chemically Exfoliated Graphene Sheets with the Assistance of Microwave Irradiation

by

Ahmet Alptekin TOPÇU

A Thesis Submitted to the
Graduate School of Engineering
in Partial Fulfillment of the Requirements for
the Degree of

Master of Science

in

Material Science and Engineering

Koç University

August 2012

Koç University

Graduate School of Science and Engineering

This is to certify that I have examined this copy of a master's thesis by

Ahmet Alptekin Topçu

and have found that it is complete and satisfactory in all respects,

and that any and all revisions required by the final

examining committee have been made.

Committee Members:

Mehmet Suat Somer, Ph. D. (Advisor)

Uğur Ünal, Ph. D.

Zeki Çizmecioglu, Ph. D.

Date: _____

ABSTRACT

Graphene is a network of monolayer, sp^2 hybridized Carbon (C_6) atoms packed into a 2D honeycomb structure, which is the basic building block of all existing carbon allotropes. Graphene's high crystal, electronic quality along with its exceptional mechanical ($E = 1.0\text{TPa}$), electrical, thermal ($k = 5000\text{ Wm}^{-1}\text{K}^{-1}$) and optical (Opt. Transm. = 97.7%) properties have attracted the widespread attention of the world of science. None other proof is required for the rising importance of this novel material, especially after the nomination of 2010 Nobel Prize Award to Novoselov, Geim for their research on graphene.

The research presented in this MSc. thesis focuses on the production of reduced Graphene Oxide (RGO) / few layer graphene sheets with a more facile, rapid and environmental-friendly methodology in comparison to those presently available. For this purpose, RGO is chemically derived by a two-step reaction pathway. An improved method is selected for the production of Graphene Oxide (GO) that eliminates the evolution of noxious gases during synthesis (NO_2 , N_2O_4) from the commonly selected Hummers' method, while offering increased efficiency. Secondly, as produced GO sheets are reduced to RGO by replacement of toxic reducing agents with specifically selected solvents (TEG, DMF) under the assistance of Microwave Irradiation at a relatively mild temperature (120°C).

As-synthesized GO and RGO layers are characterized by XRD, FTIR, Raman, XPS, Optical Microscopy, FESEM and Elemental Analysis measurements which indicate RGO layers are successfully produced after the two-step reaction pathway.

The chemical exfoliation method for production of RGO developed in this thesis has several advantages in comparison to previous chemical techniques. It is scalable, low cost, efficient, ecological friendly, while exhibiting simplicity and short processing times. In regard of the graphene's evolution into a feasible nanomaterial and elevated importance for production, the improved process might find practical applications in the preparation of graphene-based composite materials.

ÖZET

Grafen, mevcut olan tüm karbon allotroplarının temel yapıtaşı olan tek katmanlı, sp^2 hibritleşmiş karbon (C_6) atomlarının 2 boyutlu balpeteği yapıdaki ağına verilen addır. Grafen'in yüksek kristal, elektron kalitesi ile sıradışı mekanik ($E = 1.0\text{TPa}$), elektrik, termal ($k = 5000\text{ Wm}^{-1}\text{K}^{-1}$) ve optik (Opt. Geçirgenlik = 97.7%) özellikleri bilim dünyasında geniş ilgi uyandırmıştır. Grafen üzerine çalışmaları nedeniyle 2010 Nobel Ödülleri'nin Novoselov, Geim'a takdiminden sonra bu yeni malzemenin artmakta olan önemine dair herhangi bir kanıtla gerek kalmamıştır.

Sunulmuş olan bu Master tezindeki araştırma redüklenmiş Grafen Oksit (RGO) / az katmanlı grafen yüzeylerinin mevcut olan yöntemlerle karşılaştırıldığında daha kolay, hızlı ve doğa-dostu bir metod ile üretimi üzerine yoğunlaşmıştır. Bu amaç için, RGO kimyasal bazlı iki adımlı reaksiyon yöntemi ile türetilmiştir. GO üretimi için sıkça kullanılan Hummer metodu ile yapılan sentez sırasındaki zehirli gazların (NO_2 , N_2O_4) çıkışını ortadan kaldıran, aynı zamanda da yükseltilmiş verimlilik sunan gelişmiş bir metod tercih edilmiştir. İkinci olarak, üretilen GO katmanları zehirli redüksiyon ajanlarının yerine spesifik olarak seçilmiş solventler (TEG, DMF) kullanılarak, Mikrodalga Işınımı desteği ile nispeten uygun sıcaklıklarda (120°C) RGO'ya redüklenmiştir.

Üretilmiş olan GO ve RGO katmanları X-Işını Difraksiyonu, Kızılaltı Spektroskopisi, Optik Mikroskop, Tarayan Elektron Mikroskopi, X-Işını Fotoelektron Spektroskopisi, Element Analizi ölçümleri kullanarak karakterize edilmiş olup RGO katmanlarının iki adımlı reaksiyon yöntemi ile başarılı olarak üretildiğini göstermektedir.

Bu Master tezinde geliştirilmiş olan RGO üretimi için kimyasal eksfoliyasyon metodu daha önceki kimyasal tekniklerle karşılaştırıldığında birçok avantaja sahiptir. Ölçeklendirilebilir, düşük maliyetli, verimli, doğa dostu olduğu gibi basitlik sunup kısa işlem süresine imkan tanımaktadır. Grafen'in elde edilebilir bir nanomalzeme haline evrildiği ve üretiminin önem kazanmaya başlaması nedeniyle geliştirilmiş metod, grafen-bazlı kompozit malzemelerin hazırlanmasında pratik uygulamalar bulabilir.

ACKNOWLEDGEMENT

Human life is in a progressive transformation, and I have severely felt that during these years at MSc. Degree. Initially I was striving with courses, projects, reports and exercises in the rowing team which later on suddenly changed to preparations for the wedding and then searching for a job. All has been too fast for my perceptions that made me finally notice that I became a grown up. But isn't life really sudden about anything?

The most important influence on the successful completion of this thesis has been my advisor, Prof. Dr. Mehmet Somer, to whom I am deeply grateful for his support and guidance. He has had great professional influence on my development both in terms of human traits and professional scientific approach. As a mentor, he pushed me to develop my weaknesses and exploit my strengths. Just like a father, he has his own way of directing the student into the right direction at the moments of cruciality.

I would like to thank Dr. Durata Hacıu, with whom I worked as an assistant since so many years in different courses. I am grateful for her guidance and strong –Leo- character who always taught by inspiring me. Asst. Prof. Dr. Özgür Birer's encouragement and motivation aroused my excitement, while for his boundless help and anytime assistance I am deeply grateful. I appreciate Asst. Prof. Dr. Uğur Ünal, for his aid, as well as his extremely polite and humble personality. I would like to express my gratitude to Prof. Dr. Zeki Çizmecioglu, Prof. Dr. Levent Demirel and Dr. Annamaria Miko for their support and valuable hints.

Life in the laboratory would be incomplete without friends and especially Selçuk Acar, our lab's second chief, who inspired me ever with his work discipline and helped me with overcoming any type of a problem. And we miss Burcu Uslu, who is far away now. I would like to express my gratitude to Recep Kaş, my dearest friend (LOTR?), who still continues his education in the fields of Netherlands; Caner Nazlı, the referee, who has a unique personality; Ali Baş and İbrahim Hoccoğlu with whom we shared many moments and many common opinions; Muharrem Güler –the Lord of the Glass- for his technical support and friendship during coffee breaks. Thanks to Begüm for being my slave in the laboratory and helping with the synthesis, who unfortunately and mysteriously disappeared near to the end. I am deeply thankful to Bekir Yenilmez-Bekirpedia- and Erhan Aysan for their empathy

with whom we shared two enjoyable years. I also would like to thank all the dear people whom I could not mention one by one.

Finally, I am deeply grateful to my family, parents, brothers, sister and especially my dearest wife. Without her endless empathy, support and encouragement, none of what I have accomplished would be possible.

TABLE OF CONTENTS

ACKNOWLEDGEMENT	V
LIST OF TABLES	IX
LIST OF FIGURES	X
NOMENCLATURE	XIII
GENERAL INTRODUCTION	15
Chapter I : INTRODUCTION.....	16
1.1 History of Graphitic Compounds	17
1.2 Chemistry of Graphitic Compounds.....	20
1.2.1 Chemistry of Graphene	23
1.3 Production Methods.....	25
1.3.1 Reduction of Graphite Oxide	28
1.4 Characterization of Graphene	30
1.5 Properties and Applications of Graphite	33
1.5.1 Properties and Applications of Graphene	33
1.6 General Aspects of Microwave Radiation.....	37
Chapter II : EXPERIMENTAL PROCEDURE	40
2.1 Experimental Materials.....	40
2.2 Experimental Methodology	40
2.2.1 Synthesis of Graphite Oxide	41
2.2.2 Reduction of Graphite Oxide	44
2.3 Characterization Methods/Instruments	45
2.3.1 Microwave Radiation System	45
2.3.2 X- Ray Diffraction	45
2.3.3 Fourier Transform - Infrared Spectroscopy	46
2.3.4 Raman Microscope	47
2.3.5 Thermo Gravimetric / Differential Thermal Analysis	47
2.3.6 Optical Microscopy.....	48

2.3.7 Field Emission Scanning Electron Microscopy (FESEM)	49
2.3.8 Elemental Analyzer.....	49
2.3.9 X-Ray Photoelectron Spectroscopy	50
2.3.10 Water Purification System	51
Chapter III : RESULTS AND DISCUSSION.....	52
3.1 Microwave Solvothermal Approach.....	54
3.2 The Choice of an Appropriate Solvent	59
3.3 Optical Microscopy Results.....	59
3.4 SEM Results	60
3.5 FT-IR Results	68
3.6 Raman Results	74
3.7 XRD Analysis.....	77
3.8 XPS Results	80
3.9 Elemental Analysis Results	84
3.10 TGA/DTA Analysis.....	85
Chapter IV : SUMMARY AND FUTURE WORK.....	87
Appendix A : Raman Microscope Images	90
Chapter V : BIBLIOGRAPHY	92

LIST OF TABLES

Table 1.1 : Physical Properties of Graphite and Diamond.....	6
Table 2.1 : Hansen Solubility Parameters of selected.....	43
Table 2.2 : Comparison of selected solvents (DMF, TEG, Water).....	44
Table 2.3 : Comparison of utilized Reaction parameters.....	45
Table 3.1 : The Result of Elemental Analyses.....	61

LIST OF FIGURES

Figure 1.1 : A Representation of timeline of the universe [6].....	16
Figure 1.2 : The renowned Egyptian Hieroglyphics: “The Book of the Dead” 1275B.C. [11]	18
Figure 1.3 : Eight important allotropes of Carbon a) Diamond b) Graphite c) Ionsdaleite d-f) Buckminsterfullerenes g) Amorphous Carbon h) Carbon Nano Tube [16].....	19
Figure 1.4 : Physical Appearance of Graphite, pencil made of graphite (right, down)	20
Figure 1.5 : a) Atomic orbital diagram showing sp^3 hybridization of Carbon b) hybrid orbitals of carbon [12].....	21
Figure 1.6 : Atomic Force Microscopy (AFM) image of highly ordered pyrolytic graphite, C_6 hexagons indicated by white lines [12]	22
Figure 1.7 : The sequence of layers in hexagonal α -graphite, ABAB in z-direction [12]	23
Figure 1.8 : Graphene, “the mother of all graphitic forms of carbon”, from left to right; 0D Buckyballs, 1D CNT, 2D Graphene, 3D Graphite [1]	24
Figure 1.9 : Number of publications on graphene in the last 20 years [35]	25
Figure 1.10 : Image of a multilayer Graphene flake with thickness ~ 3 nm on a Si wafer [2].	26
Figure 1.11 : Categorization of graphitic thin film sheets [39].....	27
Figure 1.12 : Structure of Graphite Oxide proposed by Lerf-Klinowski Model [43].....	28
Figure 1.13 : Molecular model displaying the pathway for Graphene production; Graphite is oxidized to GO and reduced to Graphene [46]	29
Figure 1.14 : Optical Image of mono-,bi-, tri- and tetra-layer graphene on SiO_2/Si substrate [54]	31
Figure 1.15 : AFM Image of RGO on HOPG surface with line profile (red line) [55]	31
Figure 1.16 : High Res. STM Image displaying the honeycomb network of single layer graphene [56].....	32
Figure 1.17 : Raman Spectra of bulk graphite and graphene at 514nm [58]	32
Figure 1.18 : Single layer graphene has an optical absorbance of 2.3% per layer [62]	34
Figure 1.19 : An assembled Graphene layer over PET membrane with outstanding flexibility [74]	36
Figure 1.20 : Components of a Microwave.....	38
Figure 2.1 : Molecular model representing the pathway for Graphene production	41
Figure 2.2 : Millipore Membrane Filter; 100 pack filter (left), Type GS(right)	43
Figure 2.3 : Vacuum Assisted Membrane Filtration Setup	44
Figure 2.4 : CEM MarsXpress Microwave Radiation System.....	45
Figure 2.5 : X-Ray Diffraction Spectrometers. Huber G670(left), Bruker D2 Phaser (right) .	46
Figure 2.6 : Thermo Fisher Inc. Nicolet iS10 FT-IR Spectrometer	46
Figure 2.7 : Renishaw inVia Raman Microscope	47
Figure 2.8 : Thermo Gravimetric/Differential Thermal Analyzer	48
Figure 2.9 : Nikon Eclipse Ti Optical Microscope	48
Figure 2.10 : Zeiss Evo Ultra Plus FE-SEM	49
Figure 2.11 : Leco Elemental Analyzer.....	50

Figure 2.12 : Thermo K-Alpha X-Ray Photoelectron Spectrometer.....	51
Figure 2.13 : ELGA Purelab Option Q Water Purification System	51
Figure 3.1 : Millipore Membrane Filter blank (left) and Graphite Oxide (right).....	54
Figure 3.2 : Graphite Oxide (left) in comparison with reduced GO (right)	54
Figure 3.3 : Optical Microscopy Image of Graphene Oxide, Scale bar: 10 μ m, (left:100X Magnification, right:200X)	59
Figure 3.4 : Optical Microscopy Image of Graphene Oxide, (left:200X Magnification, Scale bar: 10 μ m, right: 1000X, Scale bar: 1 μ m)	59
Figure 3.5 : Optical Microscopy Image of a Graphene Oxide sheet, 500X Magnification, Scale bar: 2 μ m(left), 1000X, Scale bar: 1 μ m(right)	59
Figure 3.6 : Optical Microscopy Image of RGO sheets, 100X Magnification, Scale bar: 10 μ m(left), 200X, Scale bar: 5 μ m(right)	60
Figure 3.7 : FESEM Image of Graphene Oxide, 2460X Magnification, Scale bar: 10 μ m	60
Figure 3.8 : Epoxy group stretching the C-C bond	61
Figure 3.9 : An illustration displaying the wrinkle on a thin-film layer	61
Figure 3.10 : FESEM Image of Graphene Oxide, 21.170X Magnification, Scale bar: 1 μ m ...	62
Figure 3.11 : FESEM Image of Graphene Oxide, 52.320X Magnification, Scale bar: 300nm	62
Figure 3.12 : FESEM Image of Graphene Oxide, 101.780X Magnification, Scale bar: 200nm	63
Figure 3.13 : FESEM Image of Graphene Oxide, 172.960X Magnification, Scale bar: 100nm	63
Figure 3.14 : FESEM Image of Reduced Graphene Oxide, 4.410X Magnification, Scale bar: 2 μ m.....	64
Figure 3.15 : FESEM Image of Reduced Graphene Oxide, 31.140X Magnification, Scale bar: 1 μ m.....	64
Figure 3.16 : FESEM Image of Reduced Graphene Oxide, 28.630X Magnification, Scale bar: 1 μ m.....	65
Figure 3.17 : FESEM Image of Reduced Graphene Oxide, 200.060X Magnification, Scale bar: 100nm.....	65
Figure 3.18 : FESEM Image of Reduced Graphene Oxide, 358.110X Magnification, Scale bar: 100nm.....	66
Figure 3.19 : FESEM Image of Reduced Graphene Oxide, 236.260X Magnification, Scale bar: 100nm.....	66
Figure 3.20 : FESEM Image of Reduced Graphene Oxide, 313.170X Magnification, Scale bar: 100nm.....	67
Figure 3.21 : ATR-FTIR Pattern displaying Oxidation of Graphite to Graphite Oxide	68
Figure 3.22 : Structure of Graphite Oxide proposed by Lerf-Klinowski Model [43].....	69
Figure 3.23 : Starting Material Effect: FTIR Spectrum of flake Graphite vs HOPG.....	70
Figure 3.24 : Oxidation Method Effect: FTIR Spectrum of Hummers Method vs Improved Method	71
Figure 3.25 : Hydrogen Network formed between the functional oxygen of GO and water molecules [43]	71
Figure 3.26 : FTIR Spectra: Reduction of GO to RGO	72
Figure 3.27 : FTIR Spectra: Reduction of GO to RGO	73

Figure 3.28 : Raman spectra of Graphite - GO	74
Figure 3.29 : Raman spectra of GO - RGO.....	75
Figure 3.30 : Raman spectra of Graphite - RGO.....	76
Figure 3.31 : XRD Diagram of Graphite - literature data	78
Figure 3.32 : XRD Diagram of Graphite - GO	79
Figure 3.33 : XRD Diagram of Graphite - GO – RGO1	79
Figure 3.34 : XPS Spectrum of Graphite Oxide.....	81
Figure 3.35 : XPS Spectrum of RGO-1.....	82
Figure 3.36 : XPS Spectrum of RGO-2.....	83
Figure 3.37 : TGA Curve of Graphite - GO	85
Figure 3.38 : TGA Curve of Graphite - GO	86

NOMENCLATURE

AG : Artificial Graphite

AFM : Atomic Force Microscopy

ATR – IR : Attenuated Total Reflectance Infrared Spectroscopy

DMF : N,N – Dimethylformamide

DSC : Differential Scanning Calorimetry

DTA : Differential Thermal Analysis

FESEM Field Emission Scanning Electron Microscopy

FT - IR Fourier Transform Infrared Spectroscopy

GO : Graphite Oxide

NG : Natural Graphite

RGO : Reduced Graphite Oxide

HOPG : Highly Oriented Pyrolytic Graphite

RGO Graphite Oxide

SEM : Scanning Electron Microscopy

TEG : Tetraethylene Glycol

TEM : Transmission Electron Microscopy

TGA : Thermogravimetric Analysis

THF : Tetrahydrofuran

XPS : X-Ray Photoelectron Spectroscopy

XRD : X-Ray Diffraction

GENERAL INTRODUCTION

Carbon is an extraordinary element with many different allotropes including diamond, graphite, Carbon nano tubes, amorphous carbon and graphene. Constituting more than 90% of all known chemical substances, it is a crucial element that forms the very basis of life, such as DNA and proteins.

Among Carbon allotropes, Graphene has recently attracted great interest from the scientific community, especially chemists, physicists and material scientists due to its excellent mechanical, thermal and electrical properties [1]. After discovery of graphene by Geim and Novoselov in 2004 [2] and their Nomination for 2010 Nobel Prize in Physics, the rising importance of this novel material has become particularly explicit.

As the thinnest material known in universe [3], a single layer of graphene is a high strength material, with a higher Young's modulus (1000 GPa) in comparison to bulk steel (200GPa). Thermal conductivity ($5000 \text{ Wm}^{-1}\text{K}^{-1}$) and electrical conductivity are high, with more current density than that of conventional conductors, like copper[4]. Its optical transmittance is also very high, 97.7% for single layer and combined with the excellent electrical properties, it offers a high potential for use in many diverse fields such as electronic, optoelectronic devices, chemical sensors, nanocomposites and energy storage materials.

The Research conducted in this MSc. Thesis focuses on production of graphene with a green production pathway which include utilization of microwave radiation, usage of non-toxic solvents and elimination of hazardous reducing agents for the exfoliation of graphite to graphene layers.

Introduction sections will provide information on the origin of carbon, its history, other carbon allotropes and production techniques available in the literature in addition to major concepts in microwave chemistry.

Chapter I : INTRODUCTION

In the beginning there was only Hydrogen. Then it transformed into helium, element of the stars and then to star ashes, including every element and the Carbon. [5]

About 13.7 billion years ago, the universe was an extremely hot place condensed in just some millimeters of space according to The Big Bang theory [6]. Only one second after the Big Bang, the temperature of the universe was approximately 10 billion degrees and it was filled with an excess of neutrons, protons, electrons, positrons, photons and neutrinos.

As the universe expanded and cooled, neutrons combined with protons to form deuterium, ^2H . Light elements like ^1H , ^4He and ^7Li are synthesized during the first few minutes after the Big Bang. Elements heavier than ^7Li have been produced from the nuclear fusion of lighter elements about 400 mil. years later, known as nucleosynthesis in stars.

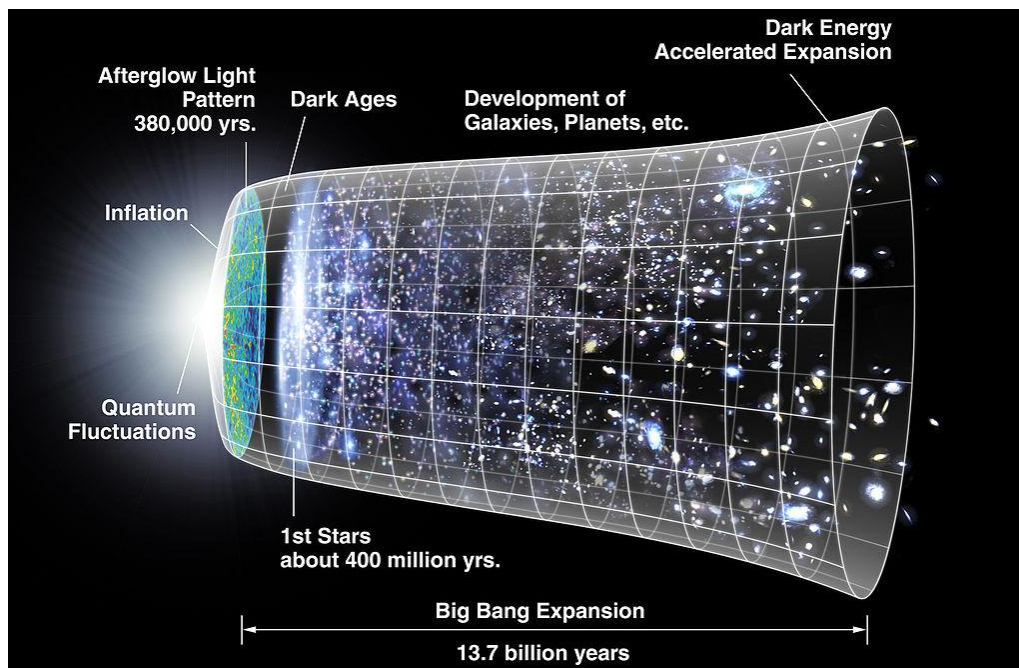


Figure 1.1 : A Representation of timeline of the universe [6]

Stars are extremely hot furnaces burning Hydrogen (^2H) basically, like the Sun of the solar system. Thus, ^4He is burned to produce ^{12}C , ^{14}Si , ^{16}O , and up to ^{56}Fe , which is the most stable form of nuclear matter. Elements heavier than ^{56}Fe are formed during death of massive stars, known as Supernova explosions [7].

From an explosion much smaller than that of the Big Bang, an orbit of the sun, named earth, has been formed 4.54 billion years ago [8]. As the fireball cooled and earth's crust solidified, a water and carbon based life form started in the oceans with simple bacteria (prokaryotes) 3.5 billion years ago. The development of photosynthesis and formation of ozone paved the way to more complex cells, the eukaryotes. Development of eukaryotic multicellular organisms led to the first appearance of keynote mammals. As recently as 200,000 years ago have appeared the species "Homo sapiens", known as the ancestors of modern humankind [9].

Basically, the foundation for the planet earth has literally started from "stardust". Not only ^{12}C has already played a major and substantial role, but from the recent developments in the field of nanotechnology, it is obvious that it will continue to do so in the 21st century.

1.1 History of Graphitic Compounds

Carbon is a naturally abundant nonmetallic element with a greyish-black, opaque appearance. It has the chemical symbol C and atomic number 6. As the 17th most abundant element on earth's crust, it plays a significant role as a central atom. There is a rich array of known Carbon allotropes differing in the way atoms bond in the structure; Graphite, Diamond as well as the recently discovered Buckminsterfullerenes, Carbon Nano Tubes (CNT) and recently Graphene.

Carbon in its various forms such as charcoal and soot has started playing a substantial role in human daily life since its discovery in 5000 BC. Earliest use of carbon dates back to 3750 BC, for reduction of metals in the production of bronze by Egyptians and Sumerians. The first recorded application of charcoal, as an adsorbant for medicinal purposes is cited in Egyptian papyri in 1500 BC [10].

The black ink used for Egyptian hieroglyphs were produced from soot [11], a form of carbon. Moreover, documents indicate that it has been excavated for use as a dark pigment to blacken pottery and in cave writings near France [12]. Pencils made of graphite/clay mixture from Middle Ages show that humankind has discovered this material's writing ability and implemented it from early on, which is still widely used today.



Figure 1.2 : The renowned Egyptian Hieroglyphics: “The Book of the Dead” 1275B.C. [11]

In fact, the name “Carbon” is derived from the Greek word “carbein”, which means “to draw”. Lavoisier, who is known as “the Father of Modern Chemistry” [13], named the element Carbon in 1789 from the Latin word “carbo” that means charcoal. After the experiments of British chemist Tennant at the end of 18th century, it was understood that graphite, soot and diamond are all but allotropes of the same element.

In the 19th century, progress in the field of Carbon rapidly increased after the distinction between inorganic and organic matter by Berzelius in 1807 [14] and that Carbon is the main player in organic chemistry. Kekule proved the benzene ring is a cyclic entity, paving the bricks of organic chemistry. Van’t Hoff, the very first Nobel Prize Laureate in 1901 [15], proved the concept that carbon is an element with four-fold coordination and a tetrahedral structure.

Research in 20th century is boosted after the studies of A.S. King and Birge proving the ^{12}C and ^{13}C composition. Radioactive ^{14}C 's detection in 1936 provided a tool for mankind to determine the age of organic matter, known as radioactive dating, for which Libby received the 1960 Nobel Prize in Chemistry [15].

In 1985, a molecular sphere which resembles a ball is discovered and named Buckminsterfullerenes (Buckyball) after the Buckminster Fuller Structure's geodesic dome in North Carolina, USA.

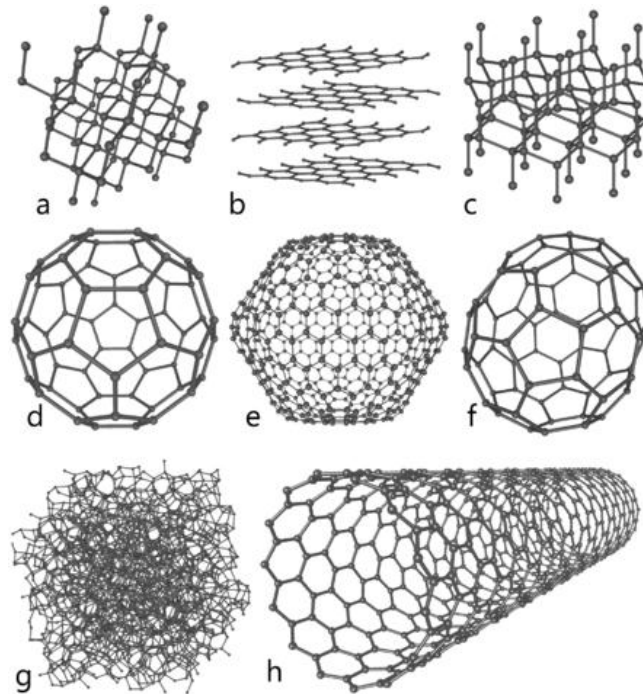


Figure 1.3 : Eight important allotropes of Carbon a) Diamond b) Graphite c) Ionsdaleite d-f) Buckminsterfullerenes g) Amorphous Carbon h) Carbon Nano Tube [16]

In 1991, Iiyama discovered Carbon Nano tubes, a cylinder made of carbon network and named them “Helical Microtubules of Carbon” [17], after which research in the field has boomed, with more than 50.000 articles to this date.

In 2004, Geim and Novoselov discovered Graphene by peeling layers of graphite with a Scotch tape, an unbelievably simple yet effective method that yield them the Nobel Awards in Physics 2010. A wide interest is present in graphene as it offers tremendous potential in applications such as batteries, solar cells and composite materials.

1.2 Chemistry of Graphitic Compounds

The knowledge of essential facts on the “classical” modification of carbon, namely graphite, would be necessary to thoroughly perceive the huge developments in the field of graphitic compounds. A solid understanding of basic concepts and principles is required for the comprehensive development of new ideas. Therefore, this section starts with the key facts on graphite, its structure and continues with those of graphene.



Figure 1.4 : Physical Appearance of Graphite, pencil made of graphite (right, down)

The sixth element in the periodic system, Carbon has the element symbol C. It is the 17th most abundant element on earth’s crust [18]. Despite the low abundance, it plays a central role in the assembly of living beings and organic matter, by constituting 18% of total mass of the human body [19].

Characteristic	Graphite	Diamond
Color	Black with metallic luster	Colorless
Refractive index $n_{D(546\text{ nm})}$	2.15 ; 1.81 \perp	2.43
Density	2.266 (exp. 1.5–2.2) g cm^{-3}	3.514 g cm^{-3}
Combustion enthalpy	393.5 kJ mol^{-1}	295.4 kJ mol^{-1}
Hardness (Mohs)	1 ; 4.5 \perp	10
Band gap	0 eV	5.5 eV
Specific resistance	0.4–0.5 $\times 10^{-4} \Omega \text{ cm}$; 0.2–1.0 $\Omega \text{ cm}$ \perp	10 ¹⁴ –10 ¹⁶ $\Omega \text{ cm}$

||: parallel to graphene layer.

\perp : perpendicular to the planes (along z-axis).

Table 1.1 : Physical Properties of Graphite and Diamond[12]

Carbon is capable of forming sp , sp^2 , sp^3 bonding and thus possesses an enormous number of different chemical, organic and biological species. This is a result of its mid position in the periodic table, as it is an ideal reaction partner to form stable species with neighboring more electronegative and also more electropositive elements.

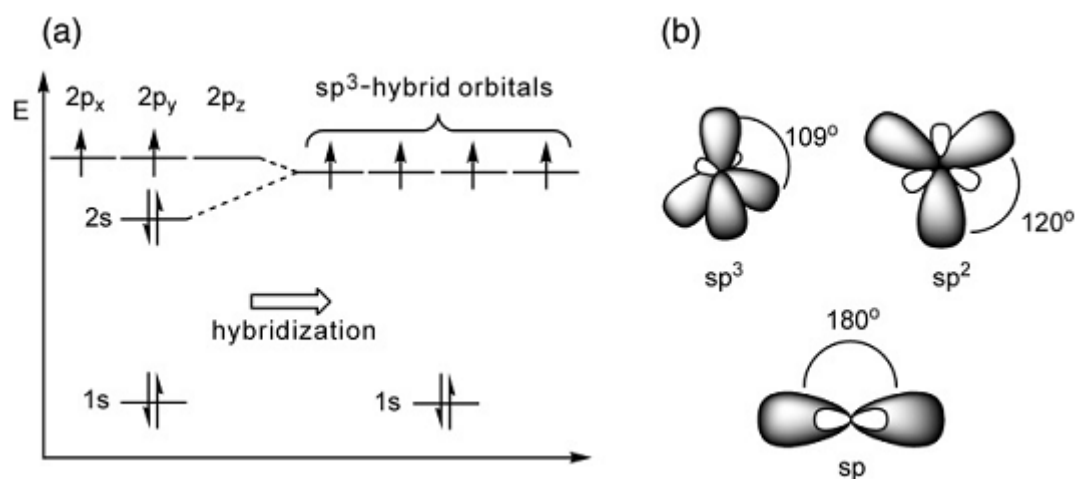


Figure 1.5 : a) Atomic orbital diagram showing sp^3 hybridization of Carbon b) hybrid orbitals of carbon [12]

Carbon atom has the electronic configuration $1s^2 2s^2 2p^2$, with a total of 6 electrons, two tightly bound to nucleus and remaining four as valence electrons. Although two valence electrons imply a bivalence, carbon atoms are tetravalent. This fact can be explained from the hybridization scheme that shows a rather low energetic difference between 2s- and 2p orbitals. As a result, wavefunctions mix to form four equivalent hybridized orbitals in sp^3 bonding scheme within a tetrahedral structure [12].

In sp^3 bonding, hybrid orbitals are directed toward the four corners of a tetrahedron as seen in *Figure 1.5 b*). Similarly 2s orbitals can mix with other 2p- orbitals to form linear chains in sp bonding, while sp^2 and sp^3 hybridization give rise to planar structures.

In a single layer, carbon atoms are covalently bonded at the corners of C_6 hexagon in a 2D lattice structure. S, p_x and p_y atomic orbitals on each carbon hybridize to form C_6 hexagons inside a honeycomb network with strong covalent sp^2 bonds and C-C-C angle of 120° [12]. The structure of graphite is characterized by succession of single graphene layers spreading over xy-plane, stacked in z-direction with weak Van der Waals interactions between them.

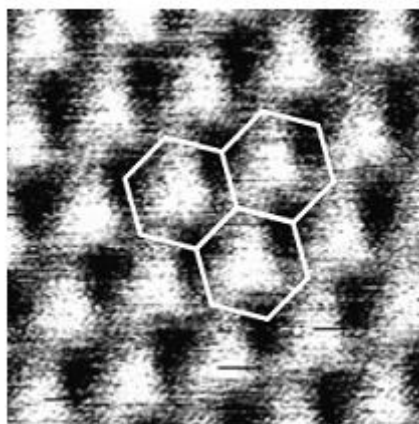


Figure 1.6 : Atomic Force Microscopy (AFM) image of highly ordered pyrolytic graphite, C_6 hexagons indicated by white lines [12]

For each C, three σ -bonds lead along the hexagons, corresponding to sp^2 hybridization. Only three of the four valence electrons participate in hybridization, while the remaining electron in p_z orbital forms delocalized π -bonding above and below the sheets, resembling a cloud of electrons. The p_z orbital of each carbon overlaps with three neighbors to form a filled π orbital (valence band) while the empty π^* orbitals constitute the conduction band.

In the graphene plane, distance between adjacent C atoms is 0.142 nm. In comparison, C-C distance in benzene is 0.139 nm. Therefore, the effect of π -bonding is clearly visible and this corresponds to a bond order of 1.5. On the other hand, the interplanar C-C distance between adjacent sheets is 0.335 nm [12], due to weak van der Waals interaction between planes that holds them more loosely. Delocalized π electrons have high electron mobility and

provide material properties such as high but anisotropic electrical conductivity, which is further explained in *Chapter 1.3: Properties and Applications*.

The lack of any chemical bonding in the c-direction results in very weak out-of-plane interactions and anisotropic material properties. The effect of this is extremely low propagation of charge and thermal carriers, thus out-of-plane electrical and thermal conductivities are more than 10^3 times lower than those of in-plane analogues [20, 21].

In its most stable form, α -graphite; a hexagonal lattice structure prevails. Individual graphene sheets are stacked in the hexagonal structure with a sequence of ABAB. Thus, a carbon atom in layer A is located right above the midpoint of the C_6 hexagon of the adjacent layer B, as displayed in *Figure 1.7*.

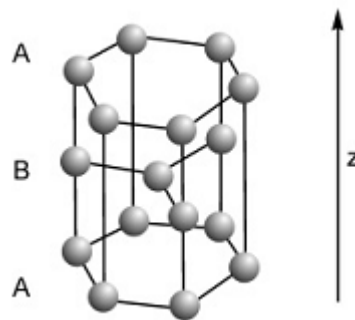


Figure 1.7 : The sequence of layers in hexagonal α -graphite, ABAB in z-direction [12]

1.2.1 Chemistry of Graphene

Graphene is a single-atom-thick planar sheet of carbon hexagons sp^2 hybridized within a honeycomb network. As the building block of all important allotropes of carbon network, it is also called “the mother of all graphitic forms” [1]. Shaped into a point particle, 0D buckminsterfullerene is formed, in 1D it is rolled to a carbon nanotube, in 2D the graphene sheet itself and finally in 3D graphene sheets are stacked to obtain graphite.

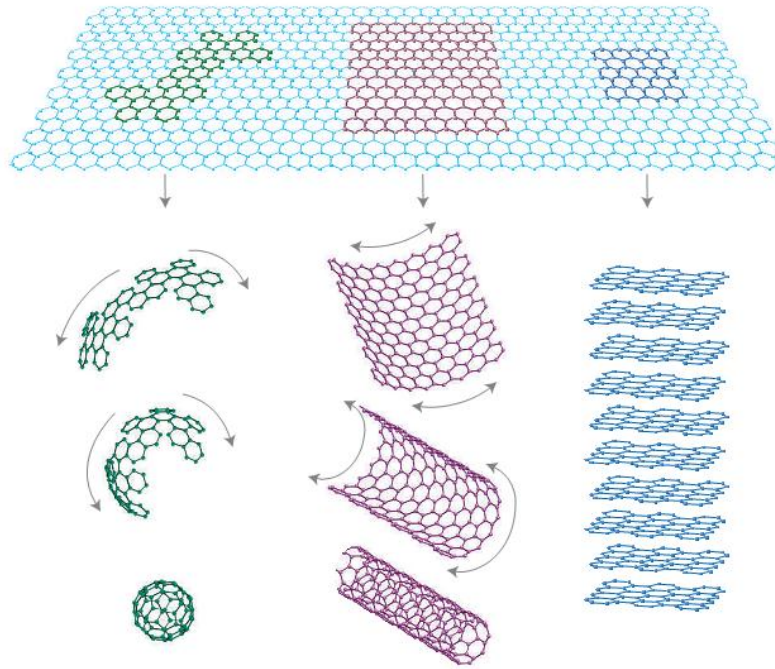


Figure 1.8 : Graphene, “the mother of all graphitic forms of carbon”, from left to right; 0D Buckyballs, 1D CNT, 2D Graphene, 3D Graphite [1]

Graphene is an attractive novel material for chemists, physicists and material scientists due to the fact that it offers not only novel properties for theoreticians but also for experimentalists as well. Surprisingly, it had been believed to be a material that should not exist; since 2D crystals were thought to be thermodynamically unstable at finite temperatures [22]. Added to theory was that experimental data also supported this belief. Indeed, thin films of few atomic layers become unstable and rapidly decompose at high temperature [23]. Therefore, there had been a wide belief that 2D materials only exist as part of larger 3D structures.

However, experimental data from single sheets of graphene obtained by Geim in 2004 clearly proved the fact that continuous and perfect crystals do exist in 2D. The experiment yields a 2D crystal, which is astounding due to two reasons; 1) that 2D crystals exist and 2) they can be stable at Room Temperature .

Graphene sheets possess high electronic quality. It shows ambipolar electric field effect, which means that charge carriers can be tuned between electrons and holes even at ambient temperature. Quantum Hall Effect is observed also at ambient temperature, a value that extends the known temperature range so far [24].

Charge carriers can travel without scattering and have a high electron mobility ($15\,000\text{ cm}^2\text{ V}^{-1}\text{ s}^{-1}$) at room temperature. Moreover, the observed mobilities are weakly dependent on temperature. The minimization of impurity scattering in suspended graphene yield exceptionally high mobility values exceeding $200.000\text{ cm}^2\text{ V}^{-1}\text{ s}^{-1}$ [25].

Electrons in graphene behave like massless relativistic particles, a phenomena that can not be explained with Schrödinger equation but that of Dirac. This also contribute to very peculiar properties such as an anomalous quantum Hall effect and the absence of localization [24].

1.3 Production Methods

After the discovery of Buckminsterfullerenes (0D Allotrope) and Carbon Nano Tube (1D Allotrope), the search for the “elusive” 2D structure of Carbon intensified, as reflected in the exponential growth of scientific publications in the past decades (see Figure 6).

A variety of techniques including Micromechanical Exfoliation of Graphite [2, 26], Chemical Vapor Deposition on metal surfaces [27, 28], epitaxial growth on SiC wafer [27, 29], unzipping of CNT [30] and Reduction of Graphite Oxide [31-34] have been utilized for the production of graphene.

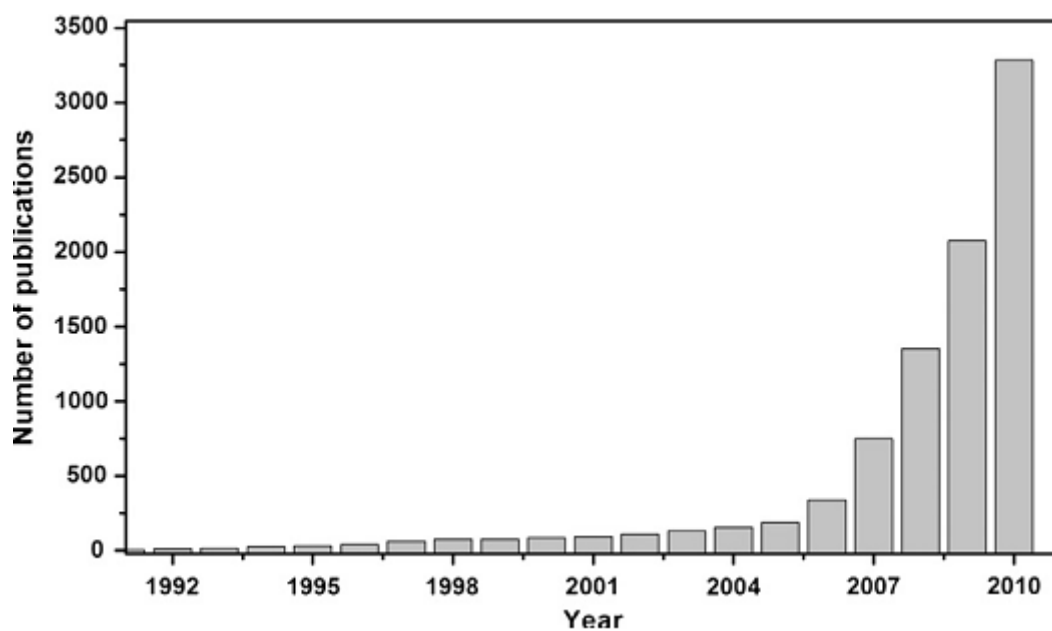


Figure 1.9 : Number of publications on graphene in the last 20 years [35]

In 1999, Ruoff aimed at tailoring graphite to obtain sheets of graphene by using Atomic Force Microscope (AFM) tip [36]. The thinnest flakes observed were more than ~ 600 layers. Kim's research group improved on by transferring the pillars to a tipless cantilever that enabled production of flakes with ~ 30 layers [37], yet still far from the single layer objective.

Micromechanical Exfoliation of highly ordered pyrolytic graphite has been the first method to successfully obtain sheets of graphene. Single layers of 2D graphene sheets are removed from graphite flakes simply by peeling a graphite flake with a cellophane tape [2]. The flakes on the tape are thick and few layers initially, but upon pressing against a Si substrate and lifting away, the number of layers are reduced. They are delaminated on Si substrate with Van der Waals interaction between the tape and substrate until single layers are obtained.

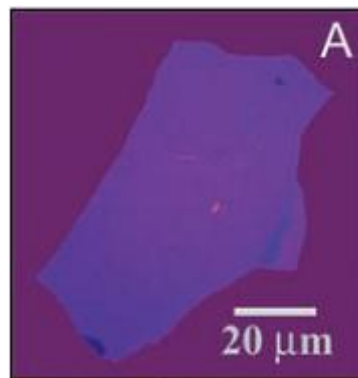


Figure 1.10 : Image of a multilayer Graphene flake with thickness $\sim 3\text{nm}$ on a Si wafer [2]

The advantage of Micromechanical Exfoliation is its ability to isolate perfect single layers of graphene [2]. The disadvantage however, is its slowness and inconvenient procedure with extremely low yields. Therefore, it is a low yield and low throughput process aimed primarily for academic intentions. Using a pencil and Scotch tape is a surprisingly simple yet effective method to acquire a Nobel in today's sophisticated World of Science. But in fact, this is the production method implemented for the production of single and few layer graphene sheets that allowed determination of the properties of this extraordinary material.

Although the aforementioned methods yield perfect crystals of graphene without any defects, they are rather slow and small-scale methods. By adopting them, availability and processability of layers become rate limiting factors for production of graphene. Instead, chemical methods are feasible, facile and scalable for the industrial bulk-scale fabrication

[38]. Therefore, reduction of Graphite Oxide to Exfoliated Graphene sheets is recently accepted as the most promising approach for large-scale production [31].

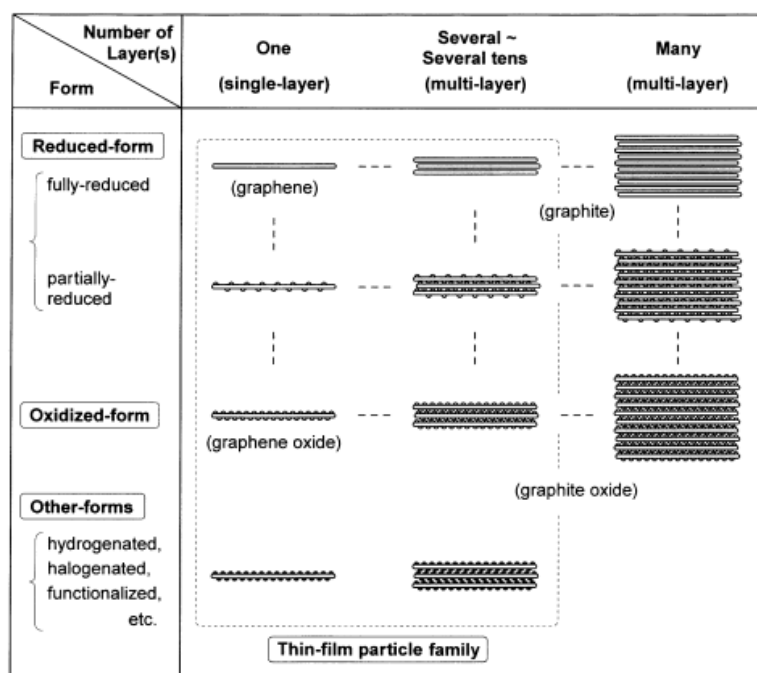


Figure 1.11 : Categorization of graphitic thin film sheets [39]

Although graphene is a novel material, the production of Graphite Oxide (GO) as precursor to its synthesis from natural graphite has been discovered for different purposes. Natural graphite is oxidized in the presence of strong acids and oxidizing agents to obtain GO, which is then reduced to exfoliated Graphene sheets, also known as reduced GO (RGO).

In the search for the structure of graphite, Brodie added Potassium Chlorate KClO_3 and Nitric acid HNO_3 to a slurry of graphite and named the resulting compound “Graphitic acid” [40] in 1859. After 40 years, Staudenmaier improved the Brodie’s method to oxidize graphite by adding KClO_3 to HNO_3 in multiple portions.

The most widely used approach is the Hummer’s method, in which graphite is reacted with a mixture of strong oxidizing agents such as potassium permanganate (KMnO_4) and concentrated sulfuric acid (H_2SO_4) [41]. The resulting product is Graphite Oxide, a nonconducting hydrophilic material.

Most of the methods used for production of GO depend on Hummer’s method, which involves toxic chemicals and generation of noxious gases. Taken into consideration the importance of GO for production of Graphene, a green approach is necessary for volume

production. The green methods utilized in this MSc. Thesis are further explained in *Chapter 2.1: Experimental Section*.

1.3.1 Reduction of Graphite Oxide

After discovery of graphene, effort has been directed on finding methods that enable large-scale production. Thus, a novel process for producing single layer graphene that is solution based was demonstrated by Ruoff in 2006 [32]

The method aimed at oxidation of graphite to produce intermediary Graphite Oxide. After oxidation by Hummers method, epoxide, hydroxide functionalities are introduced into the basal planes of graphite structure [42]. Strong interactions in the form of Hydrogen bonding occur with water and oxygen containing groups so that it can easily intercalate between sheets. Thus, the hydrophobic starting material of graphite is transformed to Graphite Oxide with excellent hydrophilicity and dispersability.

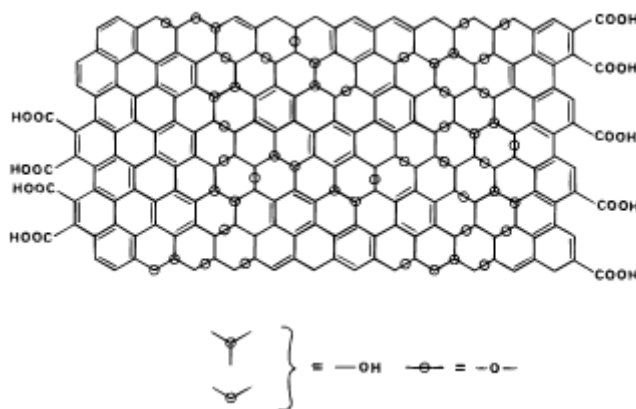


Figure 1.12 : Structure of Graphite Oxide proposed by Lerf-Klinowski Model [43]

The graphite lattice structure is disrupted by the addition of water molecules in GO that are located between layers as reflected in increase of inter-layer spacing from 0.335 nm in Graphite to more than 0.625nm in Graphite Oxide [44].

Once the Graphite is oxidized to water soluble Graphite Oxide and ultrasonicated to form Graphene Oxide, the aqueous dispersion is ultimately reduced to Reduced Graphite Oxide or exfoliated Graphene sheets. The graphene network is substantially restored from nonconducting GO through one of the following general methods; Chemical reduction using reducing agents such as Hydrazine Hydrate ($N_2H_4.H_2O$) [31], Hydroquinone [45], Sodium Borohydride ($NaBH_4$) [46], UV-assisted photocatalytic reduction [47] or high temperature annealing [48].

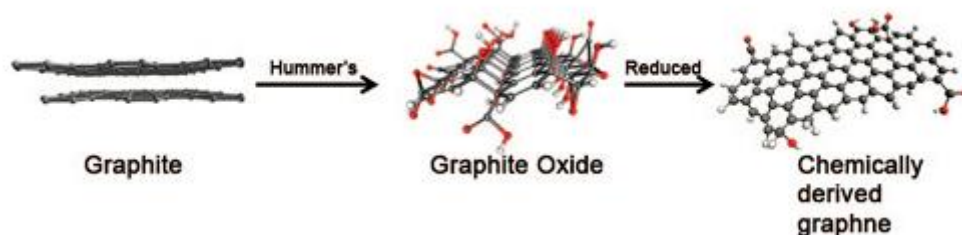


Figure 1.13 : Molecular model displaying the pathway for Graphene production; Graphite is oxidized to GO and reduced to Graphene [46]

The layers of graphene produced from these methods should be well separated from each other with the aid of appropriate solvents, otherwise graphene tends to form agglomerates and restack to form graphite through establishing Van der Waals interactions. Prevention of restacking is necessary for graphene sheets due to the fact that most of the unique properties of graphene are only associated with few layer sheets. In the case of using artificial graphite, flake graphite powder and natural flake graphite as the starting material, more than 80% of the final product has been determined to be single, double, triple and at least few-layer graphene (4-10 layers) [34] .

Many of the reduction methods include the use of hazardous chemicals that are harmful to environment such as Hydrazine Hydrate, Sodium Borohydride ($NaBH_4$) and cause the evolution of toxic gases including NO_2 and Cl_2 , respectively. Therefore, there is a search for more “green” and environmental-friendly reducing agents for the reduction process.

For this purpose, several environmental friendly methods have been probed for reduction such as use of antioxidants, Vitamin C [49], green tea polyphenols [50], aqua [51], sunlight and even *E. Coli* bacteria [52].

In a recent article, Graphene Oxide nanoribbons are prepared from CNTs using KMnO_4 , H_2SO_4 while the addition of H_3PO_4 to the reaction mixture is shown to aid in producing GO with more intact graphitic basal planes, more regular structure and higher yields. Moreover, evolution of toxic gases NO_2 and Cl_2 is prevented since NaNO_2 or ClO_2 is not used at all [53]

In summary, reduction of GO as the production method has a range of benefits. The advantages include the inexpensive starting material graphite, relative simplicity, reliability of the method and its suitability to large-scale production, all of which can not be offered simultaneously by any other method for the time being. An environmental friendly reduction process is therefore an added value to all these mentioned advantages of the reduction pathway.

1.4 Characterization of Graphene

The experimental discovery of Graphene necessitates the characterization of the layers, since some of interesting properties of graphene are dependent on thickness of layers.

Characterization is performed with adoption of various techniques including Optical Microscopy, Atomic Force Microscopy (AFM), Transmission Electron Microscopy (TEM), Scanning Tunnel Microscopy (STM), Scanning Electron Microscopy (SEM), X-Ray Diffraction (XRD) and Raman Spectroscopy.

In an effort to identify the number of layers of graphene, optical imaging such as contrast spectroscopy has been utilized. Mono- and few layer graphene is barely visible by optical microscopy but once deposited on a Si wafer coated with a specifically determined SiO_2 oxide layer thickness of 300 nm, every single layer adds to the optical path of reflected light, thereby changing the interference color with respect to the empty substrate and allowing a route for detection.

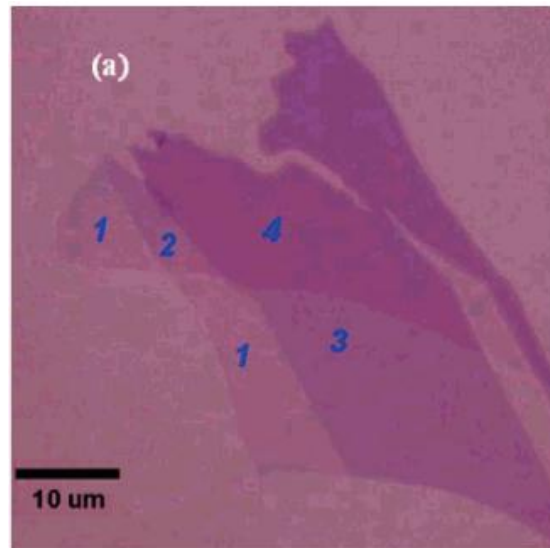


Figure 1.14 : Optical Image of mono-,bi-, tri- and tetra-layer graphene on SiO₂/Si substrate [54]

Optical microscopy is nevertheless a slow and cumbersome method for the barely visible graphene layers. Having deposited layers on a Si wafer, the 0.34nm step height for each successive layer is a basis for determination, albeit at a very slow pace. This observed change allows the detection and identification of the number of graphene layers by AFM [54]. Mechanical, frictional, electrical, magnetic and elastic properties of graphene flakes are measured by different AFM modes.

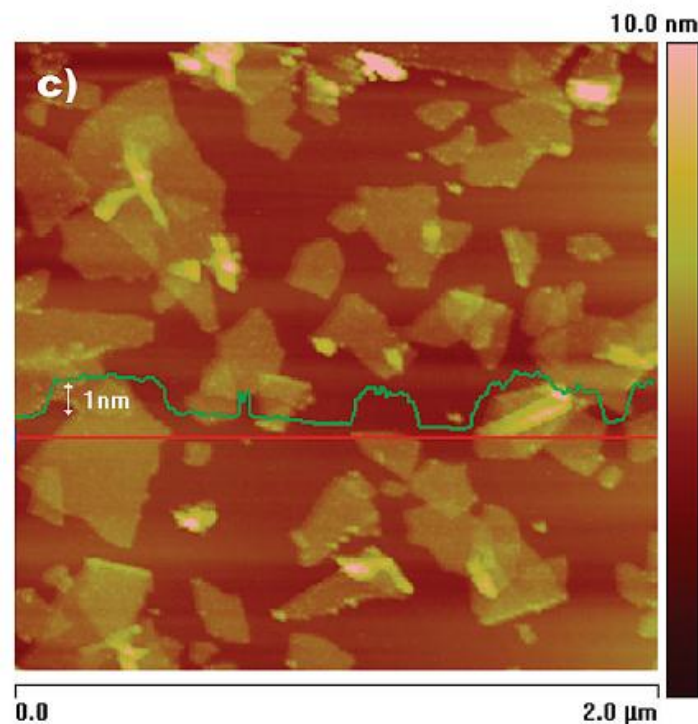


Figure 1.15 : AFM Image of RGO on HOPG surface with line profile (red line) [55]

STM [56] and TEM [57] images have been employed in the determination of morphology and structure of graphene. Each carbon of the hexagon is visible by STM as a consequence of electron density of π bonding (See Figure below)

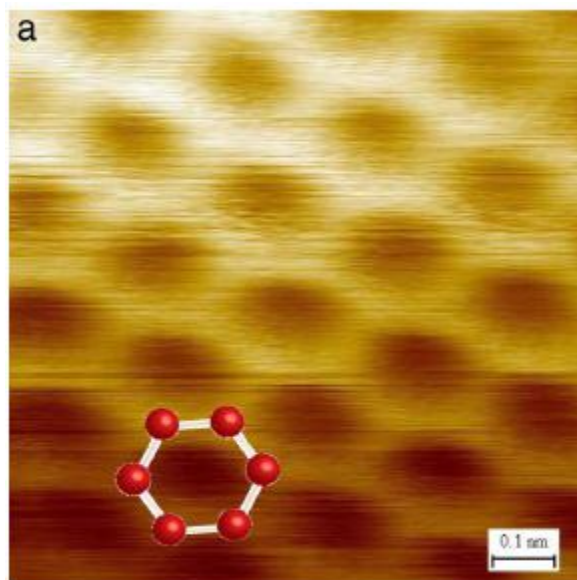


Figure 1.16 : High Res. STM Image displaying the honeycomb network of single layer graphene [56]

As a Carbon allotrope, graphene can be effectively characterized by Raman Spectroscopy. A wide range of information including number of layers, type of doping, doping concentration, effect of temperature and presence of defects can be identified from Raman spectrum. This information can be obtained as changes in the electronic band disrupt the structure of carbon hexagon. The fingerprint data of Graphene has D, G and 2D peaks around 1350cm^{-1} , 1580cm^{-1} and 2700cm^{-1} respectively.

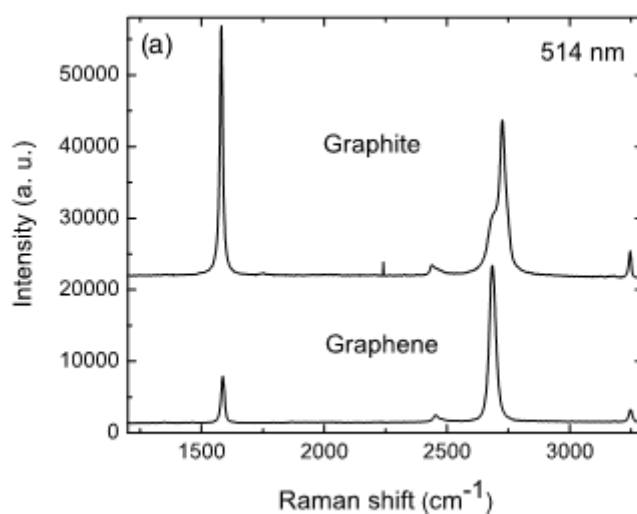


Figure 1.17 : Raman Spectra of bulk graphite and graphene at 514nm [58]

1.5 Properties and Applications of Graphite

Since Middle Ages, graphite has been used as a writing instrument due to its layered structure and weak Van der Waals forces between the adjacent sheets. With little change, graphite is still used in pencils today. As of 2011, about 4% of the total annual production of graphite is used to make pencils.

As a result of its layered structure, graphite has anisotropic material properties like electrical conductivity and modulus of elasticity [12]. The weak van der Waals interaction holding the planes of graphene within the graphite structure is the reason why sheets are easily shifted in parallel against each other. This structure have also made graphite an optimal material for use as a dry lubricant.

Electrical conductivity of in-plane graphite is remarkably high ($\sim 104\Omega^{-1}\text{cm}^{-1}$) as well as its thermal conductivity ($\sim 3000\text{ W/mK}$) make it an ideal material for use in electrodes and heating elements for blast furnaces [20].

The hexagonal network with its high mechanical stiffness (1060 GPa) has also found application in carbon fiber reinforced composites. These uses and others generate an annual demand of more than 1 million tons of graphite worldwide. [21]

1.5.1 Properties and Applications of Graphene

The novel graphene is a surprising material, with extraordinary electrical, mechanical [59] and thermal properties due to the strong sp^2 bonding between C atoms in C_6 hexagons, Π -Conjugation and delocalization of electrons that flow freely over the graphene planes.

Among its fascinating properties, graphene has a large theoretical surface area ($2630\text{m}^2\text{g}^{-1}$) [60] more than any porous material, including finely divided activated carbon favored in water purification for its high surface area. Furthermore, high intrinsic mobility ($200\ 000\text{cm}^2$) [61], high Young's modulus (1.0 TPa), excellent thermal ($5000\text{Wm}^{-1}\text{K}^{-1}$) and electrical conductivity along with the remarkable optical transmittance (97.7%) deem it a suitable material for transparent conductive electrodes.

In fact, optical absorbance of single layer graphene has been measured to be only 2.3% [62], deeming it transparent and hardly visible to naked human eye (*See Figure 8*). Graphene promises applications in various fields such as optically transparent conductive films, lithium-ion batteries, photo voltaic cells, supercapacitors and field effect transistors.

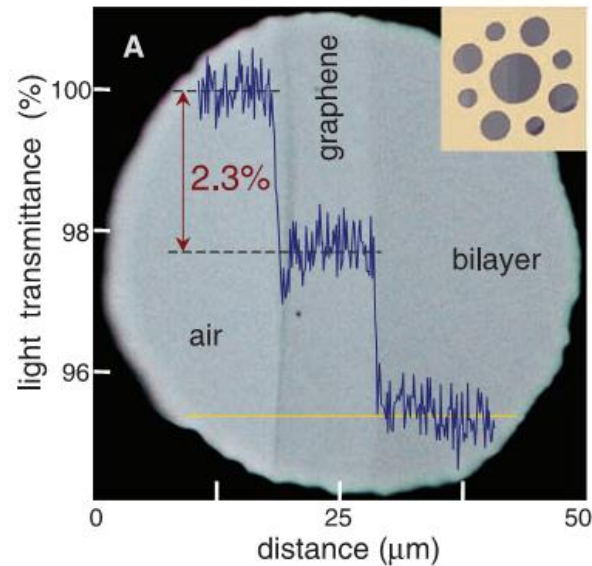


Figure 1.18 : Single layer graphene has an optical absorbance of 2.3% per layer [62]

Mechanical

Initial investigations on mechanical properties of monolayer graphene include the Young's Modulus and fracture strength measurements by numerical simulations like molecular Dynamics [63, 64]. Experimental results are determined with force-displacement measurements of micromechanically exfoliated graphene layers suspended over trenches by Atomic Force Microscopy (AFM) [65].

Experimental measurements on mechanical properties of defect-free monolayer graphene indicate that it exhibits a breaking strength of $\sim 40\text{N/m}$, approaching the theoretical limit. As the thinnest material known in the universe, single graphene sheets yield Young's Modulus of 1.0 TPa and fracture strength at 130 GPa, both of which are record high values for the time being [59].

Moreover, its mechanical properties are suited for Nanoelectromechanical (NEMS) applications [66], transparent, conductive electrodes as well as composites [67, 68]

Thermal

Thermal conductivity (κ) of a material depends on its lattice vibrations, the phonons. Due to its well-ordered 2D crystal lattice structure, graphene offers tremendous thermal conductivity.

A suspended monolayer graphene sheet obtained by micromechanical exfoliation exhibits a record thermal conductivity of ~ 5000 W/mK at Room temperature [69]. This value is much higher than that of graphitic carbon [69, 70] and all other carbon allotropes.

Therefore, it is a strong candidate to enhance the heat transport of various composites and polymer matrices, which may find applications in electronic circuit boards, heat sinks and lightweight thermal management systems.

For improvement of thermal properties, different polymer matrices such as PVC, Polyethylene and epoxy are used. Addition of 1wt % CNT with Graphite Nano platelets in epoxy matrix with a ratio of 1:9 has increased thermal conductivity by 147% [71].

Electrical

Graphene sheets possess extraordinary electronic properties like unusual electrical conductivity, higher current density than those of conventional conductor like copper, ambipolar field effect, high charge transport mobility [3]. The unusual electronic properties of graphene layers arise due to the high quality of its 2D crystal lattice.

Single layer graphene is a zero band gap semiconductor, so the highest occupied molecular orbital (HOMO) touches the lowest unoccupied molecular orbital (LUMO) at a Dirac point [21]. However, this is valid for few layers, as stacking of multiple layers lead to overlap of carrier wave functions and cause metallic behaviour.

The high electronic quality of graphene sheets and the ambipolar electric field effect provides the ability to tune charge carriers between electrons and holes. Quantum Hall Effect observed at ambient temperature [24] and massless electrons with high charge transport mobilities makes graphene a sought-after material in the field of electronics.

As the Si-based devices in semiconductor technology reach their bandwidth limits due to material and fabrication restrictions, graphene would expand the boundaries of the current

technology in the field of electronics [1]. The “graphenium inside” electronics might replace the existing Si based technology in the near future.

High electron mobility and near Ballistic carrier transport make graphene a potential material for high frequency applications in nanoelectronics. Recently, a graphene transistor is measured to reach a cutoff frequency f_T of 26 GHz [72]. Moreover, its electrical properties are suited for MEMS applications, thin-film transistors, transparent and conductive electrodes and photonics [73].

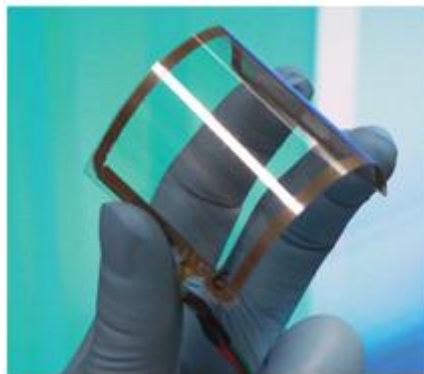


Figure 1.19 : An assembled Graphene layer over PET membrane with outstanding flexibility [74]

Graphene sheets' high transparency (97.7%), high conductivity, along with its flexible nature deem it a promising material for organic electronic and optoelectronic applications. Currently, indium tin oxide (ITO) is widely adopted as transparent, conductive electrode, yet it is expensive and offers limited mechanical flexibility. On the other hand, Graphene from GO is water soluble, easy to process with low temperature and high throughput production while being relatively inexpensive.

Graphene and GO has also found use in the production of hybrid composites by reinforcement of different polymer matrices. A range of exciting results are obtained, such as improvement of electrical and thermal conductivity (at low percolation), increase in strength and elastic modulus as well as reduced permeation of gas molecules. These properties might provide use as electrically conducting polymer [32] and packaging material for food, medicine [33] .

For instance, graphene and poly (3,4-ethyldioxythiophene) (PEDOT) composite films provide extraordinary transparency, flexibility, conductivity and thermal stability. Therefore,

it might be a promising material for future touch screens, video displays, and plastic solar cells [75]. The combination of these properties open new avenues for utilization of graphene in developing low weight – high strength polymer composites for automobile and aerospace industry.

Nevertheless, the wide range of application fields for graphene has not reached its maturity yet . Due to challenges in mass production of high quality graphene at a low cost, the explorations have not been commercialized yet . Therefore, the research has been focused more on development of viable, efficient routes for graphene production.

Moreover, Graphane is a two dimensional material that holds potential applications as a hydrogen storage material [76] Graphene nano sheets might have potential applications in electronic devices [77], biosensors and catalyst supports for energy storage materials [78].

1.6 General Aspects of Microwave Radiation

Microwave is a form of electromagnetic radiation with wavelengths in the range of 1mm – 1m and frequencies in the range of 300 MHz - 300 GHz. The prefix “micro” in microwave refers to its comparative shortness in comparison to typical radio waves and does not literally mean micrometer wavelengths.

Microwaves are generated by using magnetrons as generation source. The ballistic motion of electrons inside a vacuum tube under the influence of electric or magnetic field has been adopted for the creation of microwaves.

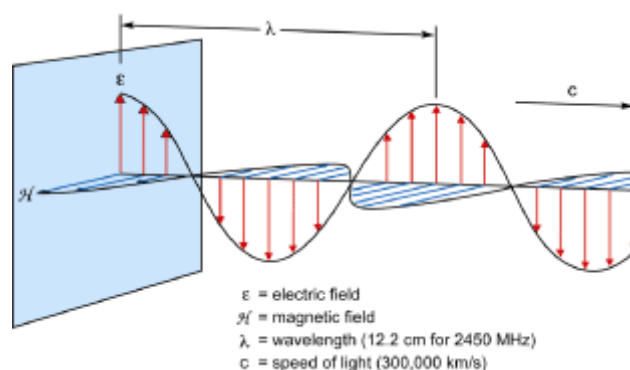


Figure 1.20 : Components of a Microwave

Microwave radiation is used as a rapid, versatile and inexpensive technique to heat species to high temperatures in relatively short times. This is accomplished through transfer of energy selectively to microwave absorbing polar solvents which have dipole moments other than zero.

Microwave Chemistry deals with implementing efficient dielectric heating mechanisms to heat reaction solutions directly, as opposed to conventional heating methods that heat the reaction vessel via conduction. Typically, Microwave chemistry is conducted in a sealed vessel under strictly controlled reaction conditions of temperature and pressure. By means of this mechanism, the reaction mixture can be superheated to temperatures high above the boiling point of the solvent in the system. The result is the dramatic enhancements in reaction rate.

According to Arrhenius equation (See Figure 8), there is a direct relationship between temperature and reaction speed. In Arrhenius equation, number of collisions that result in a reaction is denoted with k , total number of collisions with A , probability that any given collision will result in a reaction with $e^{-E_a/RT}$. It is seen that either decreasing the activation energy or increasing the temperature will result in an acceleration in the rate of reaction. T_i is the Instantaneous Temperature achieved with Microwave in opposition to T_b bulk temperature achieved with conduction.

$$k = Ae^{-E_a/RT}$$

Equation 1 : Arrhenius equation

In terms of microwave chemistry, instead of using glass beakers, sealed vessels are placed under microwave conditions. By means of enhanced reaction rates, it is shown that the reaction times are reduced from many hours down to few minutes, while improving product purity and reaction selectivity.

Scientists working with hydrothermal synthesis methods are used to high temperatures and long reaction times, some of which might take up to weeks. The aim is to produce high quality crystals slowly and thoroughly. However, same crystals can be formed in minutes with Microwave Assistance, at lower temperature due to uniform heating . Thus, Microwave Chemistry was selected as an outstanding candidate for the Reduction of GO.

Microwave irradiation transfers energy selectively to microwave absorbing polar solvents causing temperature increase in short durations along with self-generated pressure inside reaction vessels. Microwave accelerated synthesis offers an efficient, time-saving, cost-effective production method that is implemented by diverse fields.

In an effort to utilize Microwave Irradiation, Li et al has implemented a fast (<5 sec), dry synthesis of graphene using a commercial microwave oven [79]. Murugan et al employed a facile, solvothermal method for reduction of GO by using different solvents at relatively low temperatures (180-300°C) under microwave assistance[78].

Adoption of microwave chemistry in the production of graphene apparently holds a range of benefits. However, there has been only a small scope of research and inadequate advances in the field. The Research conducted in this MSc. Thesis focuses on implementation of a fast, facile and green method for Reduction of GO under the assistance of microwave irradiation by using non-toxic solvents. The details of the procedures are further explained in the following section; Chapter 2.1 Experimental Methods.

Chapter II : EXPERIMENTAL PROCEDURE

2.1 Experimental Materials

The educts used during the experiments conducted in this thesis include solid materials, acids and organic solvents, including Graphite electrode, Highly Oriented Pure Graphite (HOPG) and KMnO_4 .

Acids are specified as following; H_3PO_4 (Phosphoric acid, Purity %85, Merck KGaA), H_2SO_4 (Sulfuric acid, concentrated, Purity %95-98, $d=1,84\text{g}/\text{cm}^3$, $M=98,08\text{g}/\text{mol}$, Merck KGaA) and HNO_3 (Nitric acid, extra pure, purity %65) are used as received.

Solvents such as Tetra ethylene Glycol (TEG, $\text{C}_8\text{H}_{18}\text{O}_5$, for synthesis, Assay>%93, Density= $1.21\text{g}/\text{cm}^3$, Merck), N,N-Dimethyl Formamide(DMF, Purity<%99.8, Merck), Hydrogen Peroxide (H_2O_2 , %30), and distilled water($18.2\text{ M}\Omega\text{ cm}^{-1}$) have been used

2.2 Experimental Methodology

Although a variety of methods yield perfect crystals of graphene, they are rather inconvenient, slow and small-scale. Reduction of Graphite Oxide to Exfoliated Graphene sheets is considered widely as the most promising approach for large-scale production [31]. Furthermore, the knowledge that using the starting materials of artificial graphite, flake graphite powder or natural flake graphite results in obtaining more than 80% of the final product as single, double, triple and at least few-layer graphene (4-10 layers) [34]

For all these reasons, Reduction of Graphite Oxide has been implemented for the production of high quality graphene sheets with few layers in this MSc. thesis.

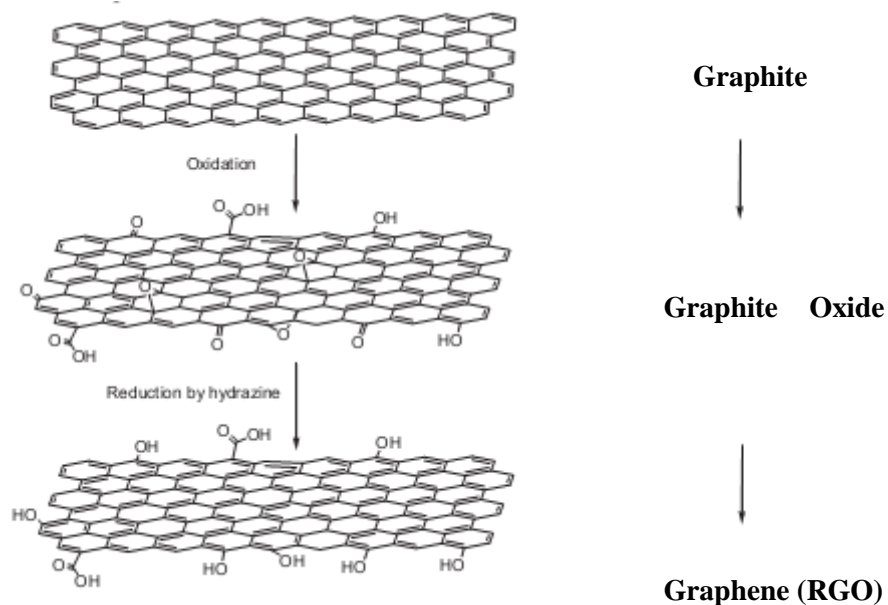


Figure 2.1 : Molecular model representing the pathway for Graphene production

The production of high quality few layer graphene sheets involves the following two key steps;

1) Oxidation of Graphite.

Substantial oxidation is necessary so that most of the graphite structure can be transformed to soluble GO and exfoliated.

2) Reduction of Graphite Oxide

Exfoliated GO or Graphene is produced. Oxygen containing epoxide, hydroxide groups should be reduced as much as possible to obtain pristine graphene

2.2.1 Synthesis of Graphite Oxide

Graphene layers are conventionally and most commonly produced by Hummer's method. . Though Hummers' method is the most common route for the production of GO, Graphite is oxidized by utilizing powerful oxidizing agents including H_2SO_4 , KMnO_4 and NaNO_3 that result in generation of NO_2 , N_2O_4 gases.

Initially, Graphite Oxide is produced with Hummers' method. Concentrated H_2SO_4 (11.5mL) is added to graphite flake (0.5g) and NaNO_3 (0.25g) with mild stirring at 300 rpm in an ice bath ($T = 0^\circ\text{C}$). 1.5g of KMnO_4 is added portionwise to this mixture in an effort to keep the reaction temperature below 20°C . The reaction is heated to 35°C and stirred for 1h. After cooling to Room Temperature, distilled water (23mL) is added slowly, forming an exotherm as Temperature goes up to 98°C . The solution is heated at 50°C for 1h and additional 70 mL distilled water is added. The solution is centrifuged at 8000 rpm for 1h with 200 ml of distilled water and then with 200 ml of 10% HCl solution to reduce the remnant materials. Finally, 4 ml of 30% H_2O_2 is added to this solution causing effervescence and color change from brown to yellow.

An innovative method is recently used to produce Carbon Nano tubes and graphene successfully. Inspired by this, Graphene is produced by utilizing an improved method which excludes the use of NaNO_3 , increases the amount of KMnO_4 and uses a mixture of $\text{H}_2\text{SO}_4/\text{H}_3\text{PO}_4$ to improve the efficiency of Oxidation.

In the Enhanced Method, 9:1 mixture of concentrated $\text{H}_2\text{SO}_4/\text{H}_3\text{PO}_4$ (60:7ml) is added to graphite flake (0.5g) and KMnO_4 (3.0 g) under mild stirring at 300 rpm. A green-black solution is obtained. An exothermic reaction occurs during addition of KMnO_4 but the temperature is kept below 40°C by using an ice-water bath. The reaction is then heated under stirring at 50°C for 12h. After 2h, color of the solution slowly transforms to brown.

After cooling to room temperature, 60 ml of ice-cold distilled water is poured onto the viscous solution while the solution is kept in ice-water bath. Distilled water is added in portions to keep the temperature under control. Addition of water changes the solution to a dark violet color due to strong coloring that arise from KMnO_4 .

For purification, a multiple-wash process with three step centrifugation is utilized. Firstly, the resulting solution is centrifuged at 8000 rpm for 1h with 200 ml of distilled water. After centrifugation, violet color supernatant is decanted away. A light brown, water dispersable solution of Graphite Oxide is obtained. 4 ml of 30% H_2O_2 is added to this solution causing effervescence. Secondly, the solution is washed with 200 ml of 10% HCl solution and centrifuged at 8000 rpm for 1h. The aim is to reduce the remnant metal and K-containing materials. The supernatant is decanted away while the centrifugate is collected. Finally, it is dispersed in 50 ml ethanol and centrifuged at 8000 rpm for 1h.



Figure 2.2 : Millipore Membrane Filter; 100 pack filter (left), Type GS(right)

The material produced after this multiple phase purification is filtered through a commercial membrane filter. The Millipore brand membrane filter is comprised of hydrophilic, mixed cellulose esters, which have 0.22 μm pore size ($\phi=47\text{mm}$). The filtering of the suspension is conducted under vacuum assistance at Room Temperature.

During the filtration of suspension through the ester membrane, the liquid water can pass through the pores, whereas the accumulated GO sheets stay on the membrane. Permeation of solvent is dependent on the amount of GO sheets at a particular location. Therefore, rate of filtration decreases on sites with more sheets, but less affected on uncovered regions.

So, the process is self-regulating and allows for reasonable control over film thickness by altering either the concentration of GO in the suspension or the volume of the suspension

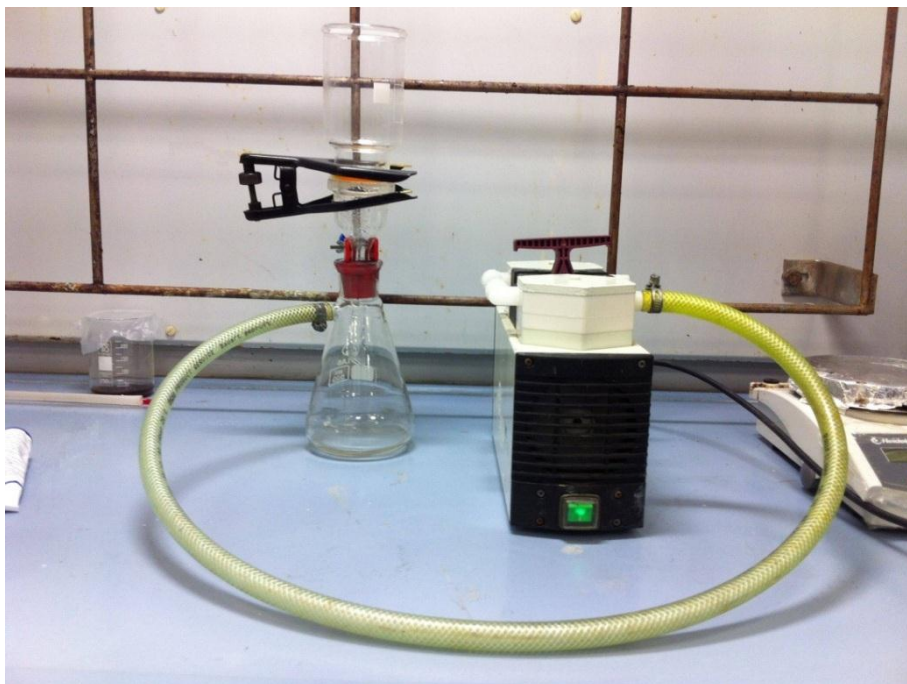


Figure 2.3 : Vacuum Assisted Membrane Filtration Setup

2.2.2 Reduction of Graphite Oxide

Reduction of Graphite Oxide is performed by using the following solvents; water(H_2O), N,N - Dimethyl Formamide (DMF) and Tetraethylene Glycol (TEG). Appropriate solvent for Reduction of GO is predicted based on dispersability of GO and RGO solutions according to Hansen solubility parameters. 9 mL of organic solvents are added 1 mL of H_2O to produce a 9:1 aqueous GO suspension. The dispersability of the selected set of solvents is displayed in Chapter III: Results.

30 mg of the as-prepared GO was placed in 100 mL of solvent (Water, DMF, TEG) to obtain a suspension (0.3 mg/mL) that is sonicated for 1h to exfoliate Graphite Oxide into Graphene Oxide. The solution is then heated under Microwave Irradiation for 1 h at the following $T = 120^\circ C$. The resulting black suspension is further sonicated in ultrasonication bath for 1h and then filtered to eliminate the remaining solvent.

2.3 Characterization Methods/Instruments

A range of different material characterization techniques/instruments are utilized during measurements; which include Microwave Irradiation, X-Ray Diffraction(XRD), Infrared Spectroscopy (FT-IR), Differential Thermometry – Thermal Gravimetry Analysis (TG/DTA), Optical Microscopy (OM), Field Emission Scanning Electron Microscopy (FESEM) and Rheometry. The settings adjusted for each individual instrument is specified in the present section.

2.3.1 Microwave Radiation System

Microwave Heating is performed by CEM MarsXpress Microwave Irradiation oven operating at a power range of 0-1600W and microwave frequency of 2450 MHz. Microwave Power is selected as 800W, 1600W. 55 mL Teflon vessels are used as sample holders. Temperature is measured and recorded with the in-built IR thermometer.

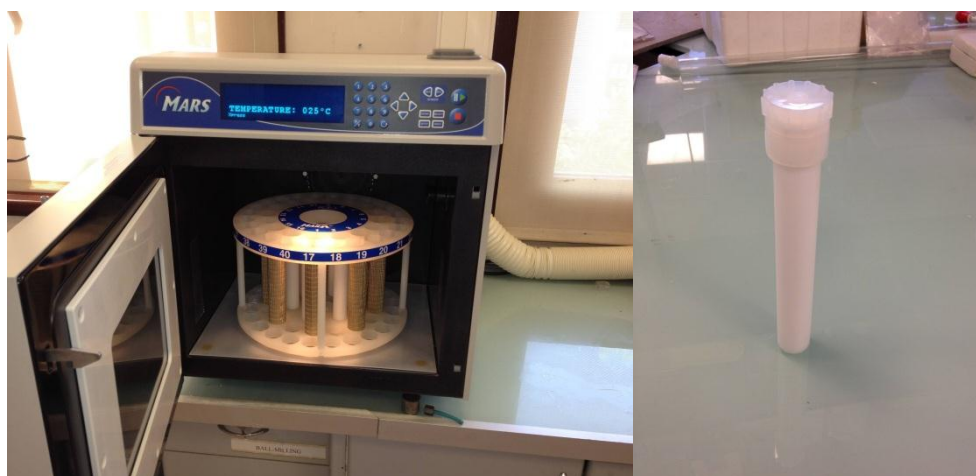


Figure 2.4 : CEM MarsXpress Microwave Radiation System

2.3.2 X- Ray Diffraction

X-ray diffraction (XRD) measurements are performed by two types of different X Ray Diffraction tools; firstly by a Huber G670 diffractometer utilizing a Germanium monochromator and Cu-K α radiation ($\lambda = 1.5406 \text{ \AA}$). Data is collected in the range of $5^\circ < 2\theta < 100^\circ$ with increments of 0.005° . Data analysis and manipulation is conducted with STOE WinXPOW Software [80].

Secondly, desktop type Bruker D2 Phaser X-Ray Powder Diffractometer is utilized, which operates at 30kV and 10mA. Workflow software DIFFRAC.SUITE is adopted for data collection/manipulation. Recorded data is collected in the range of $5^\circ < 2\theta < 80^\circ$ while scan time is adjusted to 1800s for each run.



Figure 2.5 : X-Ray Diffraction Spectrometers. Huber G670(left), Bruker D2 Phaser (right)

2.3.3 Fourier Transform - Infrared Spectroscopy

Fourier Transform – Attenuated Infrared Spectroscopy measurements are conducted with Thermo Scientific Inc. Nicolet iS10 FT-IR Spectrometer. It has a DTGS KBr detector, Diamond sample window and KBr Beamsplitter. Data is collected with built-in software OMNIC Version 8.0.342. Number of Scans is 64 for each individual run. The wavelength range of the spectrometer is between $525\text{cm}^{-1} - 4000\text{cm}^{-1}$ and the recorded spectra in the Results section has the wavelength range of $600\text{cm}^{-1} - 4000\text{cm}^{-1}$.



Figure 2.6 : Thermo Fisher Inc. Nicolet iS10 FT-IR Spectrometer

2.3.4 Raman Microscope

Raman measurements are performed with Renishaw inVia 1000 dispersive Raman microscope with an excitation wavelength of 514 nm. Laser Power is selected as %5 to prevent saturation and acquisition time is 10 sec/scan. All sample were deposited on Si/SiO₂ wafers from their corresponding solutions by dropcasting. Images of the scanned areas were also recorded and displayed.



Figure 2.7 : Renishaw inVia Raman Microscope

2.3.5 Thermo Gravimetric / Differential Thermal Analysis

The Thermo-gravimetric/Differential Thermal Analysis (TG/DTA) is performed using a SII TG/DTA 6300 thermal analyzer under the flow of Ar gas (5 sccm). The samples were heated up to 1200°C at a rate of 5 °C/min in Al₂O₃ holders for each individual run.



Figure 2.8 : Thermo Gravimetric/Differential Thermal Analyzer

Optical Microscopy

Nikon Eclipse Ti inverted microscope is utilized for imaging GO and RGO sheets. It uses a mercury arc lamp for the illumination of the sample and can perform 500X-10.000X Magnifications for an illuminated sample.

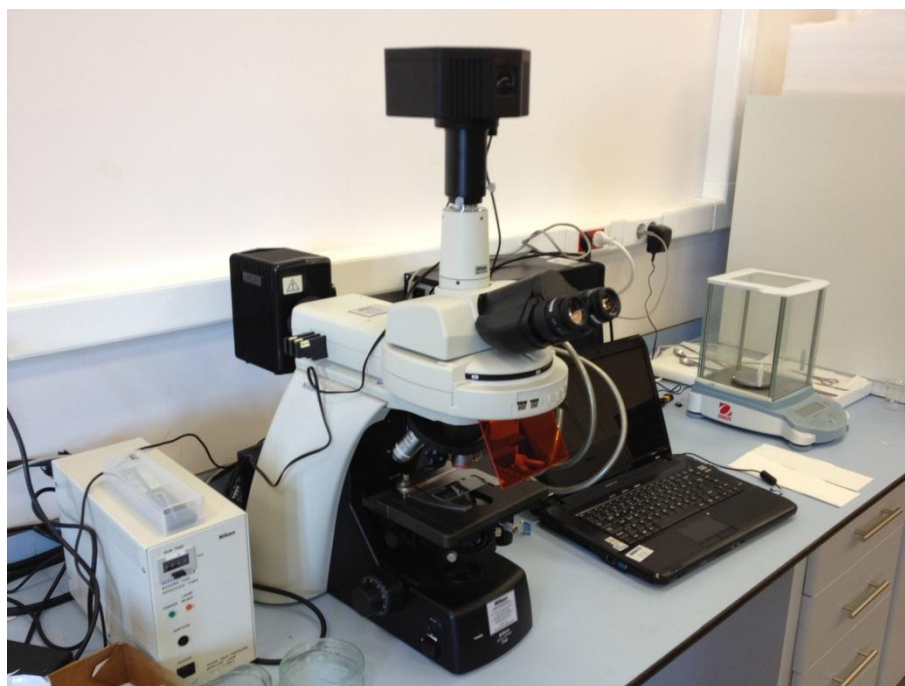


Figure 2.9 : Nikon Eclipse Ti Optical Microscope

2.3.7 Field Emission Scanning Electron Microscopy (FESEM)

The Field Emission Scanning electron Microscopy (FESEM) measurements were carried out in a Zeiss Evo Ultra Plus 40 SEM furnished with a LaB₆ electron source.

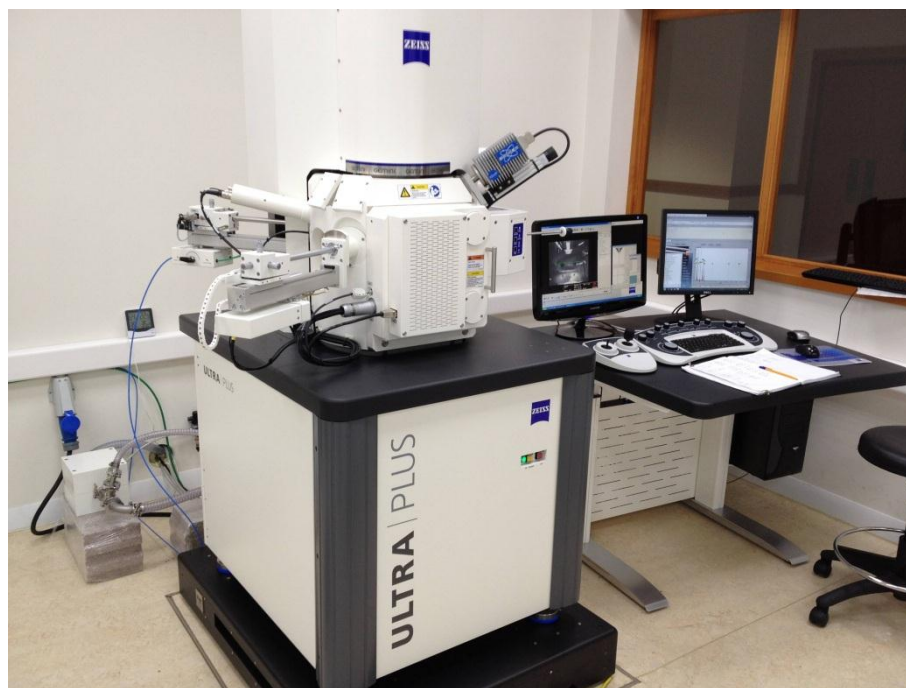


Figure 2.10 : Zeiss Evo Ultra Plus FE-SEM

2.3.8 Elemental Analyzer

Leco TCH 600 Elemental Analyzer is used to simultaneously determine O, N, and H content in Graphite Oxide and Reduced Graphite Oxide. It utilizes the inert gas fusion principle and Thermal Conductivity Difference between the carrier gas(He) and the analyte to detect the composition of the analyzed material. A weighed sample is placed in a high-purity graphite crucible, fused under a flowing He-gas stream (449 ccm) in a high temperature oven at T (2500°C) sufficient to release oxygen, nitrogen and hydrogen. Oxygen in the sample combines with the carbon from the crucible to form carbon monoxide. The nitrogen present in the sample releases as molecular nitrogen, and any hydrogen present is released as hydrogen gas.



Figure 2.11 : Leco Elemental Analyzer

2.3.9 X-Ray Photoelectron Spectroscopy

XPS spectra are recorded with Thermo Scientific K-Alpha spectrometer. Al-K α radiation is used as X-ray source and flood gun is turned on to avoid charging during the measurement. The pressure of the vacuum chamber changes between 10^{-7} to 10^{-8} Torr during the measurement. All of the spectra are corrected by using C1s binding energy 285 eV as the reference point.

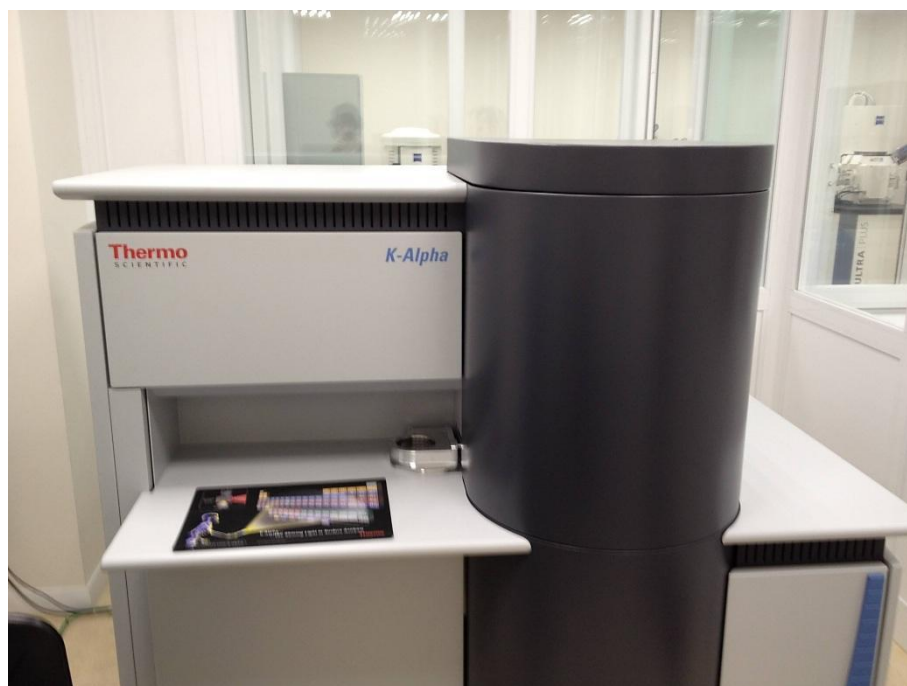


Figure 2.12 : Thermo K-Alpha X-Ray Photoelectron Spectrometer

2.3.10 Water Purification System

Elga Purelab Option Q Ultra Pure Type 1 Water Purification System is used for production of Distilled Water during experiments. DI Water with a quality of $18.2 \text{ M}\Omega\text{cm}^{-1}$, type I water suitable for sensitive applications is used.



Figure 2.13 : ELGA Purelab Option Q Water Purification System

Chapter III : RESULTS AND DISCUSSION

The motivation for this research is to produce few layer Graphene layers by a controlled, rapid, efficient and less toxic method than those reported in the literature. In order to achieve this goal, a two step pathway is implemented. In the first step, an improved method is employed for the synthesis of Graphite Oxide. Subsequently, Graphite Oxide is reduced in different solvents (TEG, DMF) in the absence of toxic reducing agents by Microwave heating only at moderate temperature (120°C).

Characterization of the products is performed with X-Ray Diffraction, FT-IR, Raman Spectroscopy, TG/DTA, Elemental Analysis, Optical Microscopy Imaging, XPS and FESEM.

Initially, a modified synthesis method was chosen for the preparation of Graphite Oxide which is based on Hummers' well-known route [31], involving the use of strong oxidizing agents such as KMnO_4 , NaNO_3 , H_2SO_4 and H_2O_2 that result in generation of NO_2 , N_2O_4 gases.

In a recent article on Graphene Oxide nanoribbons from CNT, a new preparation technique was introduced which results in more intact graphitic basal planes, more regular structure and higher yields [53]. Inspired from this idea, a 9:1 mixture of concentrated $\text{H}_2\text{SO}_4/\text{H}_3\text{PO}_4$ is used for the oxidation.

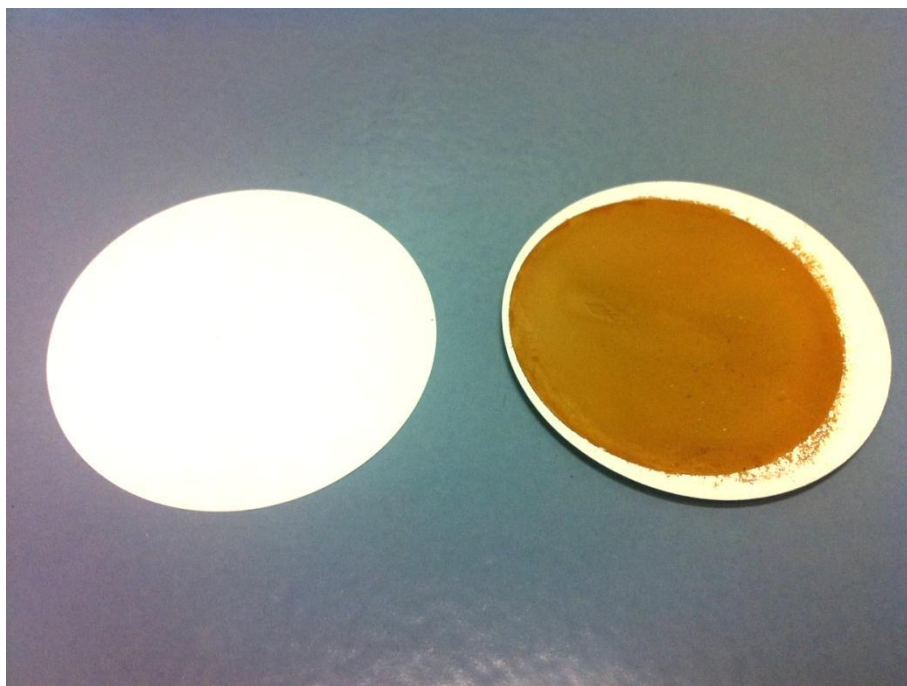


Figure 3.1 : Millipore Membrane Filter blank (left) and Graphite Oxide (right)

After Graphite flakes are oxidized to GO, a color change occurs from black to yellow-orange as shown in Figure 8. At low concentrations (0.3mg/mL), the GO suspension exhibits a light orange color that turns to dark orange brown as the concentration increases. The efficiency of Improved Method over Hummers' Method has already become obvious at the purification step. After Centrifugation, GO produced from the "Improved method" has a smoother appearance and gave a brighter orange color. Moreover, less hydrophobic graphitic flakes are left on the filter while more hydrophilic material is formed that easily dissolve. The "improved method" qualitatively provides a greater amount of hydrophilic oxidized graphite material relative to the Hummer's procedure.

Secondly, Graphite Oxide is reduced in selected solvents (TEG, DMF) under Microwave irradiation at 120°C. After reduction, a substantial color change occurs from orange to black. The black color of the Reduced Graphite oxide observed by visual inspection is considered as a pristine proof of the restoration of the graphitic network [32]. The color change results from the increase of GO absorbance. Graphene framework is reformed as functional groups are eliminated, while π -conjugation is restored that causes the graphene to absorb in the visible light region. Nevertheless, the graphitic structure is not completely restored under conditions, and significant defects are introduced [53]



Figure 3.2 : Graphite Oxide (left) in comparison with reduced GO (right)

3.1 Microwave Solvothermal Approach

Microwave Irradiation is utilized to study the possibility of Reduction of GO, as it offers advantages over solvothermal/hydrothermal methods. It does not require high temperatures, high pressure, while being facile, clean and easy to use with non-toxic reducing agents. GO is reduced to RGO with nontoxic solvents (TEG, DMF) within short reaction time of 30 min. at a relatively low temperature (120°C).

The MW pathway focuses on dielectric microwave heating of reactants by selective transfer of microwave energy to polar solvents, which in turn cause simultaneous increase in temperature and self-generated pressure inside the sealed reaction vessel. The reaction time for reduction of GO is decreased from several hours to minutes with cleanliness and savings in energy.

For dielectric microwave heating, an appropriate polar solvent is necessary. The criteria for the proper choice are explained in 3.2.

3.2 The Choice of an Appropriate Solvent

Dispersion of GO in a solvent is of importance, since the reduction of GO is a surface phenomenon which is usually carried out in a liquid phase. The solvent has a significant part in this, as it determines the extent of dispersion and the processability of GO and its derivatives. During the reduction of GO to RGO, however, surface functionality changes that leads to change in dispersibility. Yet a similar dispersion is desirable for both the precursor GO and the product RGO. So, it is deduced that an optimum solvent should be able to form a dispersion of GO as well as RGO.

As the dispersion is affected by the interaction between solvent molecules and GO and RGO, a series of factors such as polarity and solvent-GO interactions has influence on the success of the reduction [81].

Therefore, in MW process, an optimal solvent must meet the following criteria; it should be polar in order to absorb microwave irradiation to perform dielectric heating, be non-toxic, have a high boiling point to withstand local high temperatures in Microwave oven and have a low vapor pressure so as not to create extreme pressures within the vessel that might result in explosions. Last but not least, it should easily dissolve the precursor GO and also the product RGO.

For choice of a solvent, Hansen Solubility Parameters are utilized, which is a quantitative method for prediction of whether a material dissolves in a solvent [82, 83]. Solvents are classified according to their “dispersing power” and their effect on the solubility in the system. Each solvent is assigned with the three following Hansen parameters;

$$E = \Delta E_{vap} = E_D + E_P + E_H$$

$$E/V = E_D/V + E_P/V + E_H/V$$

$$\delta = \delta_D + \delta_P + \delta_H$$

Equation 3.1 : Hansen Solubility Parameters

In the Hansen Solubility equation (*Equation 3.1*), ΔE_{vap} stands for Cohesion Energy, while Solubility Parameters include δ_p , the polarity cohesion parameter represents the energy from dipolar intermolecular forces between molecules, δ_d is for dispersion cohesion parameter, the energy from dispersion forces between molecules and δ_h hydrogen bonding cohesion parameter.

The solubility of GO and RGO is tested in a series of solvents including acetone, ethanol, water, THF, DMF and NMP solutions. The ability of each solvent to form a stable dispersion, as well as δ_h , δ_d , δ_p and $\delta_p + \delta_h$ are displayed in Table 8;

Solvent	Dispersion (GO)	Dispersion (RGO)	δ_d	δ_p	δ_h	$\delta_p + \delta_h$
Acetone	√	√	15.5	10.4	7.0	17.4
Ethanol	√	√	15.8	8.8	19.4	28.2
DMF	√	√	17.4	13.7	11.3	25.0
TEG	√	√	16.0	10.3	16.4	26.7
Toluene	X	X	18.0	1.4	2.0	3.4
Water	√	X	15.5	16.0	42.3	58.3

Table 3.1 : Hansen Solubility Parameters of selected solvents[83]

From Hansen solubility coefficients, it can be deduced that solvents with high values for the sum $\delta_h + \delta_p$ (>13) produce a stable colloidal suspension of hydrophilic GO. Solvents with the sum $\delta_h + \delta_p >30$ (H_2O) or <13 (Toluene) only result in formation of agglomerates. Thus, solvents with $\delta_h + \delta_p$ sums in the range 13-30 result in stable, homogenous dispersions of GO and more importantly RGO as well. Although not every possible solvent is investigated, the Hansen solubility coefficients yield an effective pathway for the prediction of solvents with appropriate dispersion power for GO and RGO sheets.

Recently, a study is conducted to reduce GO with the solvent N,N-Dimethylacetamide (DMAc) under Microwave assistance [84]. In the present work solvents other than DMAc - which has a boiling point of $165^\circ C$ and high toxicity - were investigated. Among those, N,N-Dimethyl Formamide DMF/ H_2O (9:1) and TEG are specifically selected that conform to the required criteria for graphene solution as they prevent the agglomeration of graphene in the system. The Reduction of GO with DMF/ H_2O (9:1) is abbreviated as RGO-1, while that of TEG is RGO-2 for ease of following.

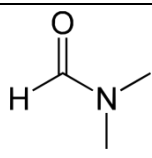
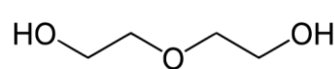
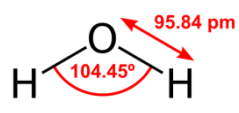
	DMF (N,NDimethylformamide)	TEG (Tetraethylene Glycol)	Water
Chemical Formula			
Mol. Formula	(CH ₃) ₂ NC(O)H	C ₄ H ₁₀ O ₃	H ₂ O
Boiling Point (°C)	153°C	244°C	100°C
Vapor Pressure (kPa, 25°C)	0.5 kPa	0.1 kPa	2.3kPa
Polarity	3.82 D	3.60 D	1.85 D

Table 3.2 : Comparison of selected solvents (DMF, TEG, Water)

As a result, the choice of the proper solvent offers the advantage of not using a stabilizer, surfactant or any other reducing agent for production of RGO sheets, which is otherwise not possible.

The series of reactions performed during the studies of the present MSc. Thesis are displayed in Table 2.3. which exhibits the processes and methods used for the Oxidation of Graphite (Hummer's and Improved Method), as well as those for the Reduction (Microwave assisted, solvents TEG, DMF).

Sample Name	Type of Process	Method	Chemical	Notes
AT002	Oxidation	Hummer's Method	KMnO ₄ , H ₂ SO ₄ , NaNO ₃ , H ₂ O ₂	
AT003	Reduction	Ultrasonication	Reducing agent : Hydrazine hydrate	
AT009	Oxidation	Hummer's Method	KMnO ₄ , H ₂ SO ₄ , NaNO ₃ , H ₂ O ₂	
AT035	Oxidation	Improved Method	KMnO ₄ , H ₂ SO ₄ /H ₃ PO ₄ , H ₂ O ₂	Starting material: Raw Graphite
AT037	Oxidation	Improved Method	H ₂ SO ₄ /H ₃ PO ₄	HOP-Graphite Abbreviation : GO
AT039	Reduction	Microwave Ass.	Solvent : H ₂ O	
AT043	Reduction	Microwave Ass.	Solvent : TEG/H ₂ O	Abbreviation : RGO-1
AT056	Reduction	Microwave Ass.	Solvent : DMF/H ₂ O	Abbreviation : RGO-2

Table 3.3 : Comparison of utilized Reaction parameters

3.3 Optical Microscopy Results

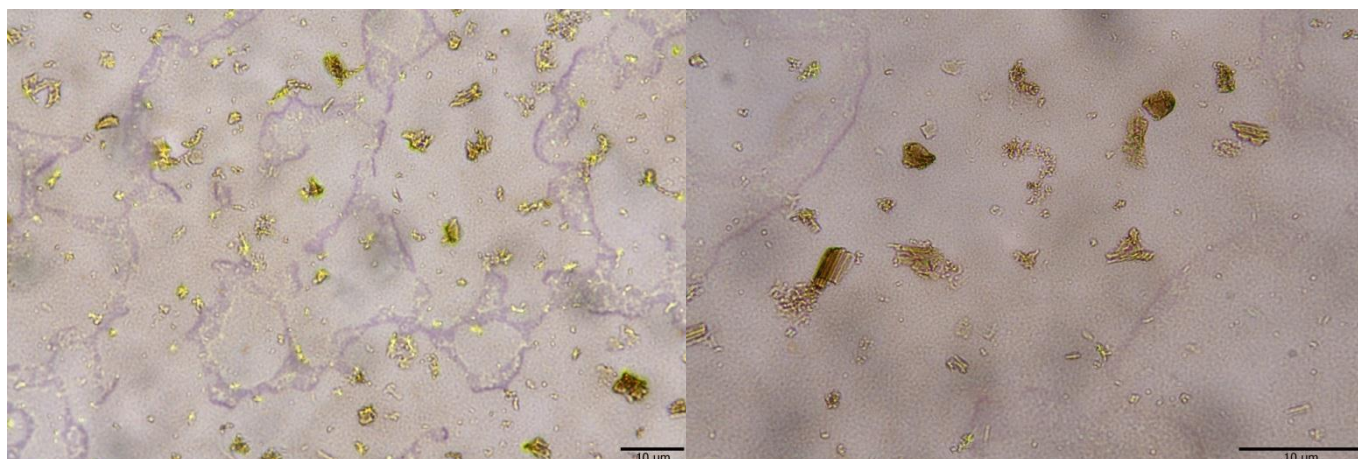


Figure 3.3 : Optical Microscopy Image of Graphene Oxide, Scale bar: 10 μ m, (left:100X Magnification, right:200X)

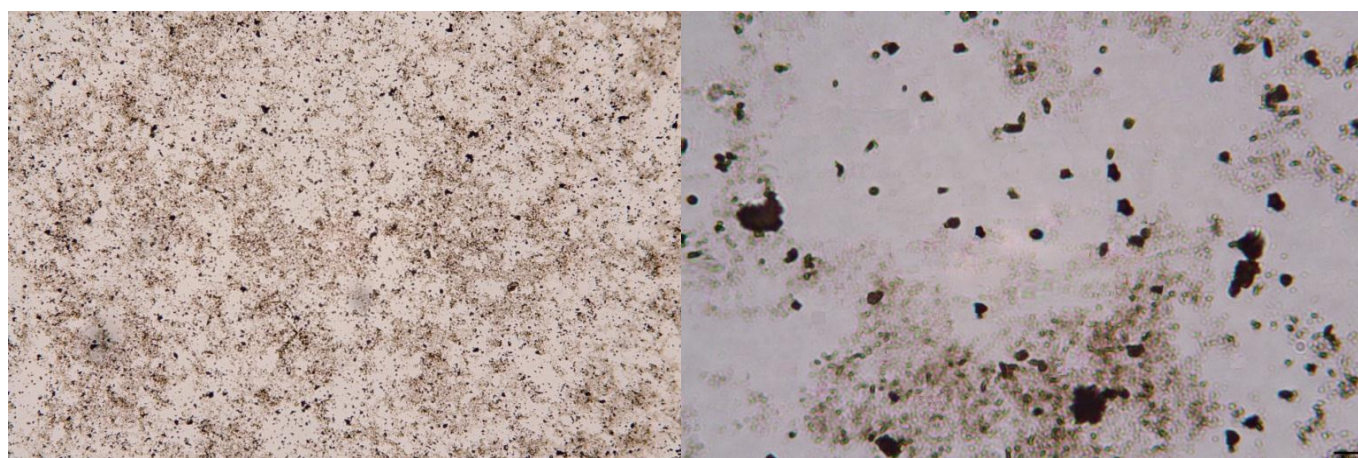


Figure 3.4 : Optical Microscopy Image of Graphene Oxide, (left:200X Magnification, Scale bar: 10 μ m, right: 1000X, Scale bar: 1 μ m)

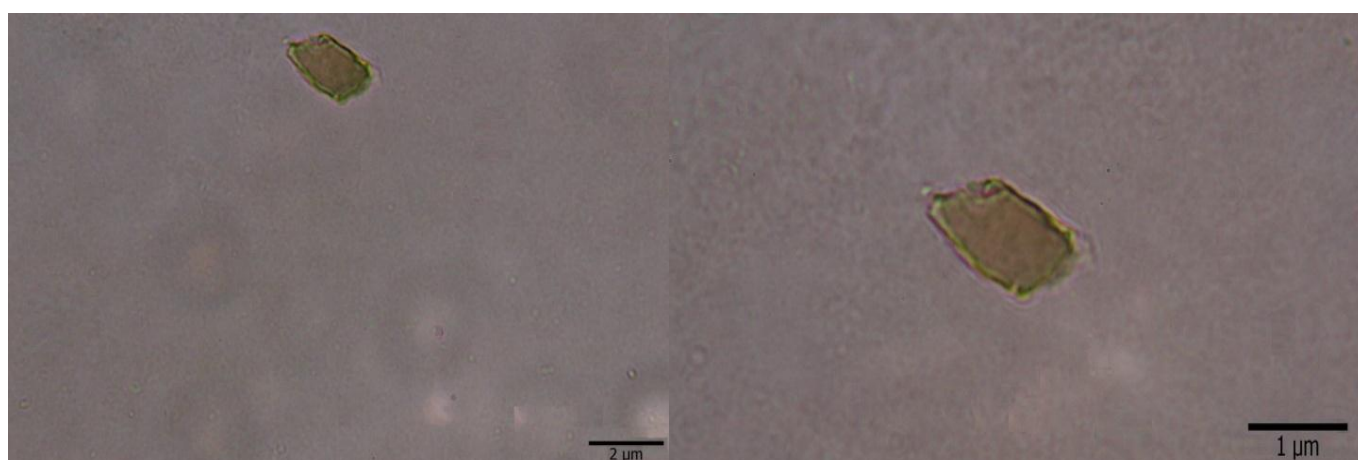


Figure 3.5 : Optical Microscopy Image of a Graphene Oxide sheet, 500X Magnification, Scale bar: 2 μ m(left), 1000X, Scale bar: 1 μ m(right)

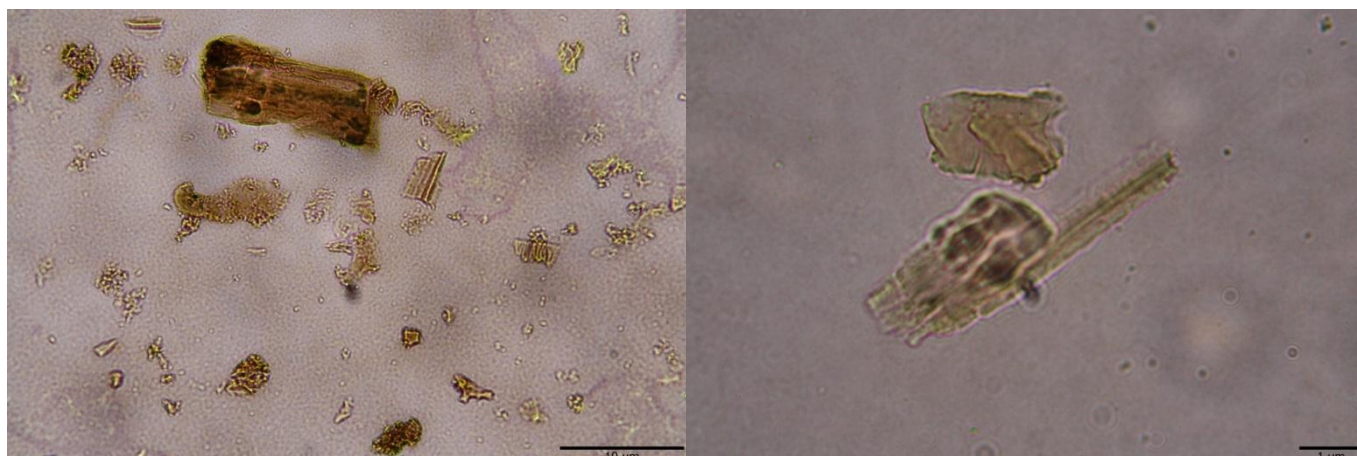


Figure 3.4 : Optical Microscopy Image of RGO sheets, 100X Magnification, Scale bar: 10 μ m(left), 200X, Scale bar: 5 μ m(right)

3.4 SEM Results

The surface morphology and structure of GO and RGO are characterized by FESEM. Figure 3.7 shows the morphology of GO, RGO at high resolution by FESEM. In low magnification images, GO sheets are visible with diameters in the range of 0.1-7 μ m. The sheets are crumpled and scrolled on top of each other. In high magnification images, GO sheets are transparent and resemble silk blankets.

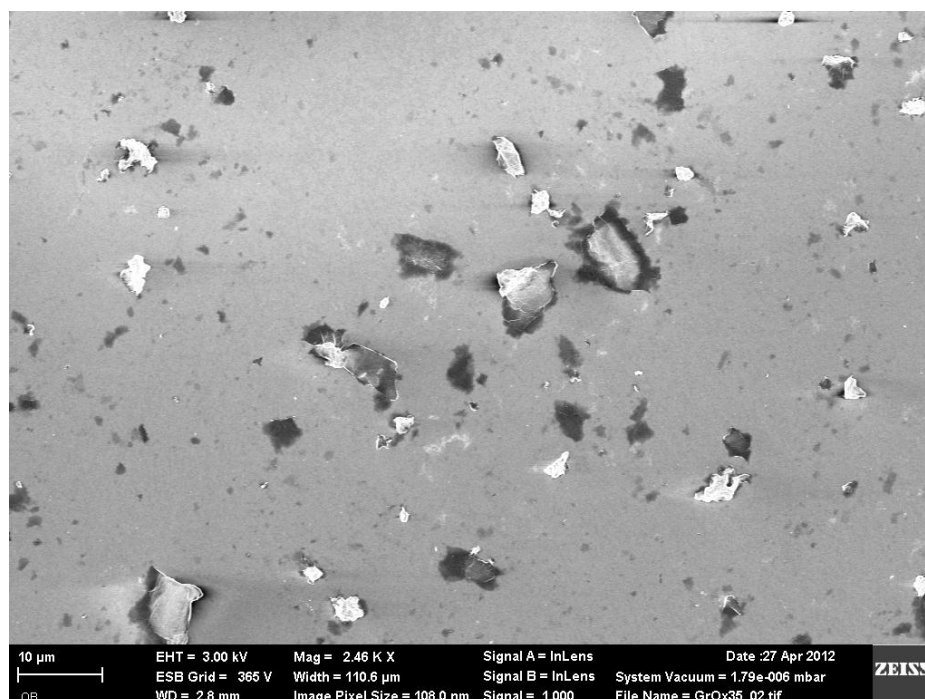


Figure 3.5 : FESEM Image of Graphene Oxide, 2460X Magnification, Scale bar: 10 μ m

Wrinkles on the surface of thin layers of GO and RGO are visible. The oxidation and process during exfoliation of graphite must be considered to interpret the existing wrinkles. During oxidation of graphite, functional groups such as carboxyls, hydroxyls and epoxy groups are introduced to the graphite framework.

Among the functional groups, epoxy group is of importance in wrinkle formation. As a single oxygen atom binds to graphite framework, epoxy group is formed as two adjacent C atoms are joined by a single bond. A three membered epoxide ring (shown in Figure 3.8) undergoes configuration change from sp^2 hybridization to distorted sp^3 - hybridized geometry, the result of which is generation of strain on C-C bond.

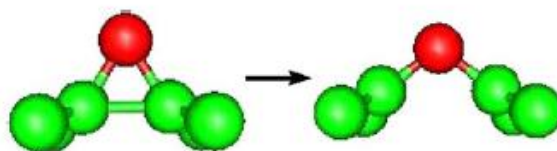


Figure 3.6 : Epoxy group stretching the C-C bond

As several epoxy groups line up, a wrinkle is formed in the sheet that partially release the energy from the strain and makes the configuration energetically favored [85]. As a result of oxidation, epoxy groups align themselves in cooperative chains on the graphite network [86]



Figure 3.7 : An illustration displaying the wrinkle on a thin-film layer

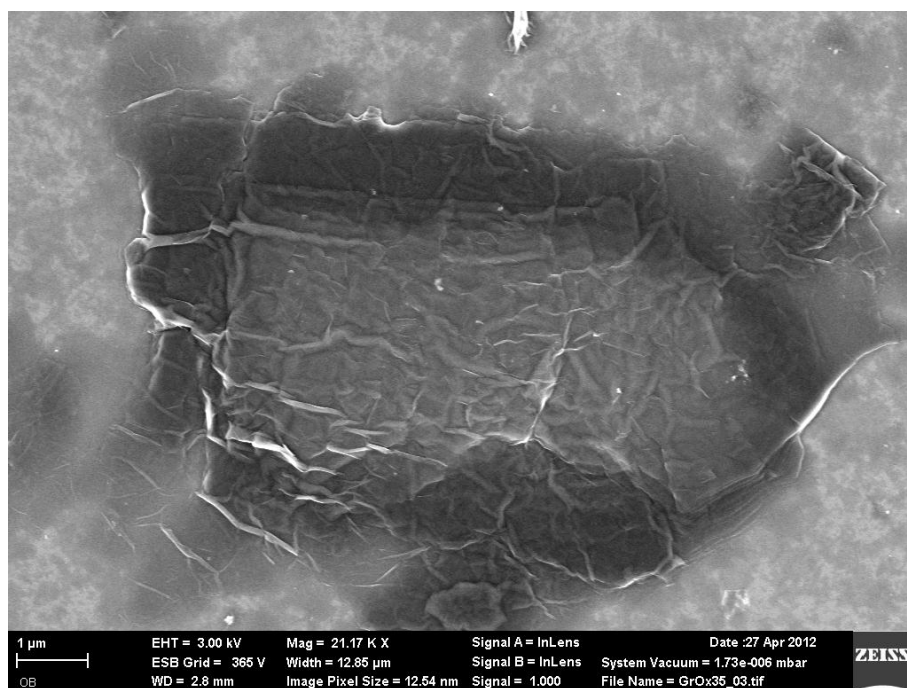


Figure 3.8 : FESEM Image of Graphene Oxide, 21.170X Magnification, Scale bar: 1μm

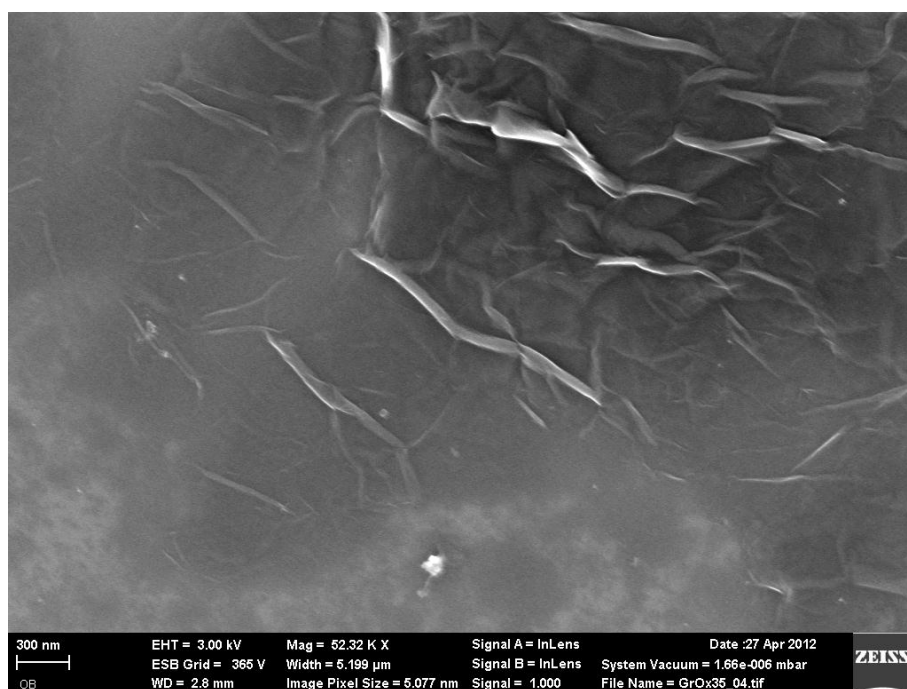


Figure 3.9 : FESEM Image of Graphene Oxide, 52.320X Magnification, Scale bar: 300nm

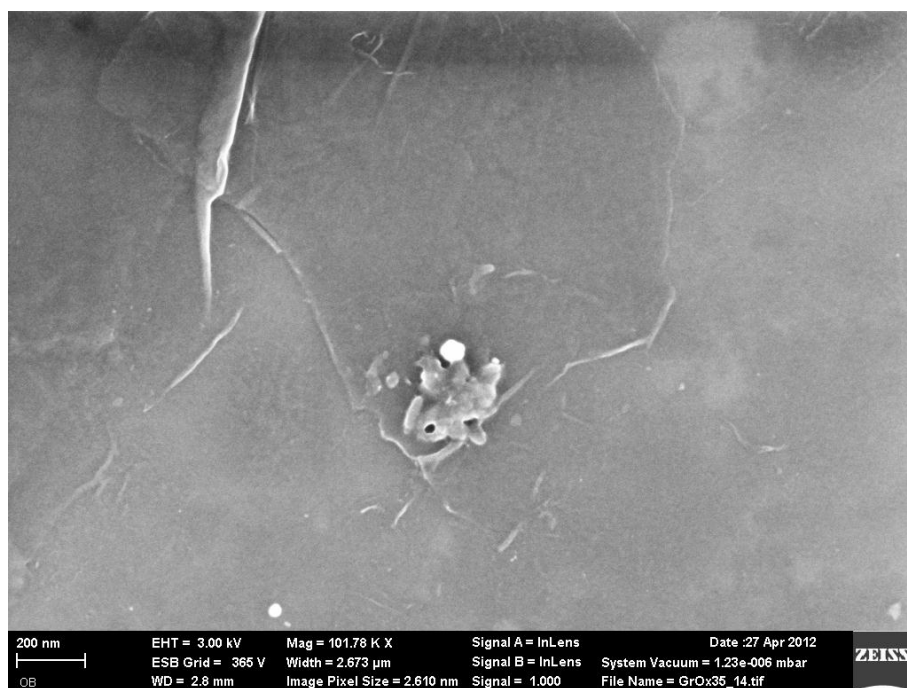


Figure 3.10 : FESEM Image of Graphene Oxide, 101.780X Magnification, Scale bar: 200nm

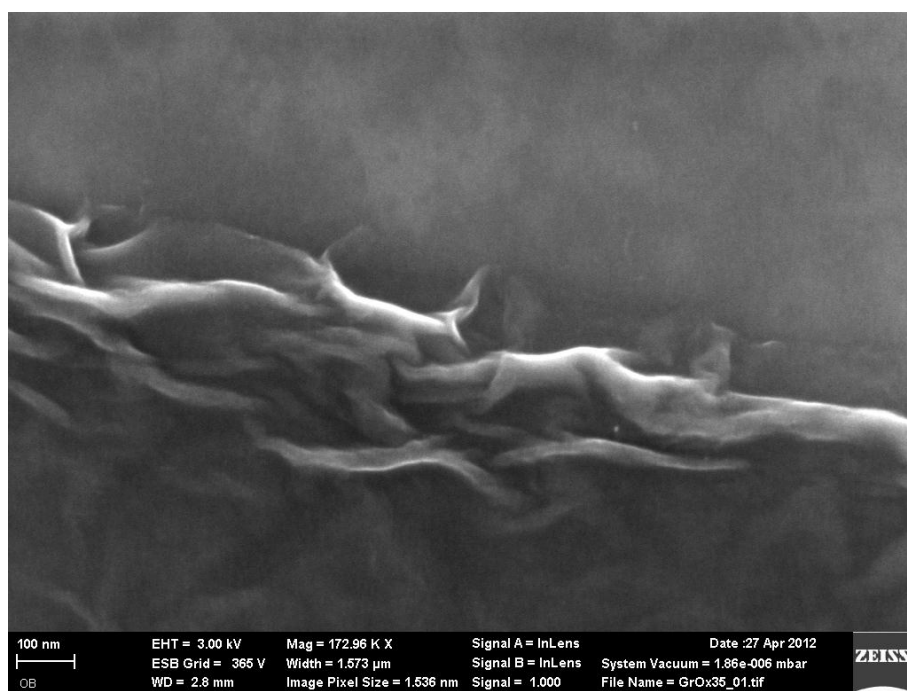


Figure 3.11 : FESEM Image of Graphene Oxide, 172.960X Magnification, Scale bar: 100nm

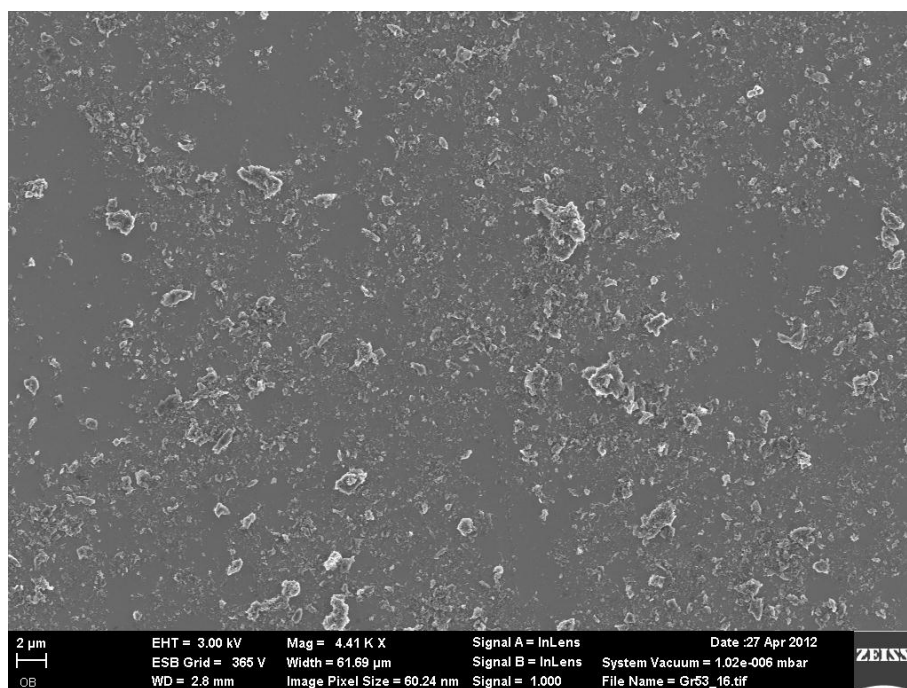


Figure 3.12 : FESEM Image of Reduced Graphene Oxide, 4.410X Magnification, Scale bar: 2μm

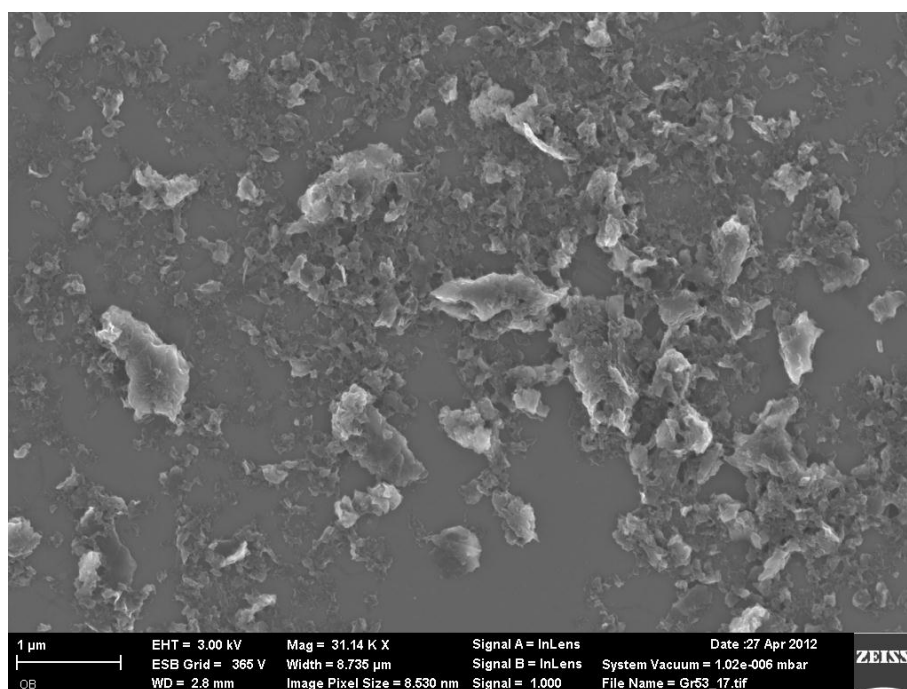


Figure 3.13 : FESEM Image of Reduced Graphene Oxide, 31.140X Magnification, Scale bar: 1μm

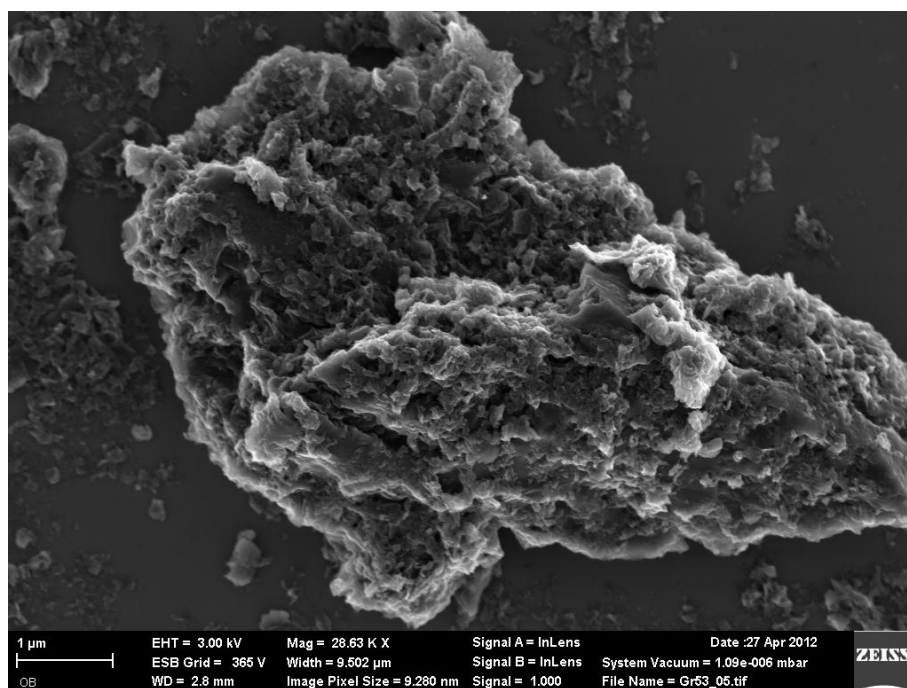


Figure 3.14 : FESEM Image of Reduced Graphene Oxide, 28.630X Magnification, Scale bar: 1μm

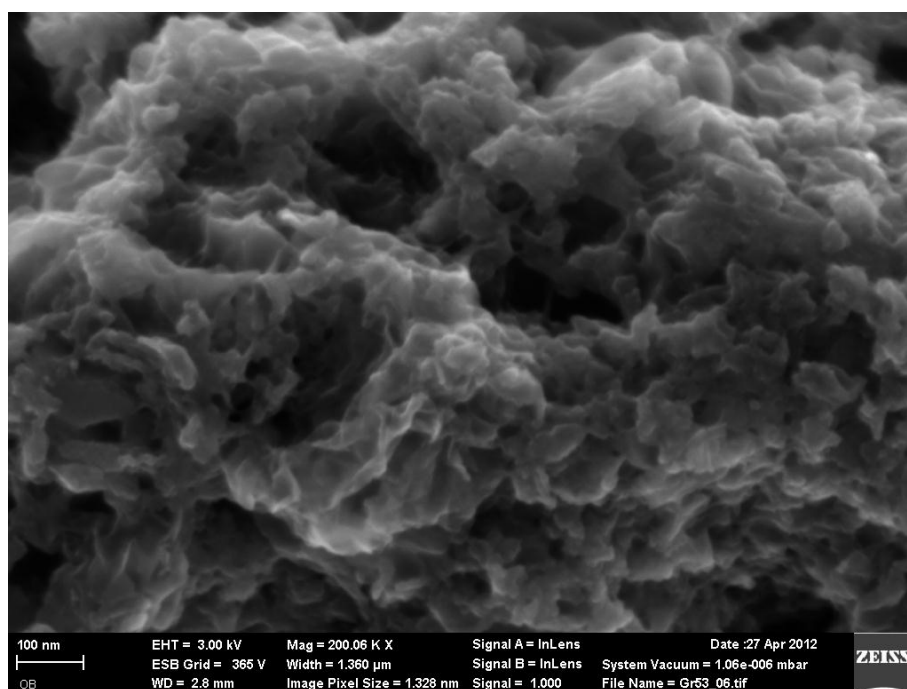


Figure 3.15 : FESEM Image of Reduced Graphene Oxide, 200.060X Magnification, Scale bar: 100nm

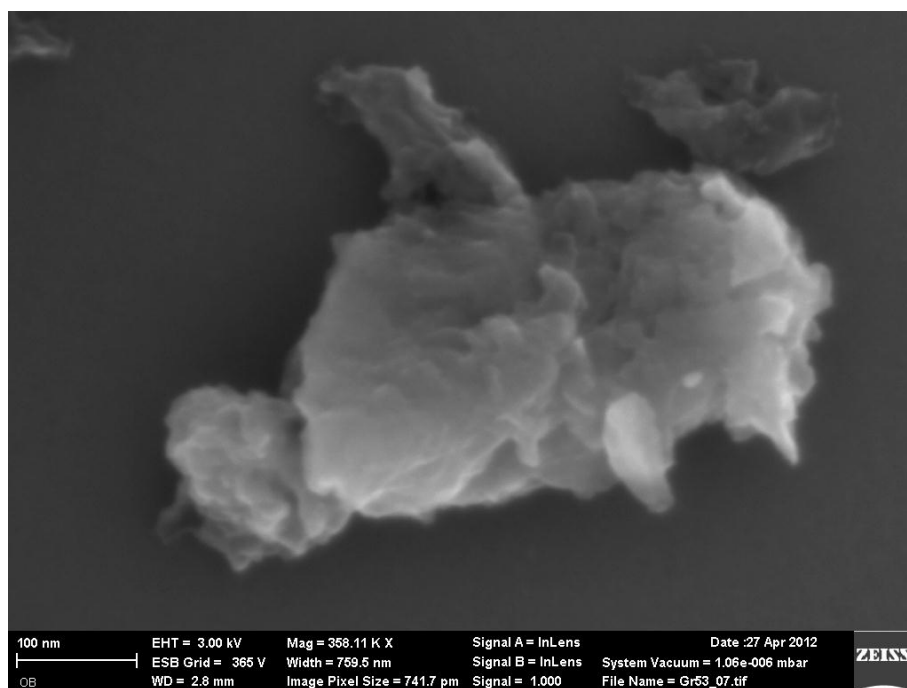


Figure 3.16 : FESEM Image of Reduced Graphene Oxide, 358.110X Magnification, Scale bar: 100nm

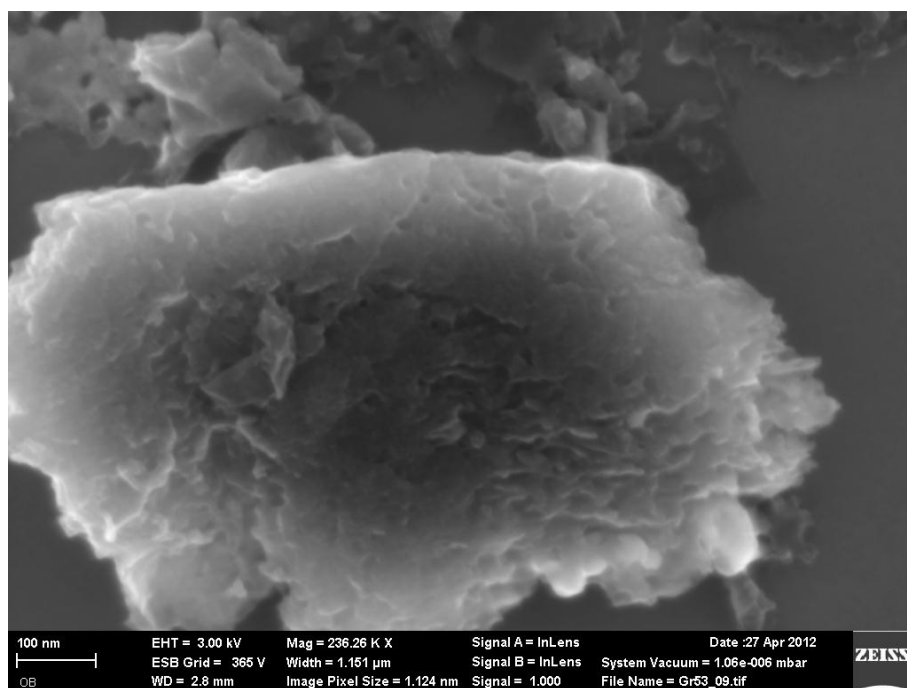


Figure 3.17 : FESEM Image of Reduced Graphene Oxide, 236.260X Magnification, Scale bar: 100nm

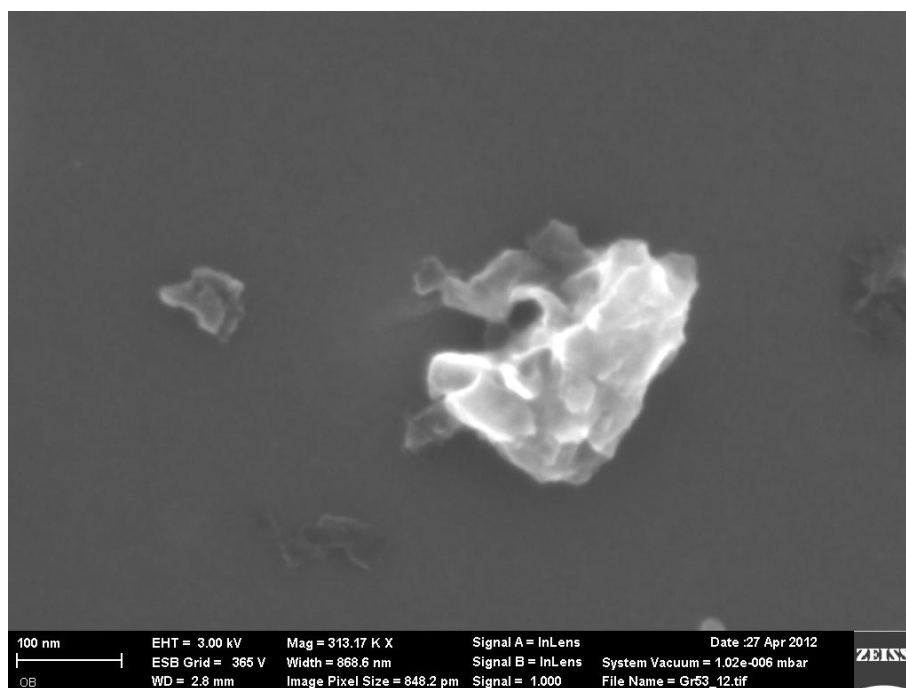


Figure 3.18 : FESEM Image of Reduced Graphene Oxide, 313.170X Magnification, Scale bar: 100nm

Figure 3.14-3-16 shows the morphology of RGO at low resolution by FESEM. In low magnification images, GO sheets are visible with diameters in the range of 0.1-7 μ m. In high magnification images (Figure 3.17-3.20), RGO sheets possess rough surface structure. The roughness arise from the harsh conditions during the oxidation and reduction processes that involve addition and removal of oxygen containing functional groups from the surface structure.

3.5 FT-IR Results

Fourier Transform Infrared Spectroscopy is conducted to gain information about the chemical structure and detect the presence of oxygen containing functional groups in the precursor GO and their disappearance after the MW-ST process. In Figure 3.21, FTIR Spectra of Graphite and Graphite Oxide are displayed. In the spectrum of pristine graphite, the peak located at 1300 cm^{-1} is assigned to the graphitic domains in C-network. The peak around 2300 cm^{-1} arises from CO_2 adsorption due to the atmospheric conditions [87].

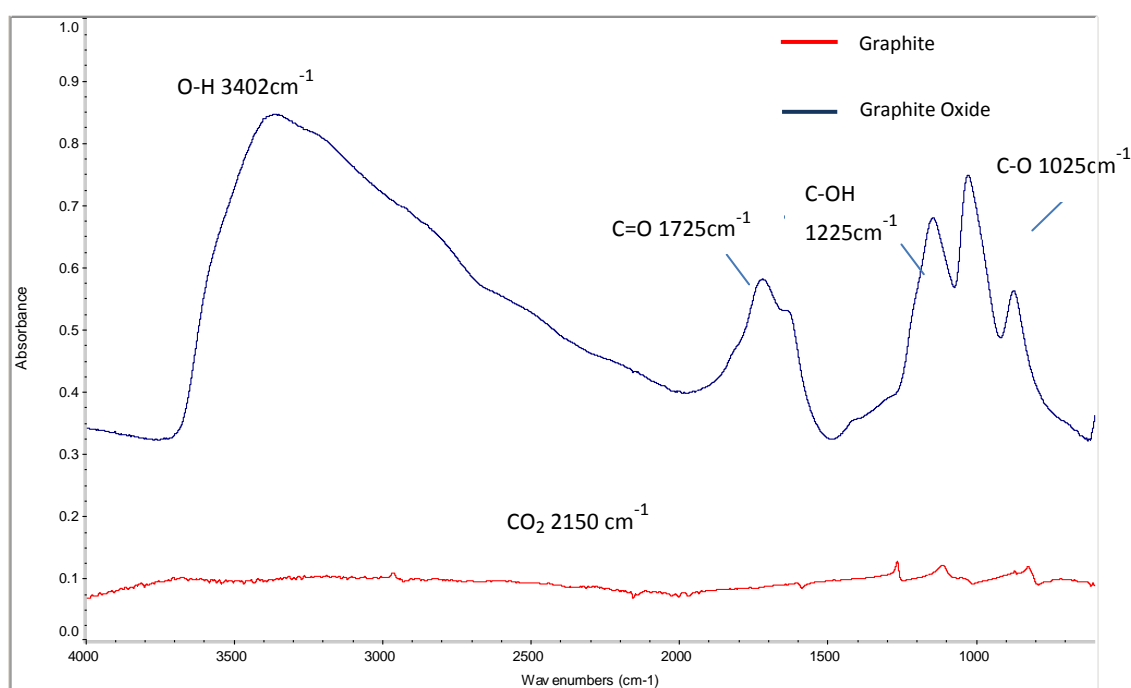


Figure 3.19 : ATR-FTIR spectra proving the Oxidation of Graphite to Graphite Oxide

In graphite oxide (Figure 3.21), a broad absorption band is observed at 3400 cm^{-1} which corresponds to the stretching modes of structural O-H groups and adsorbed water molecules. Carboxyl C=O stretching is visible at 1735 cm^{-1} , carbonyl C-O at 1390 cm^{-1} , while epoxy C-OH stretching and C-O stretching are detected at 1235 and 1025 cm^{-1} , respectively.

The FTIR spectra indicate that the oxidation of pristine graphite with H_2SO_4 and KMnO_4 results in disturbing the π -conjugation of graphite by the addition of oxygen-containing functional groups such as hydroxyls (O-H), epoxides, carbonyls (C=O) and carboxyls (C=O), as displayed in the model predicted by Lerf-Klinowski et al in Figure 3.22. These findings clearly confirm the successful oxidation of the pristine graphite.

A high degree of oxidation of Graphite is necessary since it enables more layers available for interaction with the solvent and the reducing agent. To achieve this goal, two steps are followed; firstly, a starting material with a properly ordered structure and small-sized flakes is chosen. In Figure 8, the results for production of GO with raw Graphite and Highly Oriented Pyrolytic Graphite(HOPG) is compared. It is obvious that peak positions are similar, while the peak intensities are significantly different: C-O stretching at 1025 cm^{-1} , epoxy C-OH stretching at 1235 cm^{-1} , C=O stretching at 1735 cm^{-1} , and O-H stretching at 3400 cm^{-1} . The results show that choice of the type of graphite as the starting material has a crucial role in the quality of the resulting graphene.

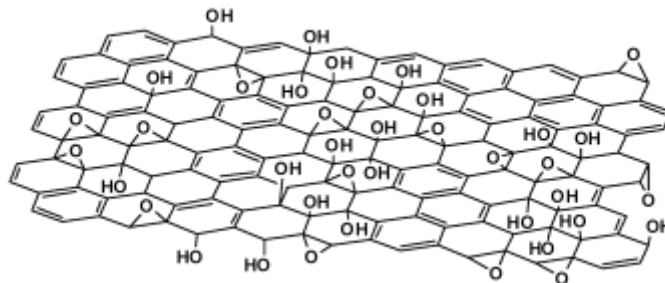


Figure 3.20 : Structure of Graphite Oxide proposed by Lerf-Klinowski Model [43]

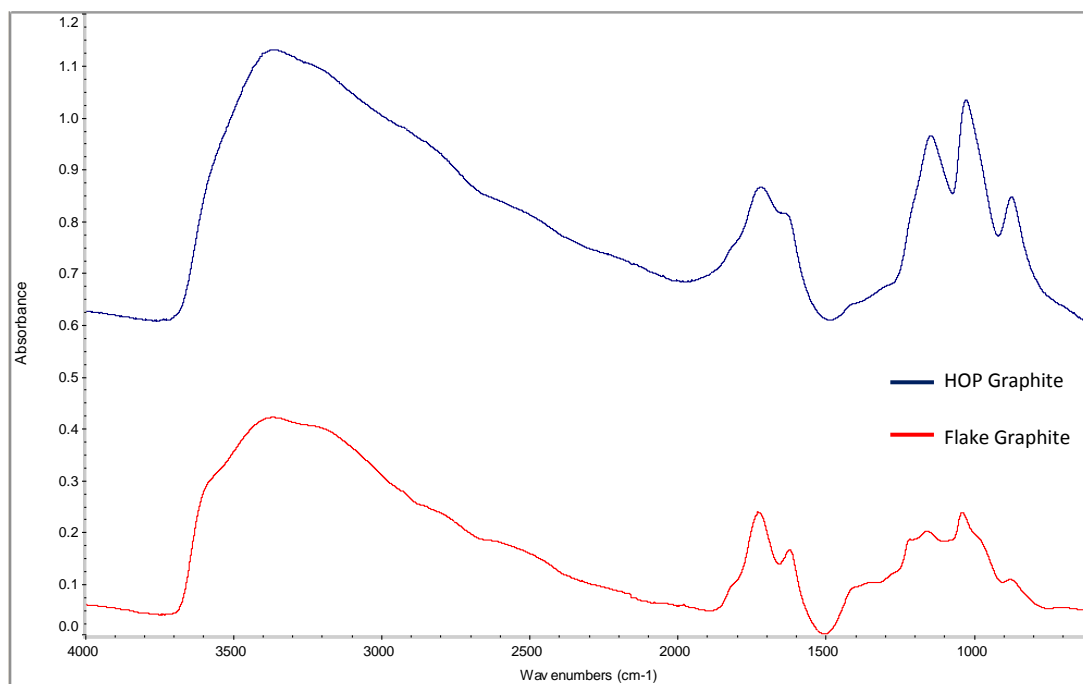


Figure 3.21 : Starting Material Effect: FTIR Spectrum of flake Graphite vs HOPG

Figure 3.24 displays a comparison of the oxidation of Graphite with Hummer's method and Improved Method. In the spectrum of GO produced according to Hummer's, the peak at 1350 cm^{-1} resulting from the skeletal vibration of unoxidized graphitic domains is present whereas it is absent in the Improved Method.

The peak positions harmonize well with C-O (1025 cm^{-1}), epoxy C-OH (1235 cm^{-1}), Carboxyl C=O (1735 cm^{-1}), and O-H (3400 cm^{-1}). The GO produced with Improved Method has the corresponding peaks but with increased intensity. Particularly, C-O (1025 cm^{-1}), epoxy C-OH (1235 cm^{-1}), Carboxyl C=O (1735 cm^{-1}) and O-H (3400 cm^{-1}) peaks are sharp and intense. This is due to the introduction of large quantities of oxygen-containing groups which leads to a higher degree of overall oxidation for the Improved Method.

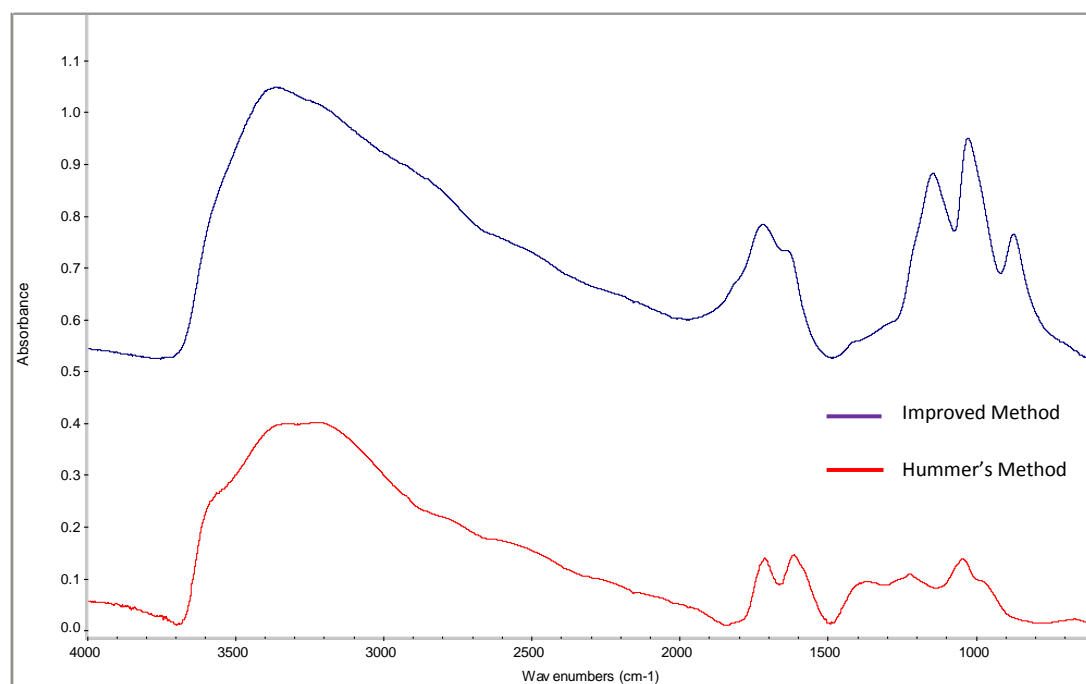


Figure 3.22 : Oxidation Method Effect: FTIR Spectrum of Hummers Method vs Improved Method

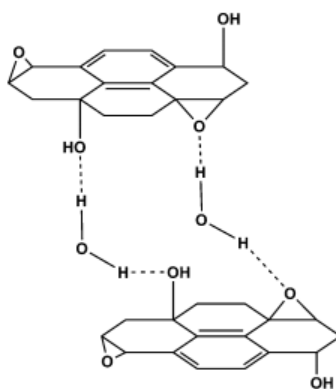


Figure 3.23 : Hydrogen bonding network formed between the oxygenated functional groups of GO and water molecules [43]

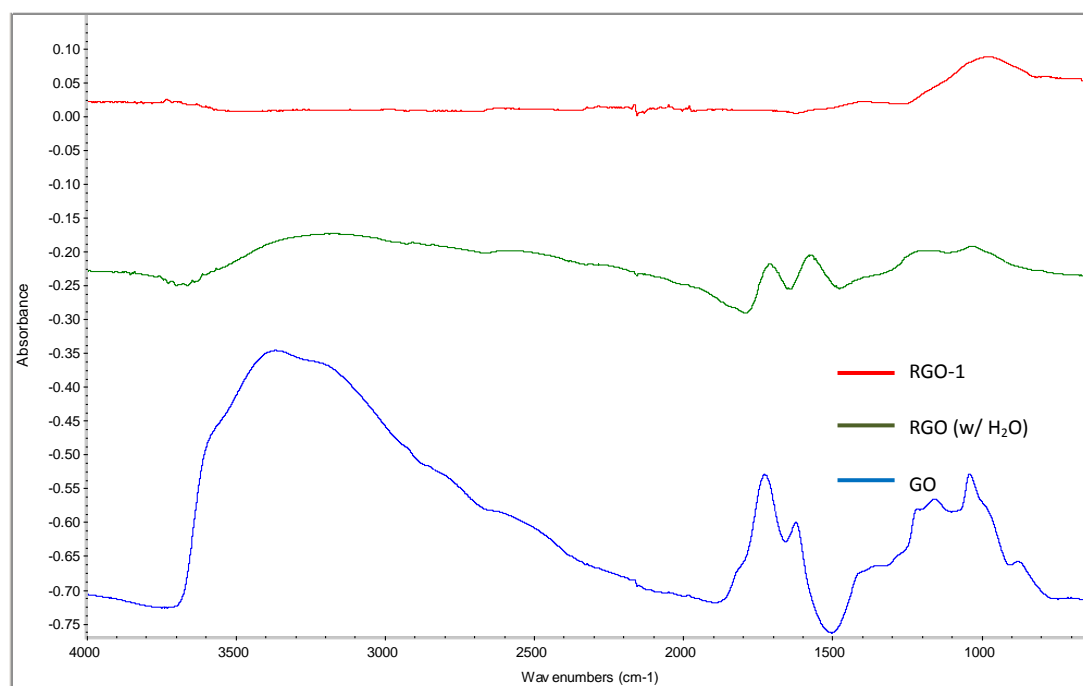


Figure 3.24 : FTIR Spectra: Reduction of GO to RGO

The Reduction of GO with H₂O at 100C removed a substantial amount of functional groups, this is proved by the disappearance of intense peaks of C-O (1025cm⁻¹), epoxy C-OH (1235 cm⁻¹), and O-H (3400 cm⁻¹). However, even after reduction, residual Carboxyl C=O (1735 cm⁻¹) and O-H (3400cm⁻¹) peaks are still visible in the spectrum, even though with very low intensity. The result indicates that the reduction with H₂O only does not completely remove the oxygenated functional groups from GO. For this reason, Microwave Assisted Reduction is utilized.

After the Microwave Reduction of Graphite Oxide, functional groups from intensive oxidation is eliminated. This is proved by disappearance of the absorption bands corresponding to oxygen containing functional group, such as O-H stretching at 3400cm⁻¹. Moreover, individual peaks of C=O stretching at 1735 cm⁻¹, C-O at 1390 cm⁻¹, C-OH Stretching at 1235 cm⁻¹ and C-O stretching at 1025 cm⁻¹ are eliminated. The peak about 1350 cm⁻¹ is due to the skeletal vibration of graphene sheets [88].

As expected, the peak corresponding to O-H stretching at 3400 cm⁻¹ is not completely vanished after reduction process. The majority of the oxygen-containing functional groups are removed from the graphite oxide structure which results in the formation of graphene. The

disappearance of peaks from functional groups indicate the result that graphite oxide have been successfully exfoliated to graphene sheets by exfoliation.

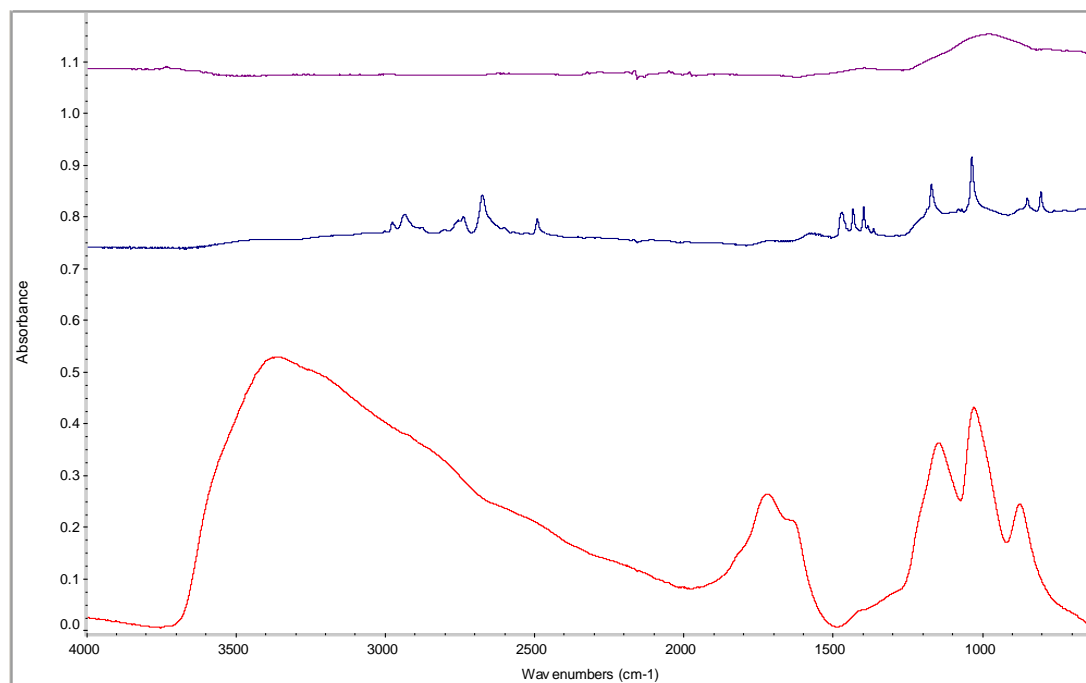


Figure 3.25 : FTIR Spectra: Reduction of GO to RGO

3.6 Raman Results

Raman Spectroscopy is a powerful tool for the characterization of single and few layer graphene sheets [58, 89]. The advantages of Raman can be listed as the following; as a non-destructive method, it can identify the number of layers of graphene [58], the order of the graphitic structure, electronic structure, type of doping [90] and any defects in the graphene. As a vibrational technique, Raman is sensitive to even minor differences in the structure of a molecule, which leads to changes in its Raman spectrum. This deems it to an ideal method for the investigation of carbon allotropes (diamond, CNT, Graphene), as they only differ in the relative position of their carbon atoms and their bonding type.

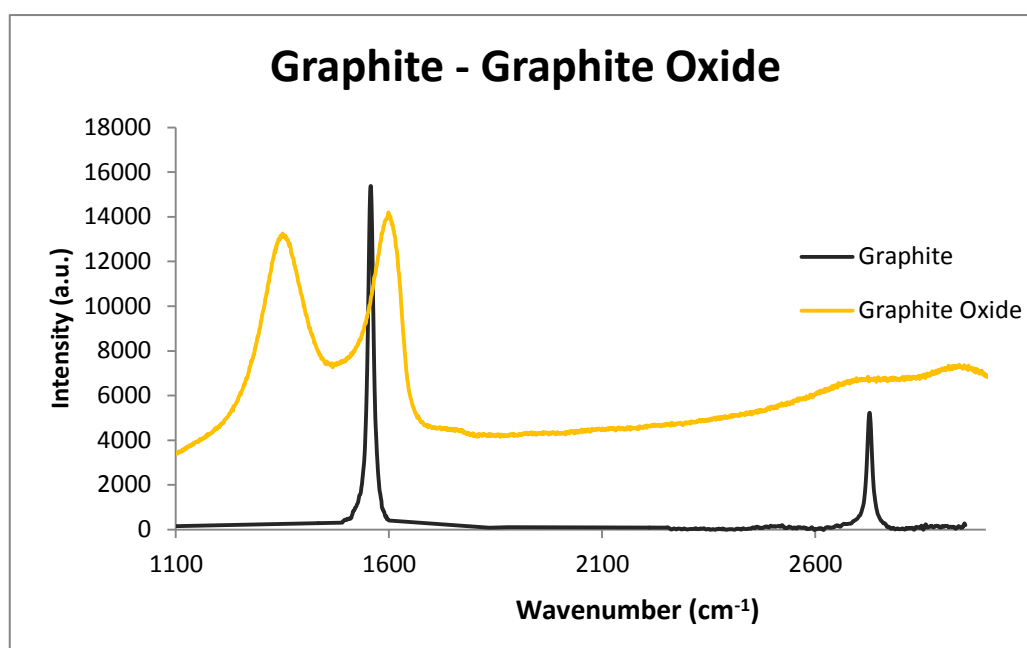


Figure 3.26 : Raman spectra of Graphite - GO

Raman spectrum of raw graphite exhibits only two intense peaks, the G band at 1578 cm^{-1} and 2D band at 2728 cm^{-1} . The G Band (1578 cm^{-1}) is related to in-phase vibration of sp^2 C atoms in the graphite lattice and named after the first order scattering of E_{2g} phonon. The second order 2D band at 2728 cm^{-1} is less intense.

As Graphite is oxidized to GO, a new peak, the D band appears at 1350 cm^{-1} which arises from the breathing mode of j-point photons of A_{1g} symmetry. An important feature of the D band is that it corresponds to defects in the graphene sheet, which is not observed in graphite. This indicates that the extensive oxidation introduces many defects into the graphitic network and thus in-plane sp^2 domains are reduced in size, which is in accordance with expectations. Moreover, the G band also undergoes a significant change as the crystalline graphite structure is transformed to amorphous GO. High disorder in amorphous GO leads to a broader G band in comparison to that of Graphite. Moreover, the G band is upshifted 30 cm^{-1} from 1578 cm^{-1} to 1608 cm^{-1} in GO, due to the existence of isolated double bonds in GO resonating at higher frequencies than those of graphite.

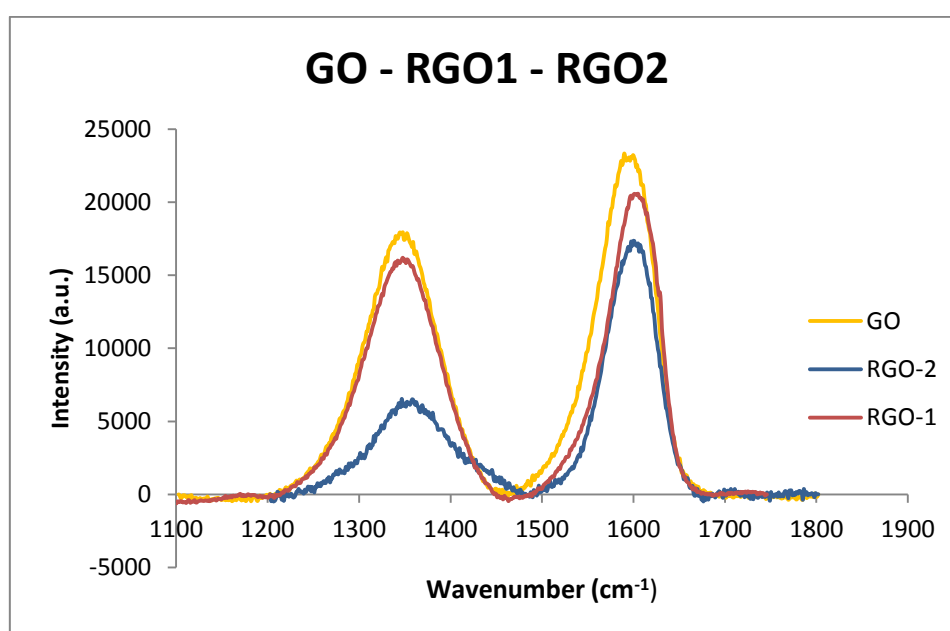


Figure 3.27 : Raman spectra of GO – RGO

In comparison to GO, RGO peak positions are slightly altered. Both the G and D band of RGO is shifted to higher frequencies (blue shift). Apparently, D band decrease in relative intensity and broadens significantly for RGO, hinting toward decrease in defect in RGO structure. With respect to GO, the 10 cm^{-1} blue shift of both D (from 1363 cm^{-1} to 1373 cm^{-1})

and G (from 1608 cm^{-1} to 1618 cm^{-1}) peaks in RGO1 indicates a higher degree of amorphization. The blue shift of RGO2 is on the order of 10 cm^{-1}

The ratio of the D to G peak intensity is also known as the I_D/I_G ratio, and it provides a valuable information on the structure of RGO. The empirical Tuinstra-Koenig relation suggests that I_D/I_G ratio is inversely proportional to the size of nanocrystalline graphite, thus an increase indicates the decrease of disorder in graphite layer. The corresponding I_D/I_G ratios for Graphite, GO and RGO are; 1.18, 1.18 and 1.18. This corresponds to in-plane crystallite size of 5nm. GO compared with RGO does not show any difference in D/G Ratio. These minor changes indicate that Microwave treatment removes most of the oxygenated groups as CO_2 , the vacant lattice sizes that are left behind remain unchanged. Also, the nanocrystalline graphite size is not affected.

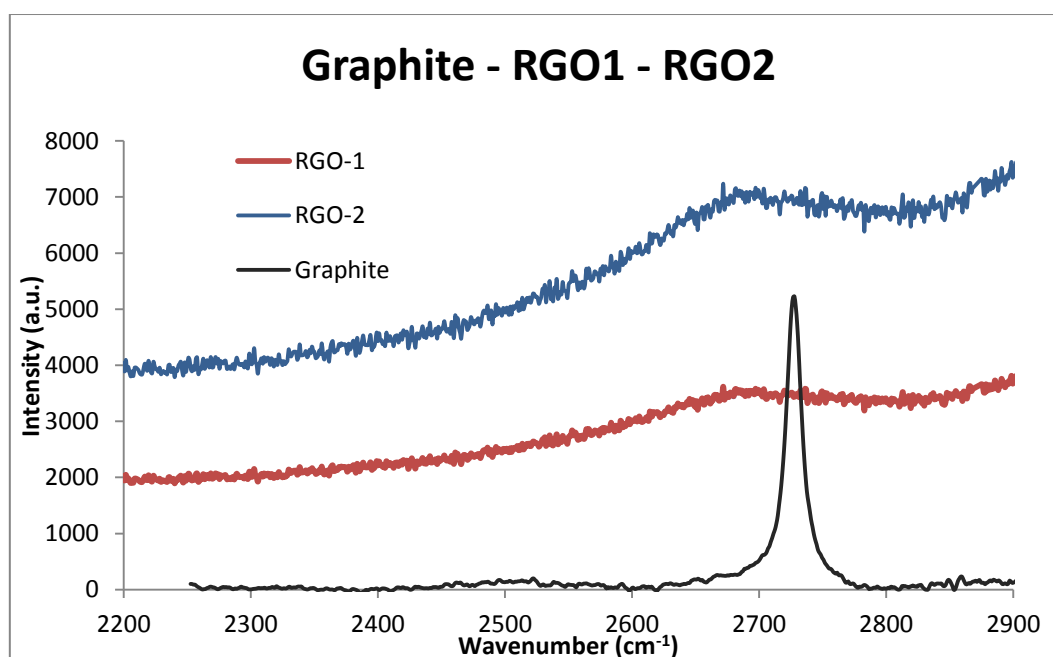


Figure 3.28 : Raman spectra of Graphite - RGO

With respect to Graphite, the G band in RGO is upshifted 20 cm^{-1} from 1580 cm^{-1} to 1608 cm^{-1} , which is attributed to transformation of crystalline graphite to sheets of graphene. Comparison of G band with D band in RGO sheets show that D band is less intense, but has almost equal full width halfmaximum (FWHM) indicating well stacked nature of graphene nanosheets.

The comparison of Graphite with RGO in Figure 3.30 displays an important feature. Position and shape of the 2D band are two cornerstone parameters that provide information by indicating the number of layers of graphene sheets [91]. The 2D position of graphite is located at 2728 cm^{-1} , while RGO have a much broader peak located at 2700 cm^{-1} (RGO-1) and 2698 cm^{-1} (RGO-2), indicating a spectrum shift of few layer graphene with respect to graphite to lower wavenumbers by 28 cm^{-1} and 30 cm^{-1} respectively. The observed 2D bands of RGO centered at 2698 cm^{-1} suggest the formation of few layer RGO sheets.

3.7 XRD Analysis

X-Ray Diffraction phenomenon is based on Bragg's law, which is expressed by;

$$n \lambda = 2d_{(hkl)} \sin \theta$$

where λ defines the wavelength of the utilized X-ray, θ is the angle of scattering, n is an integer that represents the order of the diffraction peak (which is commonly selected as $n=1$), d is the interplane distance between lattice and (hkl) stand for Miller indices. The interlayer distance is denoted as $d(002)$ in the case of (002) planes of graphite / multi layer graphene is given. As the generated X-rays are bombarded on the sample, they are scattered from each graphene plane. The angle θ between consecutive planes of graphite and also the path-length difference is an integer multiple (n) of X-ray wavelength λ , the scattering results in a constructive interference. This leads to high relative intensity of a peak located at arbitrary θ . $d(002)$ spacing can be calculated from XRD Diagram, that provides information about lattice size and quality. Moreover, multilayer graphene thickness can be estimated using Scherrer's equation :

$$D_{002} = K \lambda / B \cos \theta$$

where D_{002} stands for thickness of crystallite (thickness of multilayer graphene), K is a constant dependent on crystallite shape (0.89), λ is the wavelength of the X-Ray, B is the full width at half maximum (FWHM) and θ is angle of scattering. From Sherrer's equation, number of layers can be calculated using the following equation;

$$N_{\text{Graphene}} = D_{002} / d_{002}$$

The oxidation of Graphite and Reduction of GO is monitored by X-Ray Diffraction. Powders of GO and RGO are examined by XRD. Figure 8 shows XRD Pattern of Graphite in comparison with literature. Graphite powder has the characteristic strong (002) diffraction peak at $2\theta = 26.4^\circ$. The interlayer spacing, $d(002)$ was determined using Bragg's equation, which corresponds to (d-spacing: 0.347nm) which is in agreement with the literature XRD pattern.

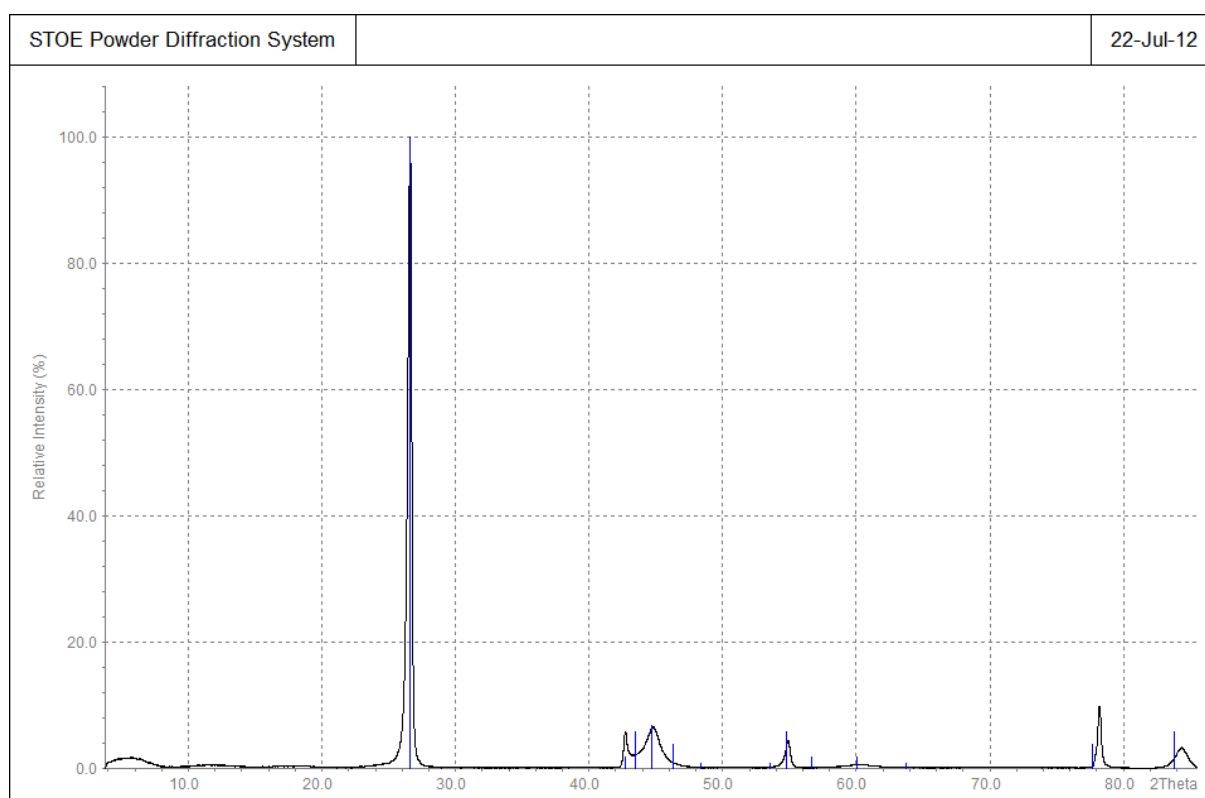


Figure 3.29 : XRD Diagram of Graphite - literature data

The oxidation of graphite eliminates the intensity of this diffraction line. (002) peak disappears, signaling the change in graphitic network as it is oxidized to GO. At the same time, a broad diffraction peak appears at $2\theta = 6.3^\circ$ (d-spacing = 1.40 nm) that corresponds to the oxidation of Graphite [45]. The significantly larger interlayer spacing of GO (1.40nm) with respect to that of Graphite (0.347nm) arises from the intercalating oxygen functional groups.

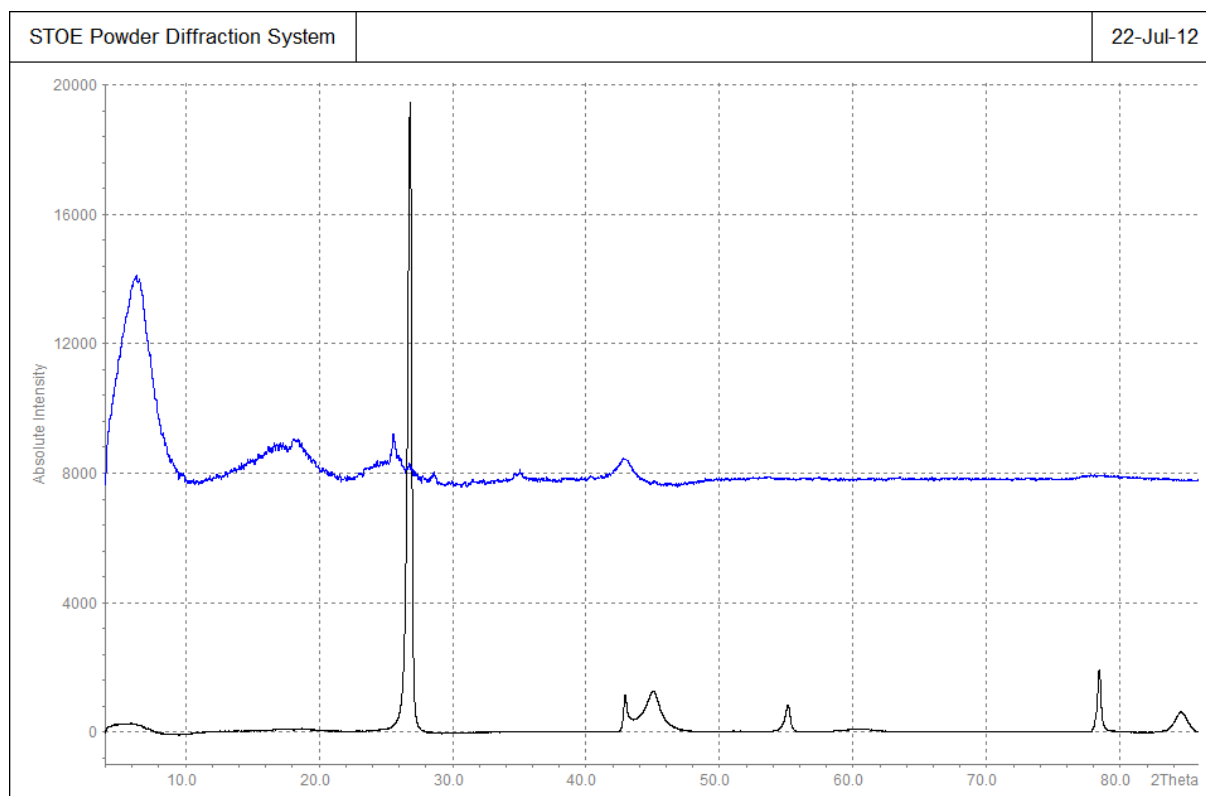


Figure 3.30 : XRD Diagram of Graphite - GO

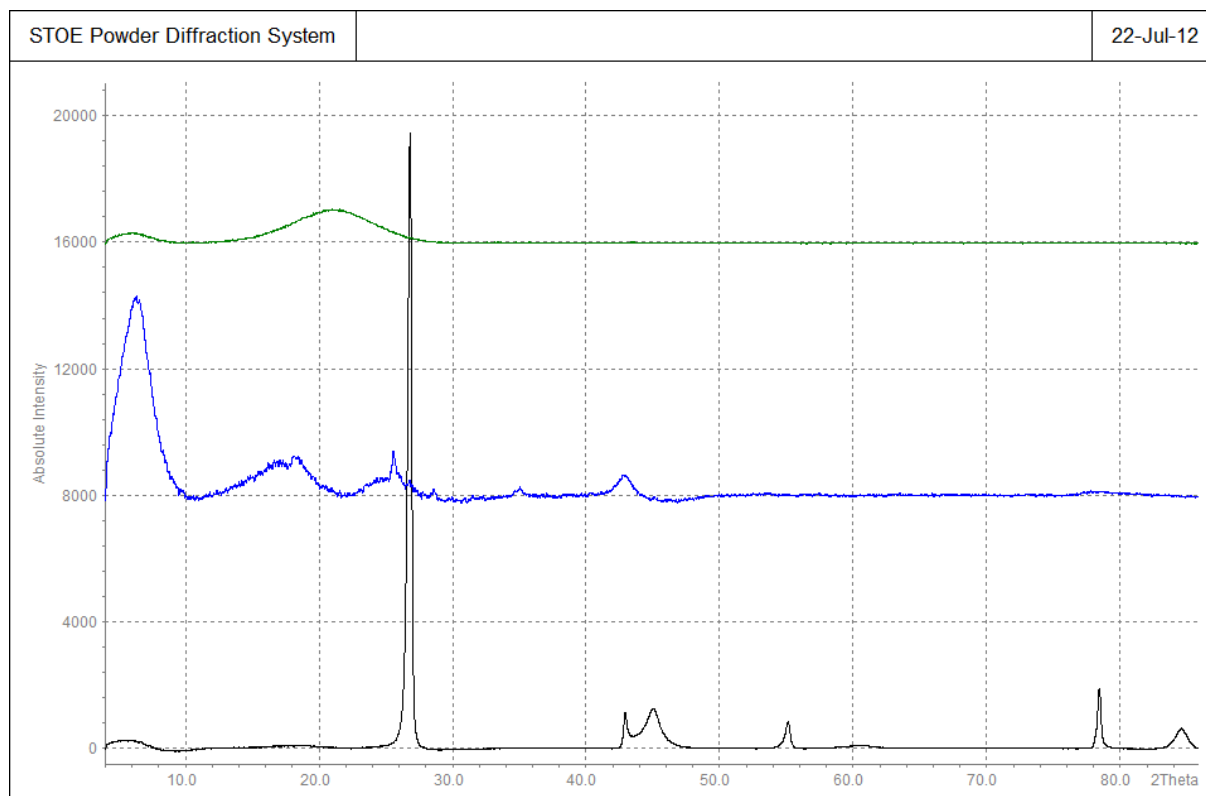


Figure 3.31 : XRD Diagram of Graphite - GO - RGO1

The substantial shift of the (002) reflection from $2\theta = 6.3^\circ$ (GO) to $2\theta = 21.5^\circ$ (RGO) after the Microwave Reduction confirms the formation of RGO/Graphene sheets from GO. RGO sheets' broad (002) diffraction peak at $2\theta = 21.5^\circ$, corresponds to d-spacing of 0.42 nm, which is slightly larger than that (0.347nm) of graphite. The slight increase in d-spacing of RGO with respect to the precursor Graphite is due to the intrinsic distortions on the graphitic framework that is subjected to powerful oxidizing agents and removal of functional groups which cooperatively damage the framework. Also, residual functional groups might be retained even after the reduction process. The broad nature of the reflection peak at 22.5° indicate poor ordering of sheets along the stacking direction.

These results suggest that GO sheets are successfully reduced while the randomly distributed RGO sheets interlayer spacing is larger than that of graphite. Moreover, aggregation and restacking of graphene sheets into graphite are prevented due to the effect of the solvent in the system. The d(002) value and broadening of the reflection is expected for randomly ordered graphitic (turbostatic) RGO platelets.

3.8 XPS Results

X-Ray Photoelectron Spectroscopy (XPS) measurement is employed to analyze the GO and the RGO which is subjected to MW-ST process. Figure 3.34 displays the C^{1s} , O^{1s} and N^{1s} XPS spectra of GO.

Especially, C^{1s} spectrum of GO bears valuable information on the oxidation state of the carbon partial structure. The spectrum is a superposition of three peaks, two of which are strong. It clearly indicates a considerable degree of oxidation of carbon atoms in three different functional groups; non-oxygenated C–C bonds (285.1 eV), followed by a shoulder of C–O bonds in epoxy and hydroxyls (287.2 eV) and carboxylate C=O (289.2 eV). The peak positions are in agreement with literature reports and are indications for the efficient oxidation of GO.

Decomposition of C^{1s} XPS spectrum into its components indicate that the fractions of C–O and C–C bonds in GO are 42% and 52% respectively. Further analysis reveals that

carbon to oxygen ratio (C/O Ratio) in GO is 1.07. Since it is energetically more favored for O to form covalent bonds with two C atoms, it is also in accordance with XPS results that graphite structure is heavily oxidized.

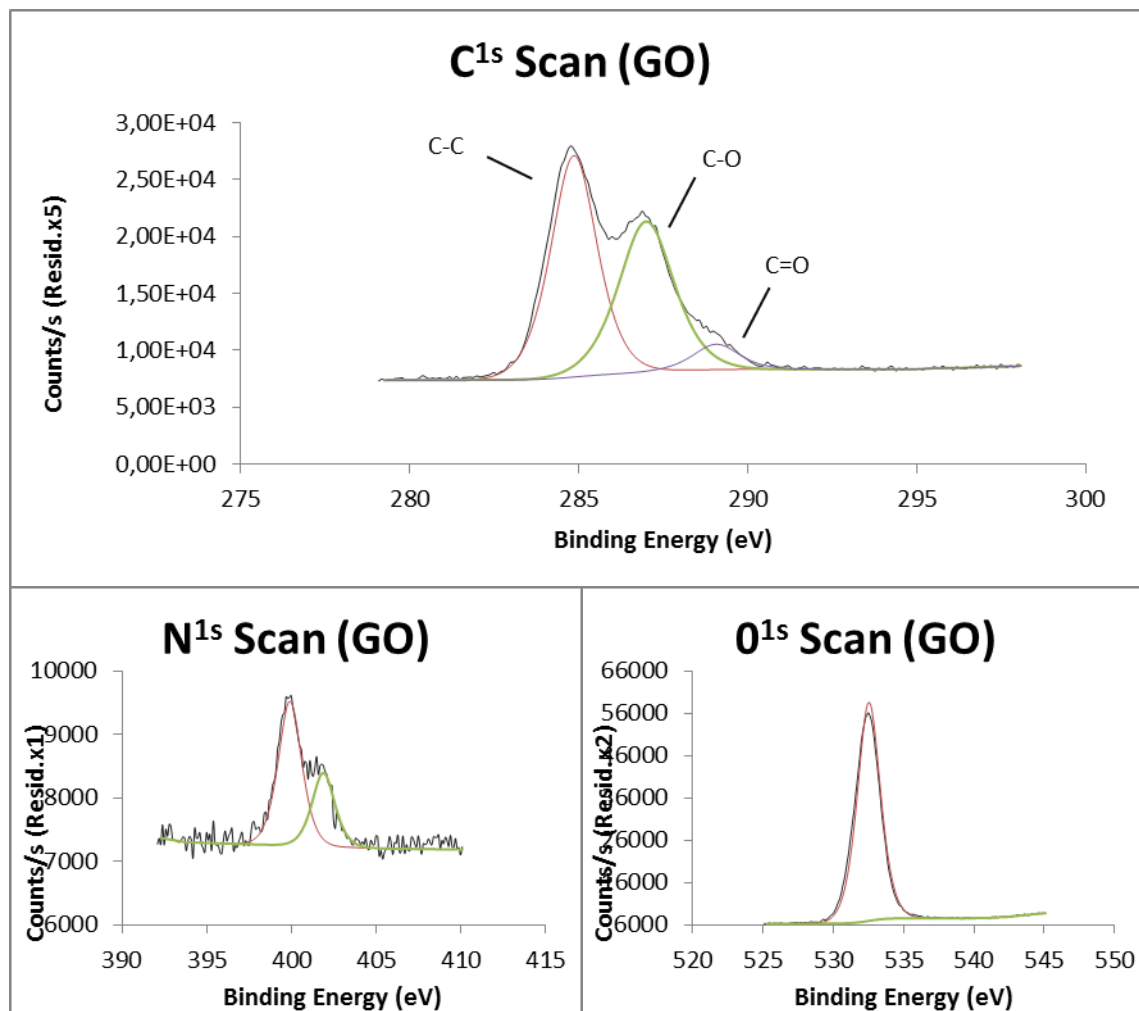


Figure 3.32 : XPS Spectrum of Graphite Oxide

XPS spectra of RGO-1 and RGO-2 is a superposition of two peaks, non-oxygenated C–C bonds (C-C, 285.1 eV) and a shoulder arising from C-O bonds in epoxy and hydroxyls (C-O, 287.2 eV). In comparison to GO, there is a significant decrease in C-O peak relative to that of C-C for RGO-1, whereas the C-O peak is relatively higher in RGO-2. This clearly indicates a considerable degree of the removal of oxygen-containing functional groups for RGO-1, whereas reduction is less effective for RGO-2

Comparison of RGO-1 and RGO-2 displays that C-O peaks Decomposition of C^{1s} XPS spectrum into its components indicate that the fractions of C-O and C-C bonds in RGO are changed to 42% and 52% respectively.

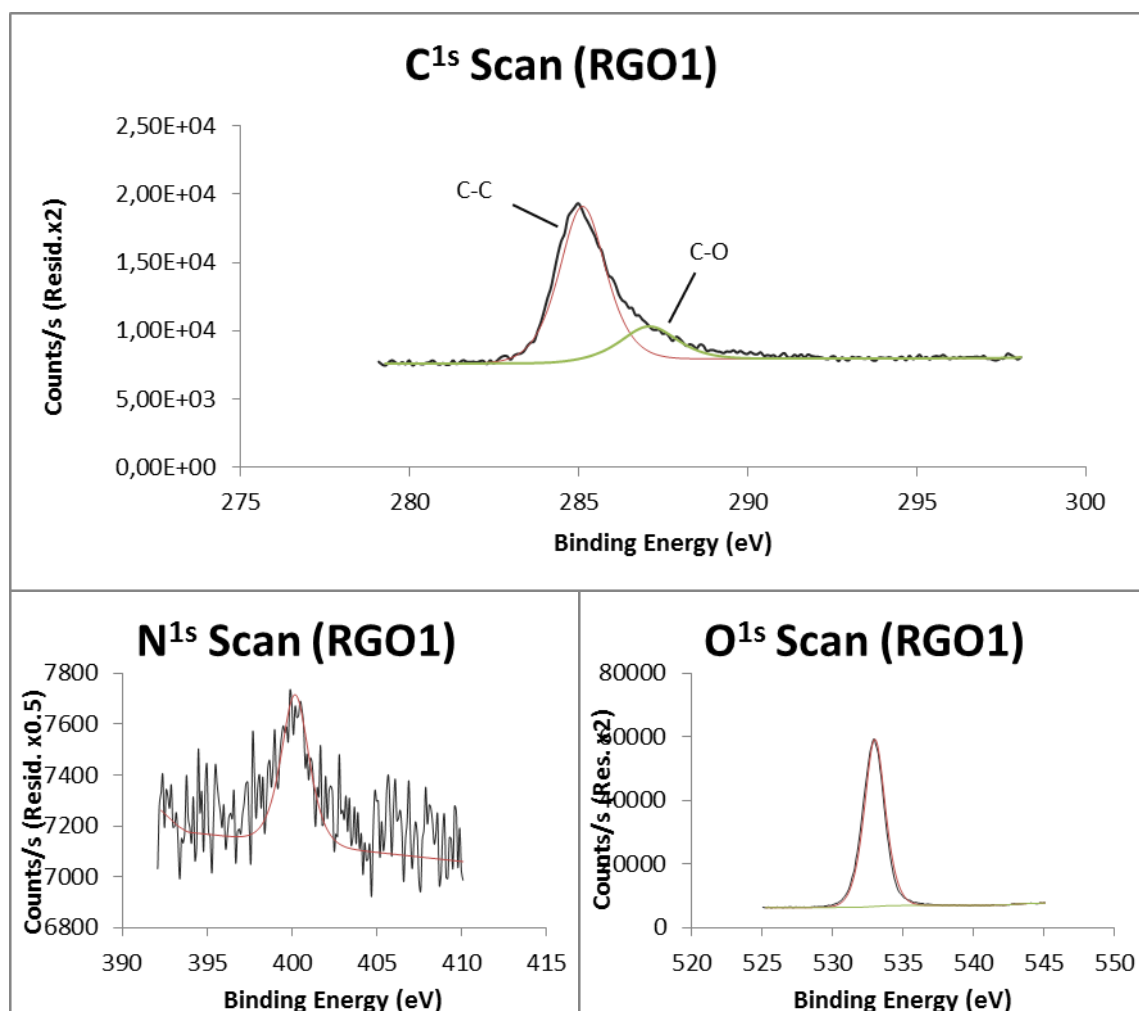


Figure 3.33 : XPS Spectrum of RGO-1

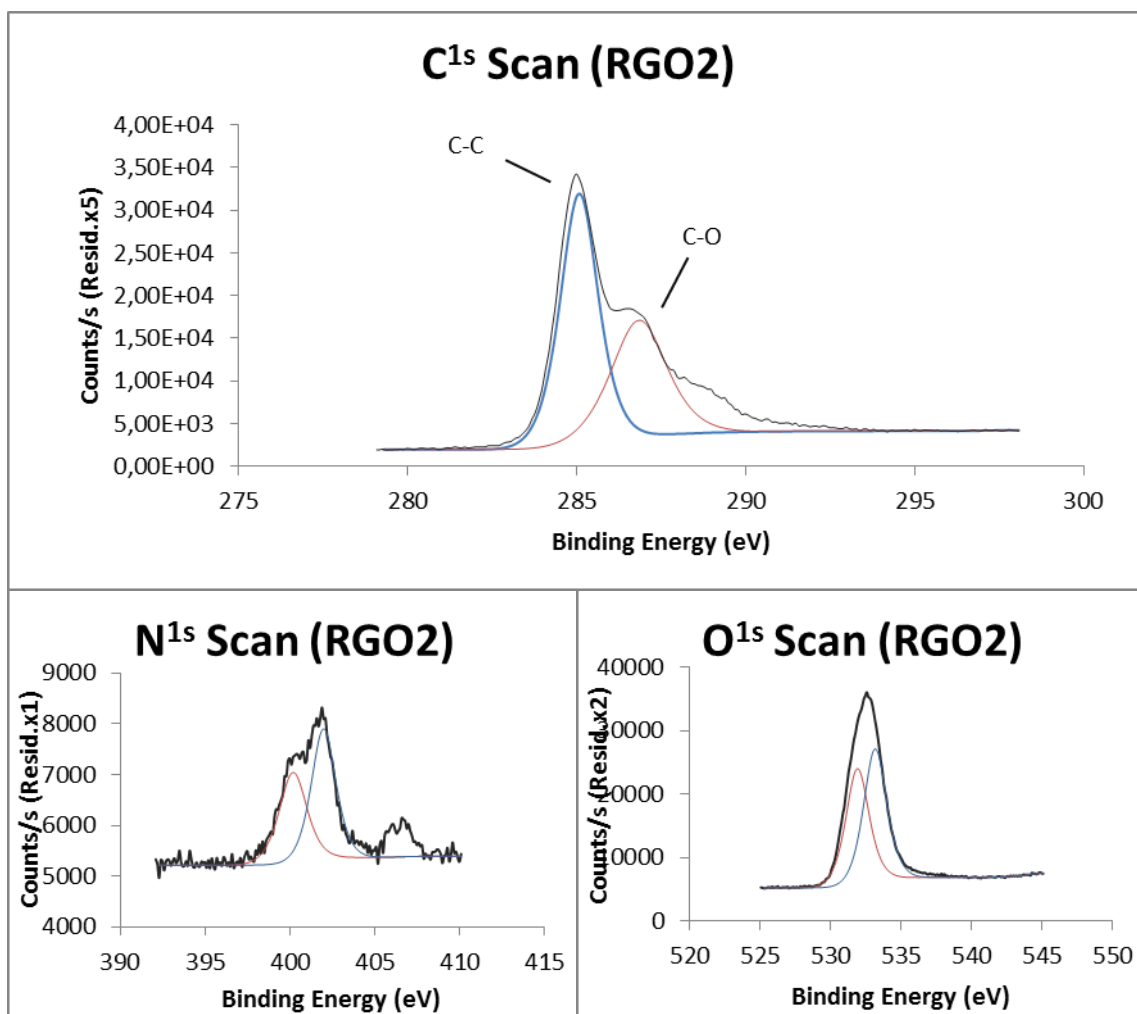


Figure 3.34 : XPS Spectrum of RGO-2

3.9 Elemental Analysis Results

Elemental Analysis is performed for the educt Graphite, the intermediate Graphene Oxide and the RGO that are reduced by different methods. C/O Ratio is specified in the table for each material, which is a value that is calculated by division of mass percent of C to that of O and provides information about the oxidation of graphite network. A high value suggests that there are less O molecules with respect to C, while a single digit value means that there is a substantial amount of O is present.

The results indicate that raw Graphite has a low O content and high C content, which results in a C/O Ratio of 99. On the other hand, GO has a C/O Ratio of 2,6, which suggests that there are 2,6 C molecules for each O atom, meaning that graphitic network is heavily oxidized. However, the reduction process decreases the ratio to 13 and 17, for RGO-1 and RGO-2 respectively. A substantial amount of functional groups should be eliminated to obtain this value, nevertheless the oxygenated groups are not completely removed. These findings are in accordance with the FT-IR, Raman, XRD and XPS measurements as well.

	O	N	H	C/O Ratio
Graphite	0.11	0.01	0.02	99
Graphite Oxide	57.39	0.47	3.52	0.7
ReducedGraphite Oxide(w. H₂O)	27.60	0.11	1.11	2.6
RGO-1	6.94	0.08	2.39	13
RGO-2	5,46	0.09	2.19	17

Table 3.1 : The result of Elemental Analyses

3.10 TGA/DTA Results

Thermogravimetric Analysis of the graphite, GO and the product RGO is performed in order to determine thermal stability of the materials and observe the presence/disappearance of oxygen containing functional groups. TGA Curves are shown in Figures 3.37 and 3.38 with temperature range of 25-1350°C for each individual run. As displayed in Figure 3.37, Graphite shows no weight loss as the temperature increases. In fact, %98 of the total weight of graphite remains at 1350°C, which indicate that graphite is quite thermally stable, in accordance with the expectations.

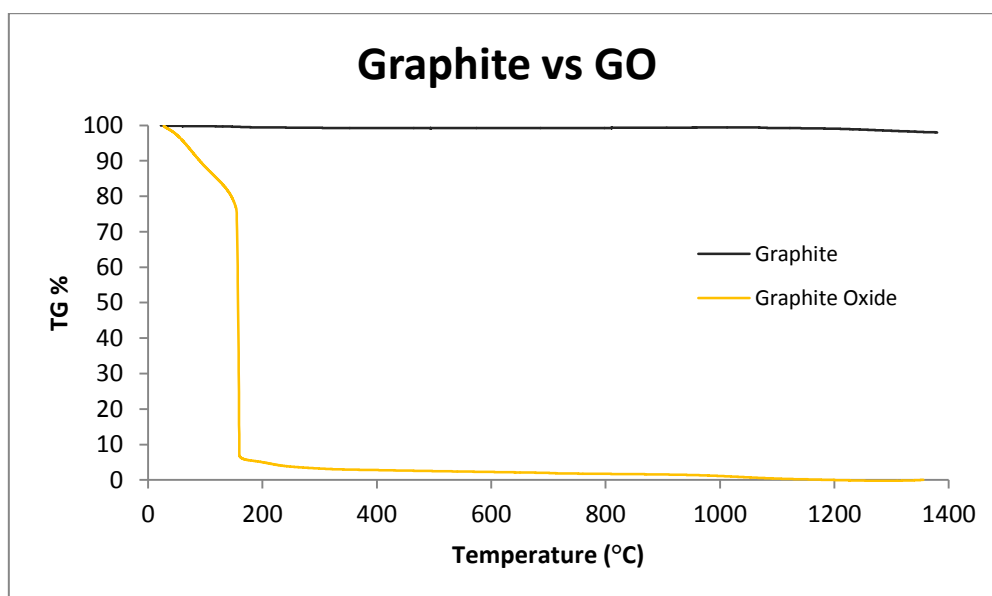


Figure 3.35 : TGA Curve of Graphite - GO

TGA Curve of GO displays that 20% weight loss is observed between 25-140°C which arise from the structural release of H₂O present on the sheets. Between 140- 200°C major weight losses occur that correspond to CO, CO₂ release from the unstable oxygen containing functional groups. In fact, only %4.9 of the total weight of GO remains at 200°C. Obviously, GO is thermally unstable at elevated temperatures.

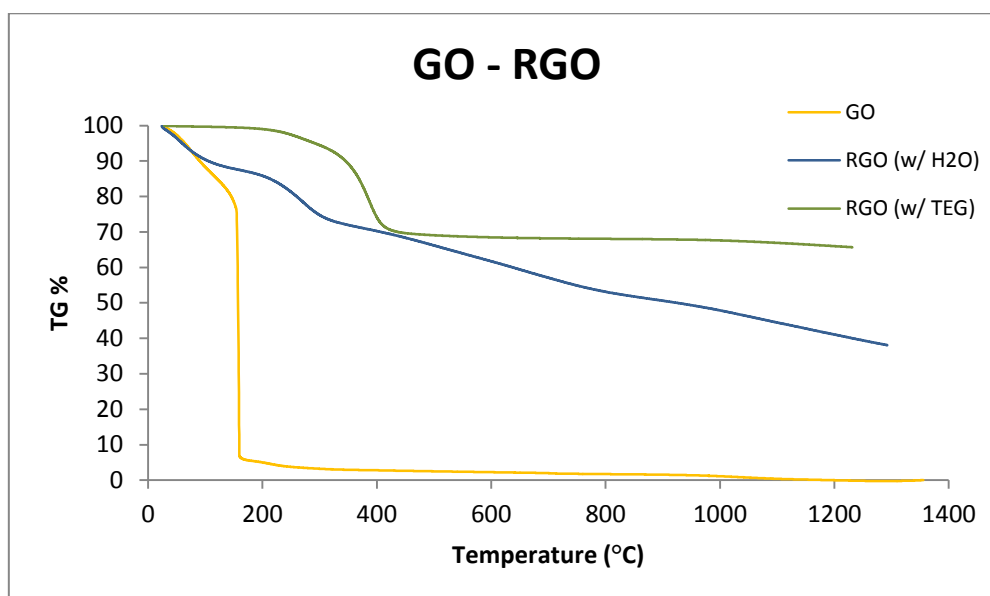


Figure 3.36 : TGA Curve of Graphite - GO

On the other hand, RGO displays different characteristics. GO reduced with using H₂O as solvent undergoes a weight loss at 160°C and constantly loses its mass as the temperature increases. At 1350°C, only 38% of the total mass is remaining. In comparison with GO, thermal stability is considerably higher, which can be explained by the disappearance of unstable oxygen containing functional groups during the reduction process. Yet GO reduced with TEG as solvent displays better thermal behaviour. It is thermally stable at temperatures up to 300°C, where 98% of its total mass retained. At 350°C a mass loss occurs, but even at elevated temperatures of 1350°C, 65% of its total mass remains. This result indicates the increased thermal stability of RGO with respect to GO and the successful completion of the reduction.

Chapter IV: SUMMARY

Graphene has been moved to the center of interest and attention since its discovery in 2004. Novel properties such as RT quantum Hall effect, high charge transport and thermal conductivity of its 2D structure are investigated by several studies in fundamental physics and chemistry. The exceptional mechanical, electrical, thermal and optical properties of graphene layers are gaining importance for various engineering applications as well.

In fact, the research in the field of graphene is fast-paced and progressive, as indicated by the exponential growth of number of publications. Though initial studies depended on micromechanical cleavage of HOPG to obtain high quality graphene layers, it was rather cumbersome, slow and low-scale. The attention is transformed recently toward methods that are scalable, higher yield and bulk-scale. In this regard, chemical reduction of GO has been an appropriate method for large-scale production. Yet it involves harsh reaction conditions, toxic reducing agents and lengthy reaction times. So, there is still a search for chemical, physical aid that should somehow ease the process.

At this point, the significantly rapid progress in the field of graphene research was personally experienced. Initially, the investigations have focused on the use of water as a solvent for the reduction of GO with the assistance of ultrasonication. The results were satisfactory and indicated indeed that rather than using hydrazine or sodium borohydrate, GO could be reduced to RGO by water. The excitement was unexplicable, yet it was understood that not only a similar research is conducted by another group, but also as soon as the GO is reduced to RGO, it tends to agglomerate and form the precursor graphite again. Thus, the investigation centered on the Microwave Assisted Solvothermal Approach with organic solvents in order to prevent agglomeration.

The research performed in this MSc. thesis investigates the production of reduced Graphene Oxide (RGO) / few layer graphene sheets with a simple, rapid and environmental-friendly approach. GO and RGO in mass production by conventional methods can lead to health risk due to handling and inhaling of toxic oxidizing agents and reducing chemicals. The health risk associated with GO and RGO is substantially reduced through use of the investigated methods presented in this study. For this purpose, chemical exfoliation is

implemented with a two-step reaction pathway. Graphite is oxidized to GO by a method that eliminates the evolution of noxious gases during synthesis (NO, NO₂) from the commonly selected Hummers' method, while offering increased efficiency.

Secondly, as produced GO sheets are reduced to RGO by elimination of toxic reducing agents. For the selection of appropriate solvents, Hansen solubility rules have been utilized that aid in the selection of an appropriate solvent. Among the probed solvents, N,N-Dimethyl Formamide DMF/H₂O (9:1) and TEG are specifically selected that conform to the required criteria for graphene solution as they prevent the agglomeration of graphene in the system. Solvent assisted Reduction of GO is performed under the assistance of Microwave Irradiation at a relatively mild temperature conditions (120°C).

As-synthesized GO layers are characterized by FTIR, Raman, XRD, XPS, Optical Microscopy, FESEM, TGA and Elemental Analysis measurements. The FT-IR results indicate that Graphite is oxidized to GO by introduction of functional groups carbonyl C-O stretching at 1025cm⁻¹, epoxy C-OH stretching at 1235 cm⁻¹, C=O stretching at 1735 cm⁻¹, and O-H stretching 3400 cm⁻¹ which disappear after successful Microwave treatment. Raman spectra of RGO exhibits a downshift of 2D band with respect to graphite from 2728 cm⁻¹ to 2698 cm⁻¹ suggesting the formation of few layer graphene. XRD Diagram indicates d(002) = 0.844 nm for GO which is then decreased to d(002) = 0.40nm in the product RGO. XPS results display that epoxy C-O (287.2eV) and carboxylate C=O (289.2 eV) functional groups disappear in RGO. Elemental Analysis results show C/O Ratio is decreased from 68 (GO) to 13 for RGO. TGA Analysis shows that 70% of total mass remains as the temperature is increased to 1400°C. In conclusion, the results indicate that RGO layers are successfully produced after the two-step reaction pathway.

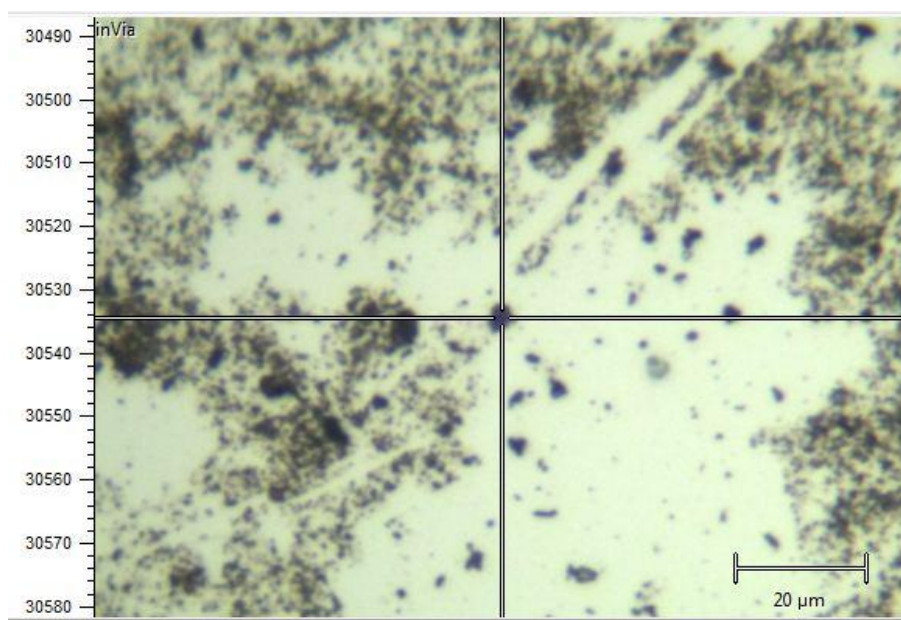
The chemical exfoliation method for production of RGO developed in this thesis has several advantages with respect to drawbacks of previous chemical techniques. It is controllable, environmental-friendly, cost-effective and energy efficient, as well as offering simplicity and short processing times. In regard of the graphene's evolution into a feasible nanomaterial and elevated importance for production, the improved process might find practical applications in the preparation of graphene-based composite materials.

Graphene based materials include potential applications in various fields including but not limited to; electronics, transparent flexible electrodes, heat transfer, graphene/polymer composites, chemical sensors and energy storage materials. However, a series of problems

have to be further investigated, such as homogenous distribution of individual graphene sheets, their orientation and bonding with matrix for composite applications. Moreover, the wrinkle formation and overlapping of RGO sheets need to be remedied, which require further research.

The further research/recommendations for future work in addition to the studies presented in this thesis might focus on the enhanced use of Microwave Assistance. Adoption of Microwave Oven gives rise to a number of restrictions; the presence of strong oxidizing agents such as H_2SO_4 , KMnO_4 under microwave conditions result in extremely rapid heat and pressure increases. This prevents the oxidation of graphite under Microwave Assistance and our efforts in these trials remained fruitless. While a proper oxidation of graphite under conventional conditions of stirring and heating requires a reaction time of 12h, the adoption of Microwave Assistance would substantially decrease the time necessary for oxidation. On the other hand, different approaches can be developed for the reduction of GO, which might include reduction by implementation of different solvents, by examination of their Hansen solubilities. Other methods may implement reduction without any solvent at all under microwave conditions, by using dry GO thin films. However, in all of the methods, the search focuses on elimination of decreasing reaction times and amount of materials used, which is in accordance with the requirements of large-scale applications.

Finally, in a time band of less than a decade after the graphene sheets were first reported, the early discoveries aroused wide interest and presently the production methods are developed which already started bearing fruits for implementation. Our efforts in this MSc. Thesis suggests an alternative route for facile, rapid, environmental-friendly and large-scale approach, which might find use in the production of RGO. There needs to be probably almost a decade for the evolution of ripe applications, but once implemented, graphene will introduce new eras in the aforementioned diverse fields.

Appendix A : Raman Microscope Images**Figure A.1 : Raman Microscope Image of GO****Figure A.2 : Raman Microscope Image of RGO-1**

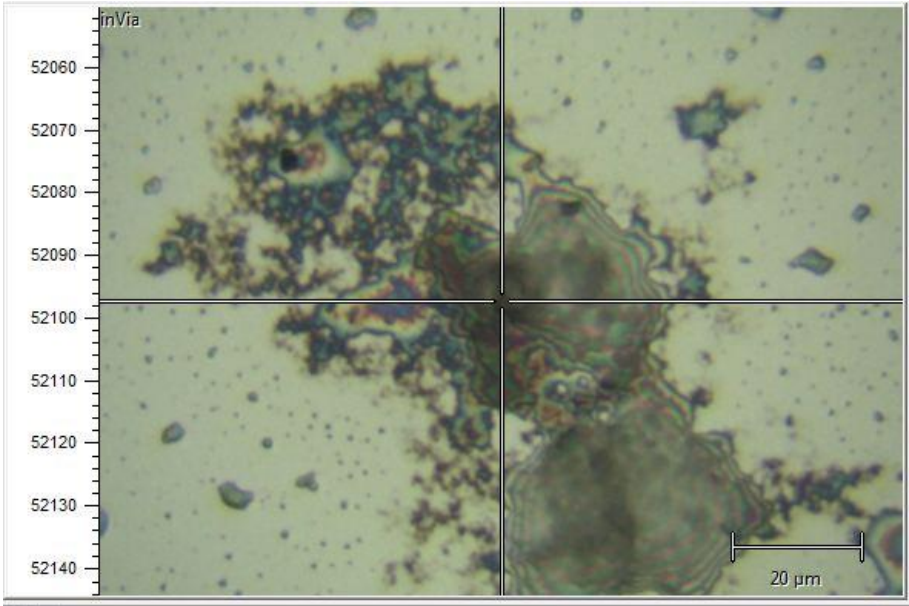


Figure A.3 : Raman Microscope Image of RGO-2

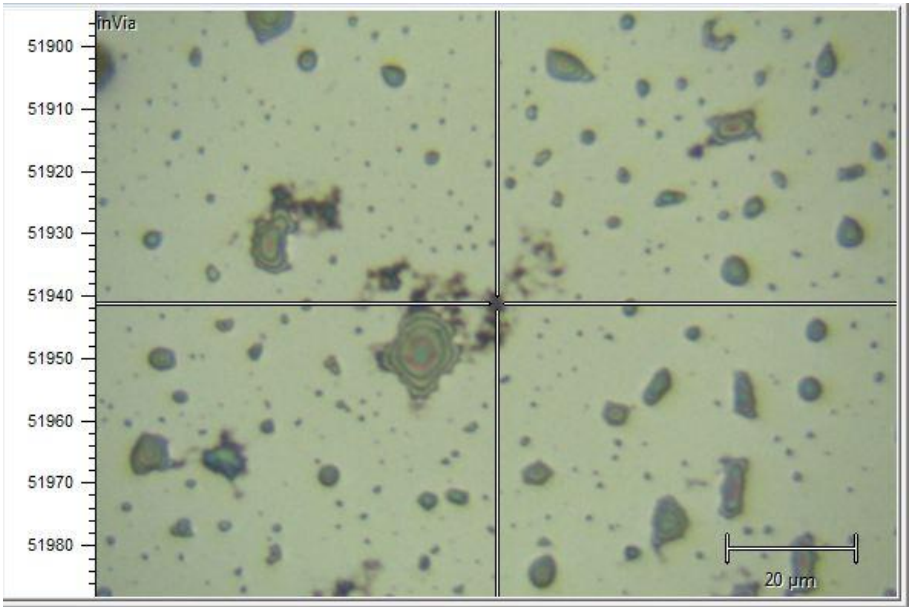


Figure A.4 : Raman Microscope Image of RGO-2

Chapter V : BIBLIOGRAPHY

1. Geim, A.K. and K.S. Novoselov, *The rise of graphene*. Nat Mater, 2007. **6**(3): p. 183-91.
2. Novoselov, K.S., et al., *Electric Field Effect in Atomically Thin Carbon Films*. Science, 2004. **306**(5696): p. 666-669.
3. Geim, A.K. and A.H. MacDonald, *Graphene: Exploring Carbon Flatland*. Physics Today, 2007. **60**(8): p. 35-41.
4. Murali, R., et al., *Breakdown current density of graphene nanoribbons*. Applied Physics Letters, 2009. **94**(24): p. 243114.
5. Lemaître, G., *Expansion of the universe, A homogeneous universe of constant mass and increasing radius accounting for the radial velocity of extra-galactic nebulae*. Monthly Notices of the Royal Astronomical Society, Vol. 91, p.483-490, 1931.
6. N. Jarosik, C.L.B., J. Dunkley, *Seven-year Wilkinson Microwave Anisotropy Probe (WMAP) Observations: Sky Maps, Systematic Errors and Basic Results* The Astrophysical Journal Supplement Series, 2011. **192**(14): p. 15.
7. Botvina, A.S. and I.N. Mishustin, *Formation of hot heavy nuclei in supernova explosions*. Physics Letters B, 2004. **584**(3-4): p. 233-240.
8. Dalrymple, G.B., *The age of the Earth in the twentieth century: a problem (mostly) solved*. Geological Society, London, Special Publications, 2001. **190**(1): p. 205-221.
9. Utah, U.o. *The Oldest Homo Sapiens: Fossils Push Human Emergence Back To 195,000 Years Ago*. 2005, February 23.
10. Patrick, J.W., *Porosity in Carbons: Characterization and Applications*1995.
11. Olsson, A.M.B., et al., *Micro-PIXE analysis of an ancient Egyptian papyrus: Identification of pigments used for the "Book of the Dead"*. Nuclear Instruments and Methods in Physics Research Section B: Beam Interactions with Materials and Atoms, 2001. **181**(1-4): p. 707-714.
12. Krueger, A., *Carbon – Element of Many Faces*, in *Carbon Materials and Nanotechnology*2010, Wiley-VCH Verlag GmbH & Co. KGaA. p. 1-32.
13. Holmes, F.L., *Lavoisier and the Chemistry of Life: An Exploration of Scientific Creativity*1977.
14. Jorpes, J.E., *Jac. Berzelius: His Life and Work*1966.
15. Levinovitz, A.W. and N. Ringertz, *The Nobel Prize : the first 100 years* 2001, London: Imperial College Press.
16. Ströck, M., http://commons.wikimedia.org/wiki/File:Eight_Allotropes_of_Carbon.png, 2006, Wikimedia Commons.
17. Iijima, S., *Helical microtubules of graphitic carbon*. Nature, 1991. **354**(6348): p. 56-58.
18. Marshak, S., *Essentials of Geology, 2nd Edition*2007: W.W. Norton.
19. Audesirk, T.A., Gerald, *Life on Earth, 5th Edition*, Prentice-Hall: 1999.
20. Enoki, T., M. Endo, and M. Suzuki, *Graphite intercalation compounds and applications*2003: Oxford University Press.
21. Allen, M.J., V.C. Tung, and R.B. Kaner, *Honeycomb Carbon: A Review of Graphene*. Chemical Reviews, 2010. **110**(1): p. 132-145.
22. Landau, L.D., *Zur Theorie der phasenumwandlungen II*. Phys. Z. Sowjetunion, 1937. **11**: p. 26-35.
23. Evans, J.W., P.A. Thiel, and M.C. Bartelt, *Morphological evolution during epitaxial thin film growth: Formation of 2D islands and 3D mounds*. Surface Science Reports, 2006. **61**(1-2): p. 1-128.

24. Novoselov, K.S., et al., *Room-Temperature Quantum Hall Effect in Graphene*. Science, 2007. **315**(5817): p. 1379.
25. Bolotin, K.I., et al., *Ultra-high electron mobility in suspended graphene*. Solid State Communications, 2008. **146**(9–10): p. 351-355.
26. Novoselov, K.S., et al., *Two-dimensional atomic crystals*. Proceedings of the National Academy of Sciences of the United States of America, 2005. **102**(30): p. 10451-10453.
27. Berger, C., et al., *Electronic Confinement and Coherence in Patterned Epitaxial Graphene*. Science, 2006. **312**(5777): p. 1191-1196.
28. Ohta, T., et al., *Controlling the Electronic Structure of Bilayer Graphene*. Science, 2006. **313**(5789): p. 951-954.
29. Oshima, C. and A. Nagashima, *Ultra-thin epitaxial films of graphite and hexagonal boron nitride on solid surfaces*. Journal of Physics: Condensed Matter, 1997. **9**(1): p. 1.
30. Jiao, L., et al., *Narrow graphene nanoribbons from carbon nanotubes*. Nature, 2009. **458**(7240): p. 877-880.
31. Stankovich, S., et al., *Synthesis of graphene-based nanosheets via chemical reduction of exfoliated graphite oxide*. Carbon, 2007. **45**(7): p. 1558-1565.
32. Stankovich, S., et al., *Graphene-based composite materials*. Nature, 2006. **442**(7100): p. 282-286.
33. Eda, G. and M. Chhowalla, *Graphene-based Composite Thin Films for Electronics*. Nano Letters, 2009. **9**(2): p. 814-818.
34. Wu, Z.-S., et al., *Synthesis of high-quality graphene with a pre-determined number of layers*. Carbon, 2009. **47**(2): p. 493-499.
35. Singh, V., et al., *Graphene based materials: Past, present and future*. Progress in Materials Science, 2011. **56**(8): p. 1178-1271.
36. Lu, X., et al., *Tailoring graphite with the goal of achieving single sheets*. Nanotechnology, 1999. **10**(3): p. 269.
37. Zhang, Y., et al., *Fabrication and electric-field-dependent transport measurements of mesoscopic graphite devices*. Applied Physics Letters, 2005. **86**(7): p. 073104.
38. Ruoff, R., *Graphene: Calling all chemists*. Nat Nano, 2008. **3**(1): p. 10-11.
39. Hirata, M., et al., *Thin-film particles of graphite oxide 1:: High-yield synthesis and flexibility of the particles*. Carbon, 2004. **42**(14): p. 2929-2937.
40. Brodie, B.C., *On the Atomic Weight of Graphite*. Philosophical Transactions of the Royal Society of London, 1859. **149**: p. 249-259.
41. Hummers, W.S. and R.E. Offeman, *Preparation of Graphitic Oxide*. Journal of the American Chemical Society, 1958. **80**(6): p. 1339-1339.
42. Gao, W., et al., *New insights into the structure and reduction of graphite oxide*. Nat Chem, 2009. **1**(5): p. 403-408.
43. He, H., et al., *A new structural model for graphite oxide*. Chemical Physics Letters, 1998. **287**(1-2): p. 53-56.
44. Hontoria-Lucas, C., et al., *Study of oxygen-containing groups in a series of graphite oxides: Physical and chemical characterization*. Carbon, 1995. **33**(11): p. 1585-1592.
45. Wang, G., et al., *Facile Synthesis and Characterization of Graphene Nanosheets*. The Journal of Physical Chemistry C, 2008. **112**(22): p. 8192-8195.
46. Tung, V.C., et al., *High-throughput solution processing of large-scale graphene*. Nat Nano, 2009. **4**(1): p. 25-29.
47. Williams, G., B. Seger, and P.V. Kamat, *TiO₂-Graphene Nanocomposites. UV-Assisted Photocatalytic Reduction of Graphene Oxide*. ACS Nano, 2008. **2**(7): p. 1487-1491.
48. Li, X., et al., *Chemically Derived, Ultrasoft Graphene Nanoribbon Semiconductors*. Science, 2008. **319**(5867): p. 1229-1232.
49. Gao, J., et al., *Environment-Friendly Method To Produce Graphene That Employs Vitamin C and Amino Acid*. Chemistry of Materials, 2010. **22**(7): p. 2213-2218.

50. Wang, Y., Z. Shi, and J. Yin, *Facile Synthesis of Soluble Graphene via a Green Reduction of Graphene Oxide in Tea Solution and Its Biocomposites*. ACS Applied Materials & Interfaces, 2011. **3**(4): p. 1127-1133.
51. Liao, K.-H., et al., *Aqueous Only Route toward Graphene from Graphite Oxide*. ACS Nano, 2011. **5**(2): p. 1253-1258.
52. Akhavan, O. and E. Ghaderi, *Escherichia coli bacteria reduce graphene oxide to bactericidal graphene in a self-limiting manner*. Carbon, 2012. **50**(5): p. 1853-1860.
53. Gómez-Navarro, C., et al., *Atomic Structure of Reduced Graphene Oxide*. Nano Letters, 2010. **10**(4): p. 1144-1148.
54. Ni, Z.H., et al., *Graphene Thickness Determination Using Reflection and Contrast Spectroscopy*. Nano Letters, 2007. **7**(9): p. 2758-2763.
55. Paredes, J.I., et al., *Atomic Force and Scanning Tunneling Microscopy Imaging of Graphene Nanosheets Derived from Graphite Oxide*. Langmuir, 2009. **25**(10): p. 5957-5968.
56. Stolyarova, E., et al., *High-resolution scanning tunneling microscopy imaging of mesoscopic graphene sheets on an insulating surface*. Proceedings of the National Academy of Sciences, 2007. **104**(22): p. 9209-9212.
57. Meyer, J.C., et al., *Direct Imaging of Lattice Atoms and Topological Defects in Graphene Membranes*. Nano Letters, 2008. **8**(11): p. 3582-3586.
58. Ferrari, A.C., et al., *Raman Spectrum of Graphene and Graphene Layers*. Physical Review Letters, 2006. **97**(18): p. 187401.
59. Lee, C., et al., *Measurement of the Elastic Properties and Intrinsic Strength of Monolayer Graphene*. Science, 2008. **321**(5887): p. 385-388.
60. Chae, H.K., et al., *A route to high surface area, porosity and inclusion of large molecules in crystals*. Nature, 2004. **427**(6974): p. 523-527.
61. Morozov, S.V., et al., *Giant Intrinsic Carrier Mobilities in Graphene and Its Bilayer*. Physical Review Letters, 2008. **100**(1): p. 016602.
62. Nair, R.R., et al., *Fine Structure Constant Defines Visual Transparency of Graphene*. Science, 2008. **320**(5881): p. 1308.
63. Reddy, C.D., S. Rajendran, and K.M. Liew, *Equilibrium configuration and continuum elastic properties of finite sized graphene*. Nanotechnology, 2006. **17**(3): p. 864.
64. Van Lier, G., et al., *Ab initio study of the elastic properties of single-walled carbon nanotubes and graphene*. Chemical Physics Letters, 2000. **326**(1-2): p. 181-185.
65. Frank, I.W., et al. *Mechanical properties of suspended graphene sheets*. 2007. AVS.
66. Bunch, J.S., et al., *Electromechanical Resonators from Graphene Sheets*. Science, 2007. **315**(5811): p. 490-493.
67. Eda, G., G. Fanchini, and M. Chhowalla, *Large-area ultrathin films of reduced graphene oxide as a transparent and flexible electronic material*. Nat Nano, 2008. **3**(5): p. 270-274.
68. Hernandez, Y., et al., *High-yield production of graphene by liquid-phase exfoliation of graphite*. Nat Nano, 2008. **3**(9): p. 563-568.
69. Balandin, A.A., et al., *Superior Thermal Conductivity of Single-Layer Graphene*. Nano Letters, 2008. **8**(3): p. 902-907.
70. Ghosh, S., et al., *Extremely high thermal conductivity of graphene: Prospects for thermal management applications in nanoelectronic circuits*. Applied Physics Letters, 2008. **92**(15): p. 151911.
71. Yang, S.-Y., et al., *Synergetic effects of graphene platelets and carbon nanotubes on the mechanical and thermal properties of epoxy composites*. Carbon, 2011. **49**(3): p. 793-803.
72. Lin, Y.-M., et al., *Operation of Graphene Transistors at Gigahertz Frequencies*. Nano Letters, 2008. **9**(1): p. 422-426.
73. Hasan, T., et al., *Nanotube-Polymer Composites for Ultrafast Photonics*. Advanced Materials, 2009. **21**(38-39): p. 3874-3899.
74. Bae, S., et al., *Roll-to-roll production of 30-inch graphene films for transparent electrodes*. Nat Nano, 2010. **5**(8): p. 574-578.

75. Xu, Y., et al., *A hybrid material of graphene and poly (3,4-ethyldioxythiophene) with high conductivity, flexibility, and transparency*. Nano Research, 2009. **2**(4): p. 343-348.
76. Sofo, J.O., A.S. Chaudhari, and G.D. Barber, *Graphane: A two-dimensional hydrocarbon*. Physical Review B, 2007. **75**(15): p. 153401.
77. Cao, Y., et al., *High-Performance Photoresponsive Organic Nanotransistors with Single-Layer Graphenes as Two-Dimensional Electrodes*. Advanced Functional Materials, 2009. **19**(17): p. 2743-2748.
78. Murugan, A.V., T. Muraliganth, and A. Manthiram, *Rapid, Facile Microwave-Solvothermal Synthesis of Graphene Nanosheets and Their Polyaniline Nanocomposites for Energy Storage*. Chemistry of Materials, 2009. **21**(21): p. 5004-5006.
79. Li, Z., et al., *Ultrafast, dry microwave synthesis of graphene sheets*. Journal of Materials Chemistry, 2010. **20**(23).
80. *Stoe WINXPOW 1.2.2000*: Stoe & Cie GmbH, Darmstadt.
81. Paredes, J.I., et al., *Graphene Oxide Dispersions in Organic Solvents*. Langmuir, 2008. **24**(19): p. 10560-10564.
82. Park, S., et al., *Colloidal Suspensions of Highly Reduced Graphene Oxide in a Wide Variety of Organic Solvents*. Nano Letters, 2009. **9**(4): p. 1593-1597.
83. Hansen, C.M., *Hansen Solubility Parameters: A User's Handbook; 2nd ed.*; 2007: CRC Press: Hoboken, .
84. Chen, W., L. Yan, and P.R. Bangal, *Preparation of graphene by the rapid and mild thermal reduction of graphene oxide induced by microwaves*. Carbon, 2010. **48**(4): p. 1146-1152.
85. Li, J.-L., et al., *Oxygen-Driven Unzipping of Graphitic Materials*. Physical Review Letters, 2006. **96**(17): p. 176101.
86. Schniepp, H.C., et al., *Functionalized Single Graphene Sheets Derived from Splitting Graphite Oxide*. The Journal of Physical Chemistry B, 2006. **110**(17): p. 8535-8539.
87. Titelman, G.I., et al., *Characteristics and microstructure of aqueous colloidal dispersions of graphite oxide*. Carbon, 2005. **43**(3): p. 641-649.
88. Guo, P., H. Song, and X. Chen, *Electrochemical performance of graphene nanosheets as anode material for lithium-ion batteries*. Electrochemistry Communications, 2009. **11**(6): p. 1320-1324.
89. Dresselhaus, M.S., G. Dresselhaus, and M. Hofmann, *Raman spectroscopy as a probe of graphene and carbon nanotubes*. Philosophical Transactions of the Royal Society A: Mathematical, Physical and Engineering Sciences, 2008. **366**(1863): p. 231-236.
90. Wei, D., et al., *Synthesis of N-Doped Graphene by Chemical Vapor Deposition and Its Electrical Properties*. Nano Letters, 2009. **9**(5): p. 1752-1758.
91. Kudin, K.N., et al., *Raman Spectra of Graphite Oxide and Functionalized Graphene Sheets*. Nano Letters, 2007. **8**(1): p. 36-41.